ABSTRACT

Influence of Hydraulic Fracturing on Overlying Aquifers in the Presence of Abandoned and Converted Oil and Gas Wells: Numerical, Spatial, Uncertainty, and Geochemical Investigations

Joshua W. Brownlow, Ph.D.

Committee Chairman: Joe C. Yelderman, Jr., Ph.D.

The association between hydrocarbon-rich reservoirs and organic-rich source rocks means unconventional oil and gas plays usually occur in mature sedimentary basins – where large-scale conventional development has already taken place. Abandoned wells in proximity to hydraulic fracturing could be affected by increased fluid pressures and corresponding newly generated fractures that directly connect (frac hit) to an abandoned well or to existing fractures intersecting an abandoned well. If contaminants migrate to a pathway hydraulically connected to an abandoned well, upward leakage may occur. This study evaluated potential risks associated with hydraulic fracturing near abandoned oil and gas wells, with attention to abandoned oil and gas wells converted into water wells. Potential risks of hydraulic fracturing on abandoned oil and gas wells were evaluated with four investigations: (1) development of a numerical model to assess magnitude of upward leakage along a leaky abandoned well in proximity of hydraulic fracturing, (2) characterization of abandoned and converted oil and gas wells and probability of their

intersection with stimulated areas surrounding horizontal wells, (3) interrogation of model uncertainty and evaluation of data crucial for future investigations, and (4) preliminary assessment of an organic geochemical fingerprint to identify potential groundwater quality impacts. Collectively, investigations suggest there is potential for abandoned oil and gas wells near hydraulic fracturing to represent a risk to groundwater quality if certain spatial and hydraulic conditions exist. Overall, the results of this study underscore a critical need to evaluate historical oil and gas activities in areas with modern unconventional oil and gas activities, and improve historical and future data contained in public records.

Influence of Hydraulic Fracturing on Overlying Aquifers in the Presence of Abandoned and Converted Oil and Gas Wells: Numerical, Spatial, Uncertainty, and Geochemical Investigations

by

Joshua W. Brownlow, B.S., M.S.

A Dissertation

Approved by the Department of Geosciences

_____

Stacy C. Atchley, Ph.D., Chairperson

Submitted to the Graduate Faculty of
Baylor University in Partial Fulfillment of the
Requirements for the Degree
of
Doctor of Philosophy

Approved by the Dissertation Committee

_____

Joe C. Yelderman, Jr., Ph.D., Chairperson

_____

Scott C. James, Ph.D.

_____

Peter M. Allen, Ph.D.

_____

William C. Hockaday, Ph.D.

_____

Sascha Usenko, Ph.D.

_____

R.L. Bassett, Ph.D.

Accepted by the Graduate School
December 2016

_____

J. Larry Lyon, Ph.D., Dean

Page bearing signatures is kept on file in the Graduate School.

TABLE OF CONTENTS

LIST OF FIGURES

LIST OF TABLES

ACKNOWLEDGMENTS

Foremost, I want to thank my committee chair Dr. Joe C. Yelderman, Jr for his unwavering support of me throughout my time here at Baylor University. I especially want thank my committee member Dr. Scott C. James for the time and effort he contributed. I also thank my committee members Dr. Peter Allen, Dr. Bill Hockaday, Dr. R.L. Bassett, and Dr. Sascha Usenko, with whom I had numerous discussions with about both research and life.

I could not have completed this journey without the help of my friends and colleagues: Stephanie Wong, Andrew Worsley, Todd Longbottom, Josh Kirby, Stephen Norair, Jim Tucker, Hunter Harlow, Tori Worrell, Kori Taylor, and many others. The Geoscience faculty and staff donated voluminous advice and time which I greatly appreciate: Paulette Penney, Jamie Ruth, Stacy and Janelle Atchley, Vince Cronin, John Dunbar, Stephen Dworkin, Joseph White, and Wayne Hamilton.

I want thank the Board of Directors for both the Evergreen Underground Water Conservation District and the Wintergarden Groundwater Conservation District, this dissertation would not have been possible without their support. The groundwater district staff were instrumental in my success: Russell Labus, Chris McFarlane, Matt Pope, and Melissa Gonzalez at EUWCD, and Ed Walker and Debbie Farmer at WGCD. In addition, support from Baylor University and the C. Gus Glasscock Foundation was indispensable.

I attribute many of my blessings to the support of my family: grandma and grandpa Brownlow, grandma and grandpa Bienek, my mom, dad, sisters Devon and Kendra. Most of all I want to thank my uncle Darrell T. Brownlow, who helped me begin

my PhD journey, the results of this research are dedicated to him and his never-ending encouragement.

Finally I want to thank my beautiful wife who is carrying the newest member of our family – my son Brooks. If I know what love is, it is because of you Morgan. Love you.

CHAPTER ONE

Introduction

A major concern of unconventional oil and gas development is the potential risk to groundwater resources. Researchers have recognized a variety of potential risks to groundwater associated with unconventional development (Vengosh et al. 2014). One controversial risk is potential contamination of overlying (shallower) aquifers due to hydraulic-fracturing operations. Hydraulic fracturing could pose a risk to groundwater if hydraulic-fracturing fluids or formation fluids (e.g., oil, gas, brine) migrate upward into shallower aquifers. Migration of contaminants may occur through natural geological features acting as preferential pathways such as faults or fractures, potentially enhanced by pressures associated with the hydraulic-fracturing process, or through anthropogenic pathways such as producing or abandoned wells (Vengosh et al. 2014; Reagan et al. 2015).

Unforced upward flow of fluids through natural features from low-permeability shale targets to an overlying aquifer is considered unlikely, or predicted to occur over especially long timescales, due to constraints on basin hydrogeology (Flewelling and Sharma 2014). In most cases, upward flow is limited by thick sequences of low-permeability interburden that separate the shale from overlying aquifers, small vertical hydraulic gradients, and high densities of deep fluids (Kreitler 1989; Flewelling and Sharma 2014). However, previous studies have documented natural migration of deep brines into overlying aquifers (Warner et al. 2012; Llewellyn 2014). Although hydraulic fracturing has the potential to interact with natural features, it is diminished by physical

constraints of the hydraulic-fracturing process. These constraints include limits on fracture-aperture growth, fracture and pressure propagation, and the stimulation of relatively small volumes of rock compared to overburden thickness (Flewelling et al. 2013; Flewelling and Sharma 2014). Gassiat et al. (2013) found that the migration of fluids through faults can occur over long timescales under certain hydrologic conditions, although they questioned whether faults could be continuous permeable features from shale to aquifer.

Compared with natural geological pathways, abandoned wells may facilitate upward migration of contaminants over shorter timescales. Abandoned wells are particularly numerous and spatially dense in mature sedimentary basins. Abandoned wells may represent large, vertically-continuous, and highly-permeable pathways through layered, low-permeability strata. Hydraulic characteristics of wells are affected by various factors, the most significant of which may be the history of oil and gas activity in the sedimentary basin.

Although hydraulic fracturing has the potential to interact with abandoned oil and gas wells, assessing the risk of upward leakage following a frac hit is a complex task due to variable field practices, regulatory requirements, materials, and subsurface conditions; often unique to each well (Nordbotten et al. 2005). Because these issues have evolved over time, the risk of leakage depends on the age and abandonment technique associated with a particular well. The risk for potential leakage is highest in mature sedimentary basins where historical oil and gas exploration and production have resulted in a high spatial density of abandoned wells (Gasda et al. 2004; Nordbotten et al. 2005). Because geographic areas of oil and gas activity often overlap, abandoned oil and gas wells can be

in close horizontal and vertical proximity to modern hydraulic-fracturing operations. Continued hydraulic fracturing in mature basins could result in increased numbers of frac hits on abandoned oil and gas wells over time as the spatial density of both horizontal and abandoned wells increases.

This study evaluated potential risks associated with hydraulic fracturing near abandoned oil and gas wells, with attention to abandoned oil and gas wells converted into water wells. Potential risks of hydraulic fracturing on abandoned oil and gas wells were evaluated with four investigations: (1) development of a numerical model to assess magnitude of upward leakage along a leaky abandoned well in proximity of hydraulic fracturing, (2) characterization of abandoned and converted oil and gas wells and probability of their intersection with stimulated areas surrounding horizontal wells, (3) interrogation of model uncertainty and evaluation of data crucial for future investigations, and (4) preliminary assessment of an organic geochemical fingerprint to identify potential groundwater quality impacts. J.W. Brownlow designed, performed the calculations and analysis, and wrote each investigation with input and feedback from J.C. Yelderman, Jr. and S.C. James. Each study is briefly reviewed below.

The first investigation used numerical modeling to investigate potential effects of hydraulic fracturing on upward flow through a leaky abandoned oil and gas wells converted into water wells (converted wells). Converted wells are usually registered with regulatory agencies, and can be completed on abandoned oil and gas wells with total vertical depths at or near modern shale plays. Conversion of abandoned oil and gas wells into water wells creates a situation of concern because converted wells are simultaneously screened in both the deep reservoir and the overlying shallower aquifer.

The objective of the investigation is to understand the potential for hydraulic-fracturing operations to influence upward leakage through a converted well subject to overpressured (10.5 MPa/km) conditions. Several factors were considered, such as proximity to hydraulic fracturing, flowback and production, and leaky-well abandonment methods. The numerical model in this study is based on the Eagle Ford Shale play in south Texas. To model realistic scenarios, industry data specific to the play and historical records from nearby converted wells were incorporated.

The second investigation used historical data and spatial modeling to characterize potential risk for frac hits on abandoned and converted oil and gas wells. The potential for frac hits was characterized by investigating the probability that abandoned or converted oil and gas wells intersect an assumed stimulated reservoir size surrounding hydraulically fractured horizontal wells. The intersection of an abandoned oil and gas well with the assumed stimulated reservoir does not mean that the abandoned well has definitely experienced a frac hit, but does indicate the potential. Public and industry data for wells were collected, classified, and integrated using a Geographic Information System (GIS). Well data were analyzed for spatial location and reservoir information to develop spatial distributions in three-dimensions. Sensitivity analyses for the number and locations of potential frac hits were conducted by varying the assumed horizontal extent of the stimulated reservoir area (SRA) assigned to horizontal wells. A simple statistical analysis estimated the potential number and locations of abandoned and converted oil and gas wells that intersect the assumed SRA of horizontal wells. The investigation focused on the Eagle Ford Shale play in south Texas because it is exemplary of a mature

sedimentary basin with data available for both abandoned and converted oil and gas wells.

The third investigation comprised a series of uncertainty analyses conducted on the original model of upward flow through an abandoned oil and gas well in the stimulated reservoir of hydraulically fractured shale. The model focused on leaky abandoned oil and gas wells converted in water wells (converted wells) in the Eagle Ford Shale study area, and is described in Brownlow et al. (2016a). The analysis is structured as follows: first, a sensitivity analysis of the uncalibrated model is performed. Second, the model was calibrated with a limited dataset of observations calculated from measurements contained in well records. Finally, predictive uncertainty of the model is interrogated using linear and nonlinear analyses. The software used for these analyses is part of the publically available PEST suite which is extensively documented (Doherty 2016). The study provides an exploratory evaluation of major contributing factors to model uncertainty in leakage and assessment of data needed towards the development of more complex models that evaluate leakage.

The fourth investigation is described in Appendix E. The investigation details a preliminary assessment of organic substances in Eagle Ford Shale crude oil and produced water. Organic compositions of crude oil and produced water are a central component in forensic investigations of potential oil and gas impacts to water quality. Column chromatography was used to separate the total lipid extract (TLE) from crude oil and produced water samples into saturate, aromatic and polar fractions. Fractions were analyzed using gas chromatography/mass spectrometry (GC/MS). Individual organic compounds were identified according to their mass spectral features, and a number of

diagnostic biomarker ratios were determined including: maximum carbon chain length (C_{max}), average chain length (ACL), carbon preference index (CPI), odd-even preference (OEP), and pristane/phytane (Pr/Ph). The results of the investigation represent an important first step towards developing a geochemical fingerprint that could be used for identification, correlation or differentiation of potential groundwater impacts from hydraulic fracturing in the Eagle Ford Shale play.

CHAPTER TWO

Influence of Hydraulic Fracturing on Overlying Aquifers in the Presence of Leaky Abandoned Wells

This chapter was published as Brownlow, J.W., S.C. James, and J.C. Yelderman, Jr. 2016. Influence of hydraulic fracturing on overlying aquifers in the presence of leaky abandoned wells. Groundwater. dx.doi.org/10.1111/gwat.12431

Abstract

The association between hydrocarbon-rich reservoirs and organic-rich source rocks means unconventional oil and gas plays usually occur in mature sedimentary basins – where large-scale conventional development has already taken place. Abandoned wells in proximity to hydraulic fracturing could be affected by increased fluid pressures and corresponding newly generated fractures that directly connect (frac hit) to an abandoned well or to existing fractures intersecting an abandoned well. If contaminants migrate to a pathway hydraulically connected to an abandoned well, upward leakage may occur. Potential effects of hydraulic fracturing on upward flow through a particular type of leaky abandoned well – abandoned oil and gas wells converted into water wells were investigated using numerical modeling. Several factors that affect flow to leaky wells were considered including; proximity of a leaky well to hydraulic fracturing, flowback, production, and leaky-well abandonment methods. The numerical model used historical records and available industry data for the Eagle Ford Shale play in south Texas. Numerical simulations indicate upward contaminant migration could occur through leaky converted wells if certain spatial and hydraulic conditions exist. Upward flow through leaky converted wells increased with proximity to hydraulic fracturing, but decreased

when flowback and production occurred. Volumetric flow rates ranged between 0 and 0.086 m^3/d for hydraulic-fracturing scenarios. Potential groundwater impacts should be paired with plausible transport mechanisms, and upward flow through leaky abandoned wells could be unrelated to hydraulic fracturing. The results also underscore the need to evaluate historical activities.

Introduction

A major concern of unconventional oil and gas development is the potential risk to groundwater resources. Researchers have recognized a variety of potential risks to groundwater associated with unconventional development (Vengosh et al. 2014). One controversial risk is potential contamination of overlying (shallower) aquifers due to hydraulic-fracturing operations. Hydraulic fracturing could pose a risk to groundwater if hydraulic-fracturing fluids or formation fluids (e.g., oil, gas, brine) migrate upward into shallower aquifers. Migration of contaminants may occur through natural geological features acting as preferential pathways such as faults or fractures, potentially enhanced by pressures associated with the hydraulic-fracturing process, or through anthropogenic pathways such as producing or abandoned wells (Vengosh et al. 2014; Reagan et al. 2015). Conclusive evidence of impacts directly related to hydraulic fracturing is not currently available, but correct interpretations will require pairing impacts with physically plausible mechanisms of flow and transport.

Unforced upward flow of fluids through natural features from low-permeability shale targets to an overlying aquifer is considered unlikely, or predicted to occur over especially long timescales, due to constraints on basin hydrogeology (Flewelling and

Sharma 2014). In most cases, upward flow is limited by thick sequences of low-permeability interburden that separate the shale from overlying aquifers, small vertical hydraulic gradients, and high densities of deep fluids (Kreitler 1989; Flewelling and Sharma 2014). However, previous studies have documented natural migration of deep brines into overlying aquifers (Warner et al. 2012; Llewellyn 2014). Although hydraulic fracturing has the potential to interact with natural features, it is diminished by physical constraints of the hydraulic-fracturing process. These constraints include limits on fracture-aperture growth, fracture and pressure propagation, and the stimulation of relatively small volumes of rock compared to overburden thickness (Flewelling et al. 2013; Flewelling and Sharma 2014). Gassiat et al. (2013) found that the migration of fluids through faults can occur over long timescales under certain hydrologic conditions, although they questioned whether faults could be continuous permeable features from shale to aquifer. Myers (2012) considered a broad set of conditions with hydraulic fracturing occurring near a natural fault, and suggested that hydraulic fracturing could result in upward flow and transport of contaminants through a natural fault into overlying aquifers in six years or less in the most aggressive scenario.

Compared to natural geological pathways, leaky wells are more likely to act as continuous pathways, potentially facilitating upward migration of fluids over shorter timescales. Leaky wells can have a significant effect on groundwater flow and transport within a system (Avci 1994) and can function as conduits for rapid vertical contaminant transport through otherwise low-permeability strata (Lacombe et al. 1995). Studies involving deep geologic storage of CO_2 indicate that leaky abandoned wells can facilitate upward leakage of contaminants (Nordbotten et al. 2008). However, questions regarding

the role of leaky wells in the context of hydraulic fracturing have not been thoroughly explored, and relatively little work has been conducted to quantitatively estimate potential leakage. Previous hydraulic fracturing models have considered upward flow and transport along leaky wells plausible, but did not simulate this effect, and instead focused on natural geologic features (Myers 2012; Gassiat et al. 2013; Kissinger et al. 2013). Recent modeling by Reagan et al. (2015) considered leaky wells, but focused on upward leakage of methane through degraded (low-permeability) cement plugs under hydrostatic conditions.

This study applies numerical modeling to investigate potential effects of hydraulic fracturing on upward flow through a particular type of leaky well – abandoned oil and gas wells converted into water wells (converted wells). Converted wells are usually registered with regulatory agencies, and can be completed on abandoned oil and gas wells with total vertical depths at or near modern shale plays. Conversion of abandoned oil and gas wells into water wells creates a situation of concern because converted wells are simultaneously screened in both the deep reservoir and the overlying shallower aquifer. The objective of this study is to understand the potential for hydraulic-fracturing operations to influence upward leakage through a converted well subject to overpressured (10.5 MPa/km) conditions. The probability of hydraulic fracturing interacting with an abandoned well depends on the depth of the horizontal well, growth of hydraulic fractures, and depth and location of the abandoned well (Montague and Pinder 2015). Several factors were considered, such as proximity to hydraulic fracturing, flowback and production, and leaky-well abandonment methods. The numerical model in this study is based on the Eagle Ford Shale play in south Texas (Figure 2.1). To model realistic

scenarios, industry data specific to the play and historical records from nearby converted wells were incorporated.

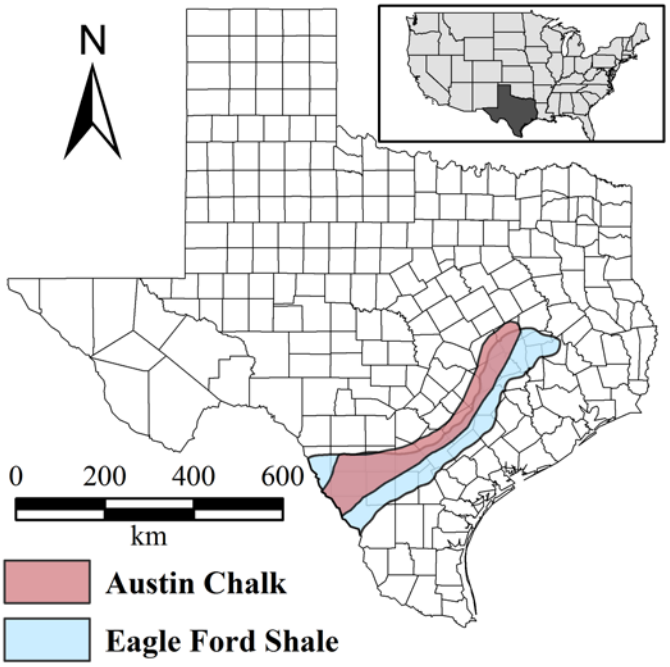

Figure 2.1. Overlapping geographic areas of two major oil and gas plays in south Texas.

Several potential limitations of this study must be emphasized. First, the system was modeled as a single-phase, isothermal fluid, in a fully saturated reservoir although these effects were accounted for indirectly using depth-dependent and multiphase relationships for hydraulic conductivities. Second, the numerical model does not account for media deformation due to hydraulic-fracturing. Finally, hydraulic fracturing is represented by a uniform transient change of shale permeability. Consequently, results are considered to be conservative (high) with respect to the potential magnitude of flow through leaky wells.

Problem Background

Conventional oil and gas plays extract fluid hydrocarbons from reservoirs sourced by organic-rich rocks. In contrast, unconventional shale plays extract hydrocarbons directly from the organic-rich source rocks. The co-location of reservoirs and source rocks means unconventional oil and gas plays usually occur in mature sedimentary basins where large-scale conventional development has already taken place. However, there are also examples of unconventional development in areas with little or no historical oil and gas activity (e.g., northeast Pennsylvania). In Texas, more than 1.1 million oil and gas wells have been drilled in sedimentary basins since the first commercial oil well was completed in 1866, the majority (>75%) of which have been abandoned (IPAA 2013). Development of mature basins resulted in spatially dense numbers of abandoned wells that represent potential pathways for upward fluid migration (Gasda et al. 2004). Both adjacent conventional reservoirs, and in some cases their associated organic-rich shales, have been drilled prior to modern unconventional production. Because geographic areas of oil and gas activity often overlap, abandoned wells can be in close proximity to modern hydraulic-fracturing operations (see Figure 2.2 for a schematic). The history of oil and gas activities in each sedimentary basin is a crucial part of evaluating abandoned wells as potential flow pathways.

Leaky abandoned wells near hydraulic-fracturing operations could be affected by the generated fractures and increased fluid pressures. Hydraulically generated fractures could directly connect to the abandoned well or propagate into natural fractures intersecting an abandoned well. Pressures associated with hydraulic fracturing could mobilize gas- or liquid-phase contaminants toward an abandoned well. If contaminant

paths are hydraulically connected to an abandoned well, upward leakage may occur through the abandoned well.

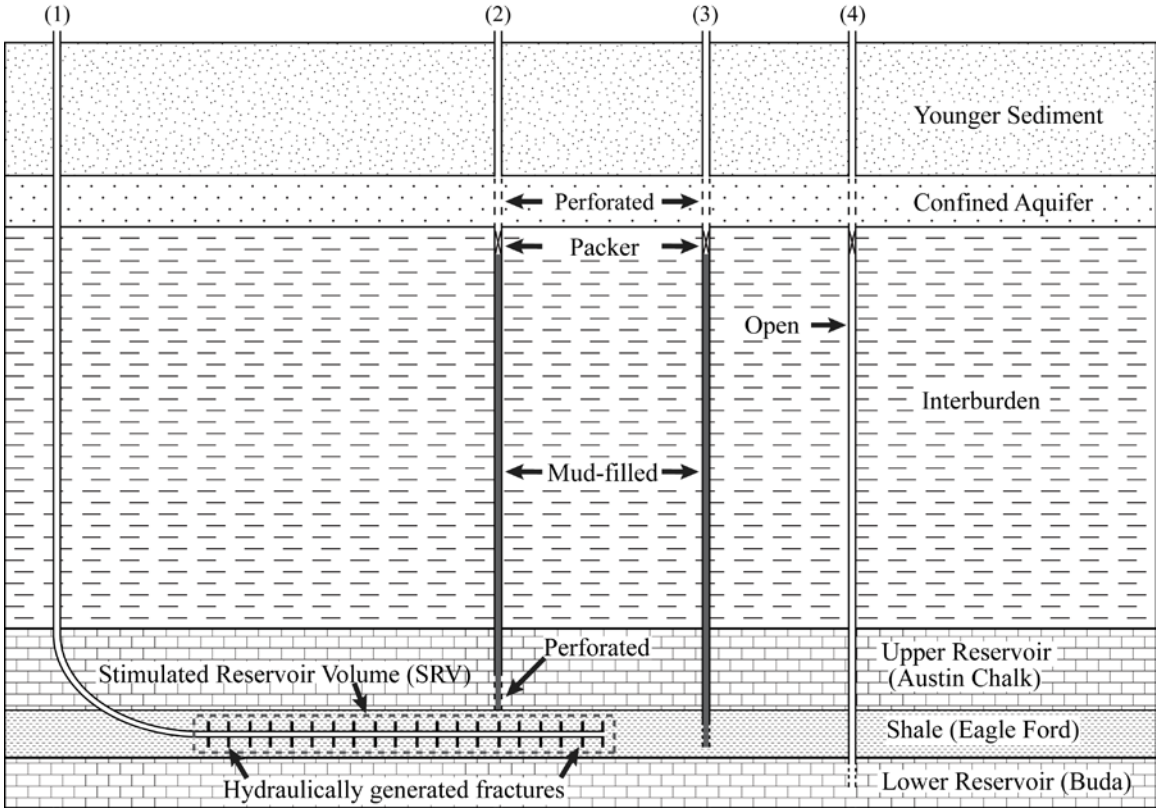

Figure 2.2. Schematic cross-section (not to scale) of spatial relationships between a horizontal well and improperly abandoned wells in unconventional plays: (1) horizontal well intersecting hydraulically generated fractures (SRV); (2) abandoned well in the upper reservoir backfilled with drilling mud and converted into a water well; (3) abandoned well in shale backfilled with drilling mud and converted into a water well; and (4) an abandoned open well in the lower reservoir converted into a water well.

Example: Eagle Ford Shale

The Eagle Ford Shale is composed of mixed siliciclastic and carbonate units deposited during the Late Cretaceous, bound disconformably above by the Austin Chalk Group, and disconformably below by the Buda Formation or Woodbine Group (Martin et al. 2011). Conventional Eagle Ford Shale wells have been drilled since the 1920s (Stapp 1977; Martin et al. 2011). Modern unconventional wells were first drilled in late 2008, and the play has since expanded to include 52,000 km^2 spanning 26 Texas counties (RRC

2016a). By 2015, the total number of wells drilled was approximately 11,460 (RRC 2016a).

The Eagle Ford Shale is a low-permeability (10^{-21} to 10^{-18} m^2) reservoir that requires a combination of laterally extensive horizontal wells and hydraulic fracturing to produce oil and gas economically (Martin et al. 2011). Horizontal wells commonly exceed 1,500 m in length. Hydraulic-fracturing treatments are unique to each well: mechanical processes, fluid characteristics, and chemical additives are specifically engineered for local reservoir characteristics. Typical Eagle Ford Shale hydraulic-fracturing treatments deliver 11,000 to 19,000 m^3 of fluid in 14 to 20 fracture stages 75 to 130 m long (Martin et al. 2011). Because hydraulic-fracturing treatments are site-specific, fractures vary by stage in orientation, aperture, length, and height. Available microseismic data show fracture half-lengths typically vary between 100 and 300 m from the horizontal well (Bazan et al. 2010; Basu et al. 2012; Suliman et al. 2013). Vertically, fractures extend throughout the shale thickness (40 to 120 m) (Fisher 2014). Out-of-formation fracturing does occur (Suliman et al. 2013), but the mechanical stratigraphies of the Eagle Ford Shale (relatively plastic) and adjacent carbonate units (relatively competent) constrain vertical growth of hydraulic fractures within the target shale more than other shale plays, like the Marcellus and Haynesville (Curry et al. 2010; Fisher and Warpinski 2011; Basu et al. 2012; Fisher 2014).

The Austin Chalk overlies the Eagle Ford Shale and has produced oil and gas since the discovery of the Giddings and Pearsall Fields in the 1930s (Haymond 1991). Matrix permeability is low (10^{-17} to 10^{-15} m^2), but the brittle lithology and dense fracture network support a long history of oil and gas production (Haymond 1991). Early

exploration strategies involved conventional drilling of vertical boreholes. However, the majority of these wells were unsuccessful (dry) wells and did not intersect the dense, but spatially isolated, fracture network (Scott 1977). Development of a key completion strategy during the 1970s – hydraulic fracturing – significantly increased well productivity in the play (Haymond 1991).

Hydraulic fracturing with vertical Austin Chalk wells notably increased the probability of intersecting existing fracture networks near the wellbore. These hydraulic-fracturing treatments were significantly smaller (total injection volume of 800 m^3) than modern hydraulic-fracturing operations (Martin et al. 2011). Operators recognized that production could be further increased by drilling deeper wells that penetrated the underlying Eagle Ford Shale or Buda Formation, and hydraulically fracturing longer intervals (Scott 1977; Martin et al. 2011). Initial production from the combination of these practices was impressive, and by 1991 over 7,000 vertical wells had been drilled throughout the Austin Chalk play (EIA 1993). Uneconomical long-term production eventually halted major oil and gas activity in the Austin Chalk play (Haymond 1991; EIA 1993).

In the exploration process, unsuccessful wells are abandoned almost immediately, while producing wells are abandoned after reservoir depletion. Well abandonment practices in Texas, regulated by the Railroad Commission (RRC), require unsuccessful wells to be properly abandoned with multiple zones of cement plugs in the wellbore (RRC 2000). After abandonment procedures are completed, the abandoned well can be converted into a water well. The application to condition an abandoned oil and gas well for groundwater production requires registration with the RRC (see RRC Form P-13).

Conversion involves scouring and perforation of the well casing in an aquifer zone (RRC 2015a). Harris (1965) noted that a number of deep oil and gas wells had been converted to water wells for livestock and domestic supplies. Discussions with local groundwater districts suggest that several hundred to several thousand converted wells may exist across the Eagle Ford Shale play. Many Austin Chalk wells were properly abandoned, although evidence from field observations and well records indicate variability in abandonment practices (RRC 2015a). One well abandonment practice was the backfilling of wells with drilling mud prior to conversion. The abandonment of oil and gas wells using mud-laden fluid was considered an acceptable practice until at least 1967 in Texas (Nicot 2009). This abandonment procedure could have consequences in the modern era of hydraulic fracturing (Figure 2.2).

Modeling Approach

We considered a three-dimensional conceptualization of a layered sedimentary model comprised of sixteen layers with five distinct hydrostratigraphic units from the oil and gas reservoirs to the overlying aquifer: (1) confined aquifer, (2) interburden, (3) upper reservoir (i.e., Austin Chalk), (4) shale (i.e., Eagle Ford Shale), and (5) lower reservoir (i.e., Buda Formation) (Figures 2.2 and 2.3). Each hydrostratigraphic unit is homogenous and vertically anisotropic. Anisotropic flow is considered because horizontal permeability often exceeds vertical permeability by more than two orders of magnitude in sedimentary basins (Neuzil 1994). Therefore, fluids injected during hydraulic fracturing would exhibit a greater tendency to move laterally than vertically (Saiers and Barth 2012). No-flow boundary conditions are imposed at the base of the

model and top of the confined aquifer model because upward flow through the lower reservoir and infiltration through the confined aquifer are assumed negligible. Constant-head boundary conditions are applied with a vertical gradient (0.165) along the sides of the model. Horizontal gradients across sedimentary basins range from 0.05 to 0.005 (Magara 1978), and flow across the model is simulated by applying a uniform horizontal gradient of 0.02. The model domain is longer (3,000 m) than it is thick (1,830 m) or wide (1,500 m) (Figure 2.3). The width and length of the model domain were selected to eliminate vertical and lateral boundary effects on the solution in the well regions. The lateral grid spacing was a uniform 5 m, and the vertical discretization varied by layer. Grid refinement studies were conducted to confirm the horizontal and vertical discretization appropriate for the solution. Numerical simulations were conducted using the MODFLOW-2005 code (Harbaugh 2005).

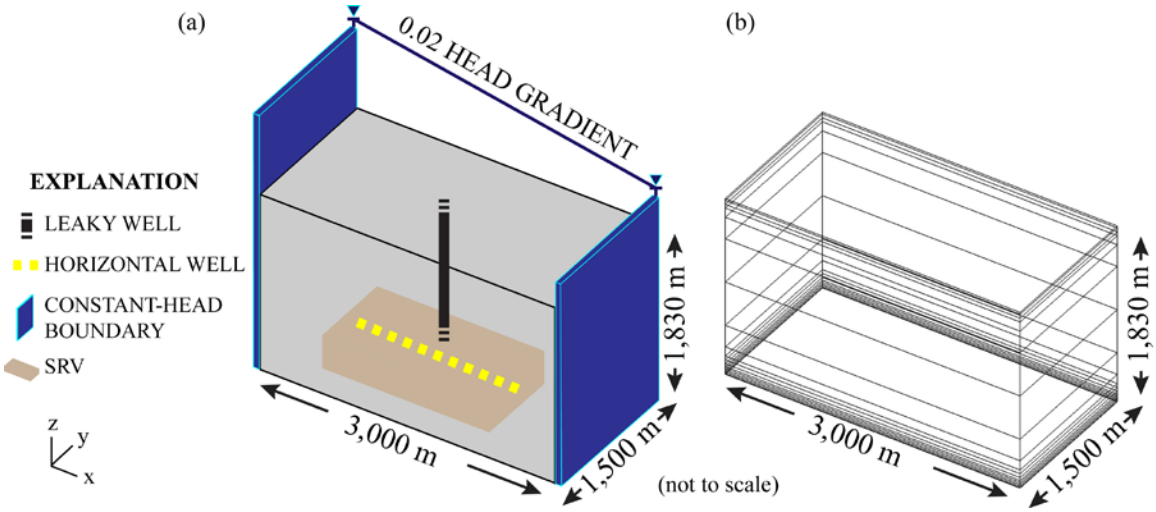

Figure 2.3. (a) Diagram of the model domain with a nonpumping multinode well, and (b) model vertical discretization.

Depth-dependent relationships were applied to certain properties (temperature, pressure, and salinity) to estimate *in-situ* reservoir pore fluid (density and dynamic

viscosity), which are used when calculating hydrogeologic parameters (storativity, hydraulic conductivity, and hydraulic head) (Table 2.1). Derivations of model parameters are available in Appendix B.1.

Table 2.1
Summary of Input Parameters for the Model

Hydrostratigraphy	Layer no.	Layer thickness (m)	Horizontal K [†] (m/s)	K anisotropy (H:V)	Specific storage (1/m)
Confined aquifer	1, 2, 3	40, 40, 40	1.0×10^{-5}	10	1×10^{-6}
Interburden	4, 5, 6, 7, 8	150, 300, 600, 300, 150	8.7×10^{-14}	100	1×10^{-5}
Upper reservoir	9, 10, 11	40, 40, 40	2.0×10^{-12}	100	1×10^{-6}
Shale[‡]	12, 13, 14	20, 20, 20	1.4×10^{-13}	1000	5×10^{-5}
Lower reservoir	15, 16	15, 15	2.1×10^{-12}	100	1×10^{-6}
SRV	-	-	8.2×10^{-11}	10	5×10^{-5}

[†]Values for interburden and reservoirs reduced to account for effects of partial saturation

[‡]Unfractured shale

The horizontal well is represented by a 1,500-m MODFLOW-2005 WELL boundary, centered vertically and laterally in the shale. Hydraulic fracturing is implemented as an instantaneous and uniform increase in horizontal permeability (7×10^{-19} to 4×10^{-16} m^2) and a decrease in vertical anisotropy (1000 to 10) in the stimulated reservoir volume (SRV) surrounding the horizontal well, followed by injection of 11,356 m^3 at formation temperature over 20 hours (a typical injection rate in Eagle Ford horizontals, see [Bazan et al. 2010; Martin et al. 2011]). The size of the hydraulically fractured network, the SRV, is established using pressure-diffusion equations (Shapiro and Dinske, 2009a; 2009b). The calculated SRV encompassed an area of 420,000 m^2 and height of 60 m (thickness of the shale). Detailed calculations of the extent and permeability of the SRV due to hydraulic fracturing are presented in Appendix B.2.

Saiers and Barth (2012) suggested hydraulic fracturing in stages may influence model results, therefore single- and multi-stage injections are tested. In single-stage, a single instantaneous permeability increase is followed by injection. The multi-stage modeling comprised twenty sequential permeability increases and injections (75 m each) along the length of the horizontal well. Because hydraulic-fracture growth is not simulated, increasing permeability in multiple stages is not expected to result in significant head differences compared to a single stage of increased permeability.

Flewelling and Sharma (2014) suggested that flowback and production affect flow within a hydraulically fractured shale. Flowback is simulated with a head-controlled flux (MODFLOW-2005 DRAIN) boundary at the horizontal well, which activates after injection stops. The DRAIN boundary was specified to remove 8% of the injected fluid (910 m^3) at surface elevation over seven days based on operator flowback data (Boschee 2014; RRC 2015a). Production of the horizontal well occurs after flowback, and is simulated by pumping 16 m^3/d (100 bbls/d) for two years followed by 3.2 m^3/d (20 bbls/d) for thirteen years, based on type-production curves for the Eagle Ford Shale (Alotaibi et al. 2015).

The converted well is simulated as a vertical well using the Multi-Node Well 2 (MODFLOW-2005 MNW2) Package (Konikow et al. 2009). The MNW2 Package was selected to simulate the converted well because it is capable of resolving complex intraborehole flow in multi-zone wells (Konikow and Hornberger 2006). The radius of the converted well is 0.07 m for accurate representation of production well-casings (5 ½" diameter). Simulations differed by varying the interval of the well screen, spatial proximity of the well to the hydraulic-fracturing injection location, and leaky-well

abandonment practices. Modeled scenarios are presented in Table 2.2. If the converted well is an abandoned production well, earlier hydraulic fracturing treatments could have resulted in a localized increase of permeability at the base of the converted well, or may suggest that the converted well is now intersected by a productive zone of fractures. For the converted well in this model, these potential effects were not considered. Abandoned wells are not considered in well-spacing requirements in Texas, and converted wells are considered to be abandoned wells. Lateral distances of 30 and 90 m from horizontal to vertical wells were selected as reasonable distances to consider. Two abandonment practices were considered: an open converted well and a mud-filled converted well. Open converted wells are abandoned oil and gas wells converted into water wells that are not plugged, and were studied because cases of open (unplugged) abandoned wells have been documented (e.g., RRC 2000). Open converted wells were simulated as nonpumping vertical wells, screened in the confined aquifer and a reservoir layer. Mud-filled converted wells were selected based on well records (RRC 2015a) and because abandonment with mud-laden fluid was historically an acceptable practice. Drilling muds used to backfill the simulated converted well have a fluid density of 1,140 kg/m^3, resulting in larger hydraulic heads at the base of the mud-filled converted well compared to the open converted well. Mud-filled converted wells were simulated as pumping wells, but drawdown was limited by the increased head at the base of the mud column. For both leaky-well scenarios, any barriers (e.g., packer) to flow in the wellbore are assumed to have failed.

Table 2.2
Explanation of Scenarios

Hydraulic fracturing[†]	**Description**	**Volume**	**Time**
Injection	Injection at horizontal well (WELL) in layer 13	(+) 11,356 m^3	20 hours
Flowback	Injection, followed by flowback (DRAIN)	(−) 910 m^3	7 days
Production	Injection, flowback, followed by production (WELL)	(−) 16 m^3/d; (−) 3.2 m3/d	2 years; 13 years
Leaky well[‡]		**Perforated Zone**	**Well Screen**
Open well	Nonpumping well (MNW2)	Upper reservoir (Austin Chalk)	Layers 3 and 11
Open well	Nonpumping well (MNW2)	Shale (Eagle Ford Shale)	Layers 3 and 13
Mud-filled well	Head-limited (2500 m) pumping well (MNW2)	Upper reservoir (Austin Chalk)	Layer 11
Mud-filled well	Head-limited (2510 m) pumping well (MNW2)	Shale (Eagle Ford Shale)	Layer 13

[†] Instantaneous change in K_h and K_v:K_h to form SRV occurs prior to injection

[‡] Leaky well simulations in shale conducted with and without hydraulic fracturing scenarios

Results and Discussion

Pre-injection, initial heads were established using the MODFLOW-2005 Link-AMG solver (Mehl and Hill 2001), and the model iteratively converged to a steady-state head distribution with 0% discrepancy. The layered structure of the model and horizontal gradient influence head distributions in the domain, consistent with flow regimes observed in young sedimentary basins such as the Western Gulf Basin (Magara 1978; Kreitler 1989; Harrison and Summa 1991). Flow in the confined aquifer is parallel to the direction of bedding. These initial steady-state heads in the interburden and reservoir layers have both vertical and horizontal flow components. Vertical fluid velocities through the interburden (5×10^{-5} cm/yr) are near the minimum range of simulated values for the region (Harrison and Summa 1991). Flows in the reservoirs were primarily horizontal, although there are vertical components. The majority of fluid discharged through the constant head boundary at the downgradient side of each layer. These initial model heads are appropriate for Eagle Ford Shale pressure data (Cander 2012). Horizontal and vertical flow between layers are presented in Table B.5. Transient model runs used initial conditions generated from this steady-state model.

Injection

Spatial distributions of heads show the effects of hydraulic fracturing occur primarily within the SRV within the model timeframe (Figure 2.4). Head changes propagate slowly from the horizontal well and small changes (0.1 m) were observed inside the boundary of the SRV and unfractured shale 15 years after injection. Peak heads and propagation are influenced by the volume and rate of injection, and lower volumes and slower rates of injection decrease peak heads resulting in slower propagation times after injection. Although this model excludes nonlinear pressure diffusion associated with fluid-rock interactions, analyses that consider such coupling show sharp pressure diffusion fronts with little pressure propagation beyond the hydraulically stimulated fractures (Shapiro and Dinske 2009a, 2009b).

Figure 2.5 plots observed heads at different distances from hydraulic fracturing in the SRV. Three curves illustrate head differences for each hydraulic fracturing scenario (i.e., injection, injection with flowback, and injection with flowback and production). Single-stage and multi-stage injection were compared by observing differences in modeled head at the horizontal well (Figures 2.5a and 2.5b). Head differences were minor between single- and multi-stage injections (< 1%), so single-stage injections were used for all subsequent model runs. Similarity between the two approaches is attributed to the method used to simulate hydraulic fracturing, low permeability of the shale, and relatively short timescale (hours) over which injection occurs. Shales with higher virgin permeability, or slower rates of hydraulic fracturing may require a multi-stage model for accurate simulation.

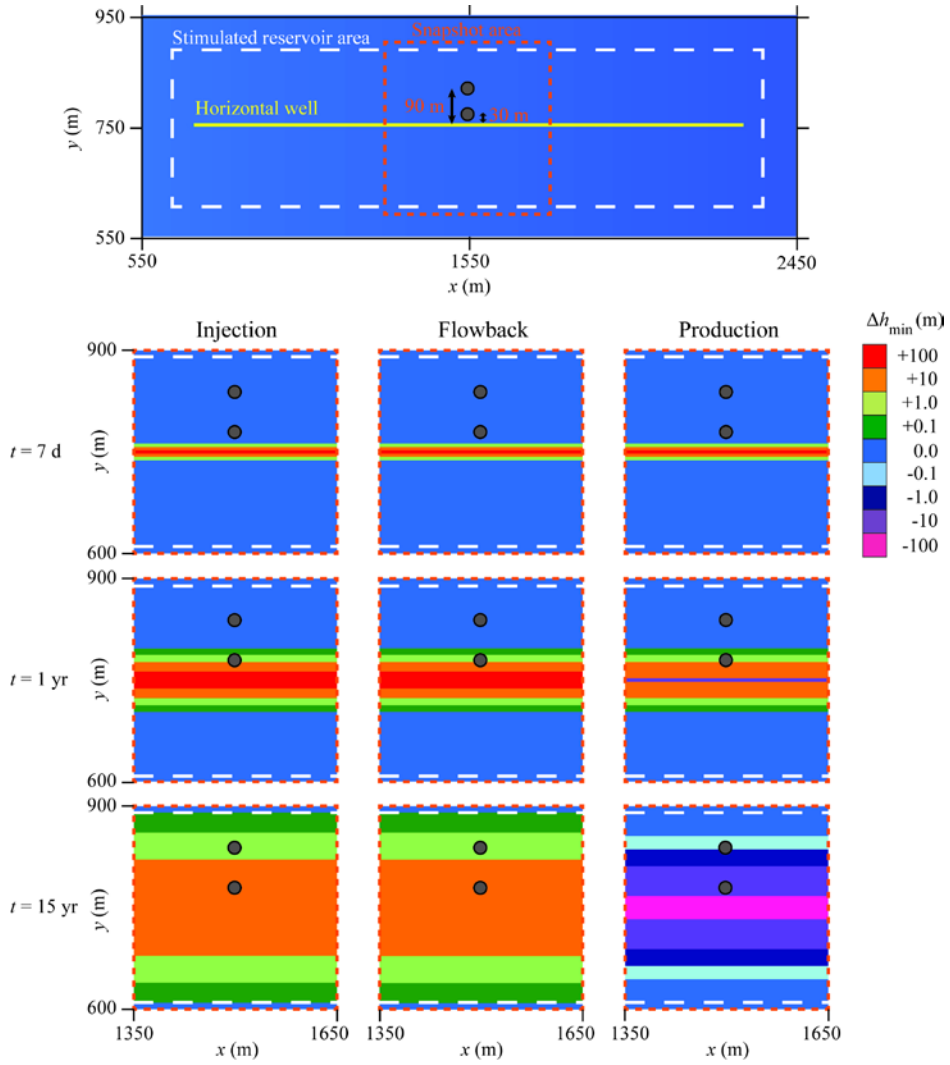

Figure 2.4. Spatiotemporal snapshots of simulated hydraulic heads near the horizontal well after seven days, one year, and 15 years under three hydraulic fracturing scenarios: (1) injection, (2) injection with flowback, and (3) injection with flowback and production. Hypothetical wells at 30 and 90 m from the horizontal well are shown for discussion purposes.

Maximum head changes were observed at time ~0 (the end of injection) (Figure 2.5a), and increased by 1,500 m at the horizontal well. Simulated heads resulting from hydraulic fracturing agree with pressures reported by Eagle Ford operators (typically 15 MPa above virgin reservoir pressure) and with previous studies (e.g., Shapiro and Dinske 2009a, 2009b). Maximum heads relaxed exponentially upon cessation of injection. Fifteen years after injection, simulated heads at the horizontal well were 54 m larger

(~2%) than initial heads. Head changes propagated laterally 30 m after 32 days, and peaked by 50 m seven years after injection (Figure 2.5c). Head changes propagated laterally 90 m after three years, and peaked at 4 m 15 years after injection (Figure 2.5d). Head changes observed in adjacent layers are shown in Figure B.3.

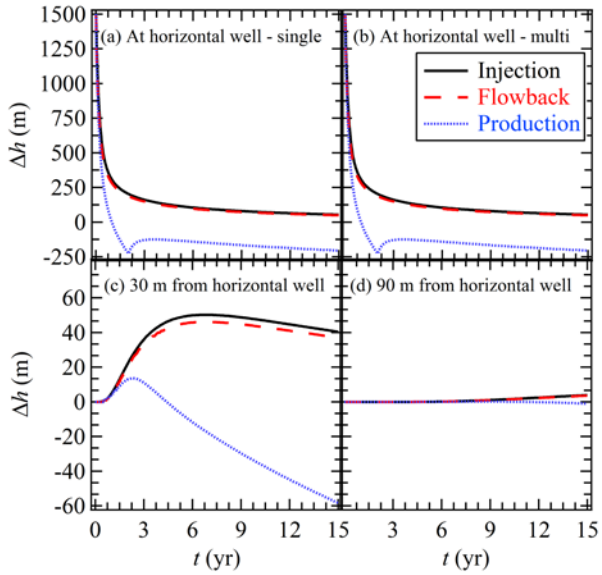

Figure 2.5. Simulated head changes (layer 13) for each hydraulic-fracturing scenario (i.e., injection, injection with flowback, injection with flowback and production): (a) Δh at the horizontal well when simulating single-stage hydraulic fracturing, (b) Δh at the horizontal well when simulating multi-stage hydraulic fracturing, (c) Δh at a lateral distance of 30 m from the horizontal well, and (d) Δh at a lateral distance of 90 m from the horizontal well.

Injection with Flowback

The addition of a seven-day flowback period reduced heads at the horizontal well, but flowback volumes were small compared to injection volumes and trends in heads were similar to injection without flowback. Approximately 910 m^3 (8% of the injected volume) of fluid were withdrawn during the flowback period at an average rate of 130 m^3/d. Eagle Ford well data (RRC 2015a) show that initial flowback rates (including hydrocarbons) vary between 100 and 200 m^3/d. At the end of the flowback period, heads decreased by 118 m at the horizontal well, compared to the injection-only simulation.

Flowback volumes in the Eagle Ford Shale are small (<15%) compared to other plays such as 15 to 40% for the Marcellus Shale (Boschee 2014). Larger flowback volumes would result in larger reductions in head after injection.

Injection with Flowback and Production

Simulation of production, after flowback, decreased heads at the horizontal well to nominal values after one year, and by an additional 200 m after 15 years (Figure 2.5). The effect of decreasing the production rate (16 to 3.2 m^3/d) after two years is evident (Figure 2.5a). The rate of head propagation from hydraulic fracturing is decreased by production (Figures 2.5c and 2.5d). Production reversed the hydraulic gradient, toward the horizontal well. Flow toward the well occurs within 30 m at five years, which grows to 140 m after 15 years. These observations are consistent with other Eagle Ford reservoir simulations. Honarpour et al. (2012) noted pressure changes less than 30 m from hydraulic fractures after five years of pumping.

Hydraulic Fracturing and Model Results

Fractures are quickly generated in the shale to form the SRV during hydraulic fracturing. Porosity versus depth relationships indicate that matrix porosity in shale is low (1 to 10%) and any flow outside of fractures, even within the SRV, would occur over long timescales. The porosity of the proppant pack is higher (~35%) due to the presence of sand-sized proppant, and fluids used during hydraulic fracturing would likely remain near or within the fractures. In contrast to fluid propagation, head propagation occurs over shorter timescales and greater distances, potentially mobilizing *in-situ* reservoir

fluids (e.g., oil, gas, brine). But, changes in permeability are bounded by the horizontal and vertical extent of the SRV and potential contaminants would be unlikely to migrate rapidly outside of this area.

Characteristics of hydraulically generated fractures correspond to changing stress fields and vary according to the brittleness and plasticity of lithofacies. Plastic shales (e.g., Eagle Ford Shale) tend to generate simple, linear fractures compared to more brittle shales (e.g., Barnett Shale), which produce highly complex fracture networks (Mayerhofer et al. 2010). Hydraulic-fracture permeability can range as high as 8×10^{-11} m^2 (Bazan et al. 2010; Chaudhary et al. 2011) and the enhanced matrix permeability (i.e., SRV permeability) varies orders magnitude (2×10^{-19} to 8×10^{-14} m^2) depending on the geometry of the fracture network (Bazan et al. 2010; Chaudhary et al. 2011; Honarpour et al. 2012; Suliman et al. 2013). This model represents the fracture network with a 585-fold increase in matrix permeability and decreased anisotropy (K_h:K_v) from 1000 to 10. Resulting heads are similar to pressures reported by operators and previous studies (e.g., Shapiro and Dinske 2009a, 2009b; RRC 2015a). Heads decreased with distance from the horizontal well and the majority of the flow was lateral, rather than vertical, in contrast to the results from Myers (2012). Lateral flow could represent a greater risk for upward leakage through abandoned wells because the lateral area of influence is larger than the vertical. Although the SRV is not completely fractured, a “frac hit” – a direct connection of a hydraulic fracture to a nearby well during hydraulic fracturing – could initiate upward leakage. Frac hits are not uncommon between two producing horizontal wells, and are predicted to increase as infill drilling proceeds (Lawal et al. 2013). Abandoned vertical wells that were previously hydraulically fractured may be more prone to frac hits

due to the increased density of fractures (either stimulated or natural) near the perforated interval.

Leaky Well without Hydraulic Fracturing

Leaky well simulations without nearby hydraulic fracturing were conducted to quantify leakage in unfractured shale and a conventional reservoir. Head differences between the reservoirs and the confined aquifer indicated that fluids should flow from the reservoirs through the lower screen into the leaky converted well and discharge through the upper screen into the confined aquifer and this scenario was modeled. The natural vertical hydraulic gradient between reservoirs and the confined aquifer ranged from 0.19 to 0.17.

Simulations of leaky wells screened in all reservoirs showed that volumetric flow rates (flow) decreased steadily over time, and larger volumes flowed through open converted wells than through mud-filled converted wells (Figure 2.6a). Cumulative volumes into the leaky well screened in the Austin Chalk ranged from 1.4 to 10 m^3 after 15 years, depending on abandonment scenario. Flow through the leaky well in the Austin Chalk averaged 2.4×10^{-3} m^3/d for open converted wells, and 3.3×10^{-4} m^3/d for mud-filled converted wells. Cumulative volumes into the leaky well screened in unfractured Eagle Ford Shale ranged from 0.08 to 0.8 m^3 after 15 years (Figure 2.6a). Flow through the leaky well in the Eagle Ford Shale averaged 1.4×10^{-4} m^3/d for open converted wells, and 1.4×10^{-5} m^3/d for mud-filled converted wells. Flow through leaky wells without hydraulic fracturing are shown in Figure B.4.

Differences in flow are primarily related to reservoir permeability, screen interval, and vertical hydraulic gradient. Intrinsic permeability of the Eagle Ford Shale is 14-fold lower than the Austin Chalk. Differences in hydraulic head, driven by overpressured reservoir conditions, create a vertical hydraulic gradient that drives upward flow through the converted well. Overpressured reservoirs are generally associated with low-permeability sediments, such as shale, while higher-permeability conventional reservoirs (i.e., Austin Chalk) are less likely to be overpressured.

Abandoned producing wells are completed (i.e., cased) and perforated into the target reservoir (RRC 2000), providing a direct pathway for upward flow. However, abandoned production wells may have been affected by previous hydrocarbon production, which decreased reservoir pressure, potentially changing the magnitude and direction of the vertical hydraulic gradient. Sustained upward flow along abandoned producing wells could exist if the reservoir was originally overpressured and minimal production occurred (e.g., uneconomical quantities of hydrocarbons produced). Original reservoir pressures are more likely to be preserved in abandoned unsuccessful (dry) wells which could provide a pathway for upward flow. However, unsuccessful wells are not completed (i.e., cased) and not perforated in the target reservoir.

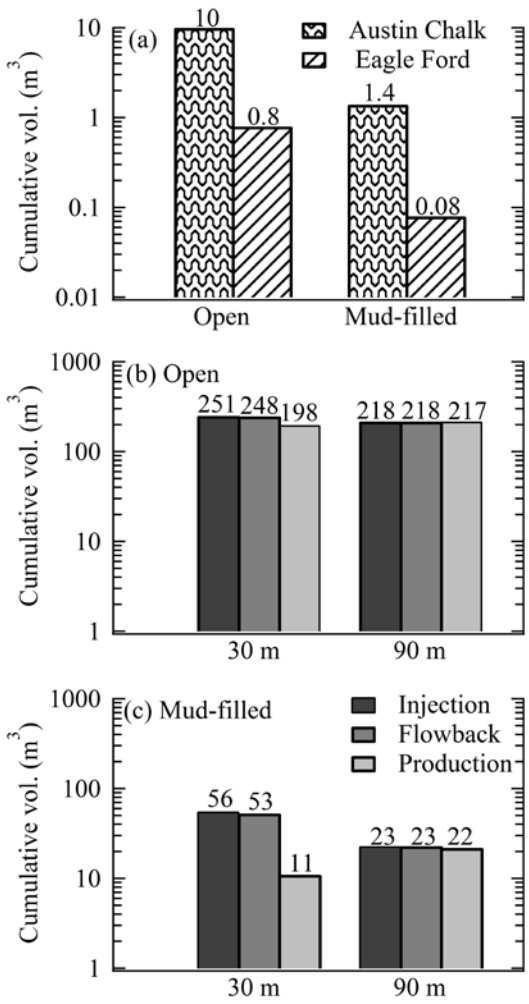

Figure 2.6. The 15-year total volume discharged through a leaky well into the shallow aquifer: (a) without hydraulic fracturing for an open or mud-filled leaky well screened in the upper reservoir (Austin Chalk) or shale (Eagle Ford Shale), and with hydraulic-fracturing scenarios (i.e., injection, injection with flowback, and injection with flowback and production) for (b) open and (c) mud-filled leaky wells at lateral distances of 30 and 90 m from the horizontal well.

Leaky Well with Hydraulic Fracturing

We performed simulations of hydraulic fracturing near leaky wells screened in the shale, where the largest head changes and highest density of fractures exist. If hydraulic fractures extend into nearby conventional reservoirs, leaky wells could be impacted but overall reservoir permeability would change little, and results would be similar to the

leaky-well scenarios without hydraulic fracturing. Leaky wells screened in unfractured shale (e.g., outside the SRV) would also exhibit flow similar to scenarios without hydraulic fracturing because virgin shale permeability limits propagation of heads generated during hydraulic fracturing.

Figure 2.7 shows flow through a leaky well at different distances from hydraulic fracturing in the SRV. Three curves illustrate flow differences for each hydraulic-fracturing scenario (i.e., injection, injection with flowback, and injection with flowback and production). Hydraulic fracturing resulted in an initial increase of upward flow through all leaky wells by orders of magnitude (more than a factor of 500) compared to scenarios without hydraulic fracturing. Flow through the open converted well at 30 m steadily decreased from 8.6×10^{-2} to 4.2×10^{-2} m^3/d after fifteen years for injection and flowback scenarios (Figure 2.7a). Simulated production after flowback reduced flow through the open converted well to 2.7×10^{-2} m^3/d after 15 years. Cumulative volumes through the open converted well at 30 m totaled between 251 and 198 m^3 after 15 years (Figure 2.6b). Flow through the open converted well at 90 m decreased from 8.6×10^{-2} to 3.7×10^{-2} m^3/d after 15 years for injection and flowback scenarios (Figure 2.7b). The addition of production reduced flow through the open converted well at 90 m to 3.6×10^{-2} m^3/d after 15 years. The open converted well at 90 m showed less variation between hydraulic-fracturing scenarios than the open converted well at 30 m, and cumulative volumes were between 217 and 218 m^3 after 15 years (Figure 2.6b). The similarity between hydraulic-fracturing scenarios for the 90-m well is due to the longer times required for the effects of production to be significant.

Simulations of mud-filled converted wells showed increased sensitivity to head changes, but overall less flow than open converted wells (Figures 2.7c and 2.7d). Flow through the mud-filled converted well at 30 m initially decreased exponentially (up to 0.5 yr) after the change in shale properties, then increased rapidly due to elevated heads from hydraulic fracturing (Figure 2.7c). Flow through the mud-filled converted well at 30 m ranged between 4.9×10^{-3} to 1.2×10^{-2} m^3/d for injection and flowback scenarios. Including production showed a significant influence on upward flow through the 30-m mud-filled converted well, and leakage essentially ceased after seven years. Cumulative volumes through the mud-filled converted well at 30 m were between 11 and 56 m^3 after 15 years (Figure 2.6c). Reagan et al. (2015) found that upward flow due to hydraulic fracturing stopped upon production. Flows through the leaky well in this model are within the range of upward flows in the shale reservoir reported by Reagan et al. (2015). Flow through the mud-filled converted well at 90 m first decreased for 6.5 years, then slowly increased during injection and flowback scenarios (Figure 2.7d). Flow through the mud-filled converted well at 90 m increased from a minimum of 3.9×10^{-3} m^3/d at 6.5 years, to 4.3×10^{-3} m^3/d after 15 years for injection and flowback scenarios. Including production steadily decreased flow through the mud-filled converted well at 90 m to 3.5×10^{-3} m^3/d after 15 years. There was little variation between hydraulic-fracturing scenarios for the mud-filled converted well at 90 m, and cumulative volumes were between 22 and 23 m^3 after 15 years (Figure 2.6c).

Leaky wells in the shale were influenced by hydraulic fracturing if located within the SRV. Outside of the SRV, the low-permeability of unfractured shale limited upward flow. Because permeability increased uniformly throughout the SRV, volumetric flow

rates potentially represent upper limits if a hydraulic fracture does not intersect the leaky well. Leaky abandoned wells that were backfilled with mud transmitted less fluid to the overlying aquifer compared to those left open because the larger head at the base of the mud-filled well decreased the vertical gradient.

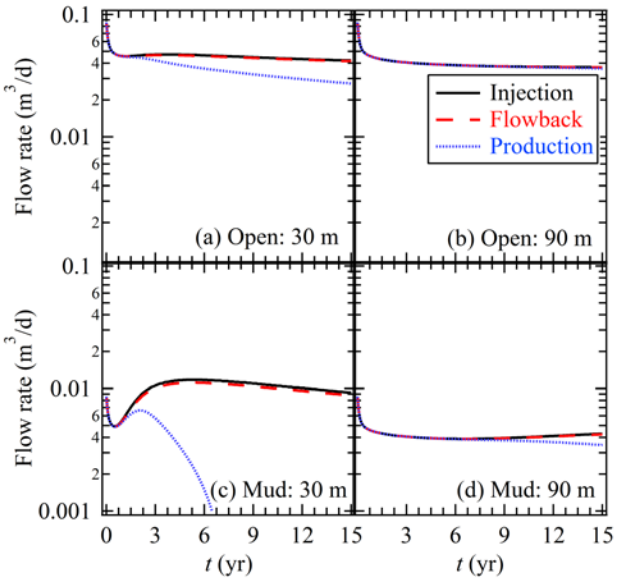

Figure 2.7. Simulated upward flow through a leaky well located within the SRV for each hydraulic-fracturing scenario (i.e., injection, injection with flowback, and injection with flowback and production): open leaky well at lateral distances of (a) 30 m and (b) 90 m from the horizontal well, and a mud-filled leaky well at lateral distances of (c) 30 m and (d) 90 m from the horizontal well.

Leaky wells connected to the SRV pose the largest risk because of increased flow related to the hydraulic-fracturing process. Although chemical detection of leakage may be difficult due to low volumetric flow rates, long-term cumulative volumes are a potential concern. Upward flow through leaky wells can also occur naturally, unrelated to hydraulic fracturing.

Flows into leaky wells do not conclusively demonstrate that contaminants from the fractured shale reservoir can migrate into the overlying aquifer because hydraulic characteristics of the well may limit migration. Contaminants would have to diffuse

through or displace the thick column of native borehole fluid. Gas-phase contaminants could diffuse through borehole materials in leaky wells at higher rates due to greater density differences. Mud-filled converted wells inhibit upward contaminant migration from the reservoir because the thick column of mud extends from the reservoir to the base of the overlying aquifer. Moreover, displacement of muds into the confined aquifer could temporarily plug pore spaces outside the well screen in the confined aquifer, decreasing potential flow into the aquifer. If an unsealed leaky well is located close to a horizontal well, hydraulic-fracturing pressures (10 to 15 MPa) are large enough to "blow out" borehole fluids through the top of the leaky well. Upward flow through a leaky well could be enhanced after a blow out if seals were disrupted, or decreased if borehole muds clogged pore space in the aquifer.

Conclusions

Leaky wells near hydraulic fracturing could facilitate upward migration of fluids over shorter timescales compared to natural geological pathways. Each sedimentary basin is unique, and evaluation of leaky wells as potential pathways for contaminants requires critical review of historical oil and gas activities. Certain abandoned wells, such as leaky converted wells, represent potential conduits for upward flow to aquifers because they are open to both a deep formation and an overlying aquifer. However, upward flow to an overlying aquifer due to hydraulic fracturing of shale requires a unique series of circumstances. Simulations of hydraulic fracturing and leaky wells revealed the following:

- Upward flow through leaky wells is influenced by both fluid pressures and corresponding generation of fractures from hydraulic fracturing. Frac hits represent a plausible mechanism for initiating upward leakage through leaky abandoned wells.
- Leaky abandoned wells located close to horizontal wells can experience large upward flows, but flowback and production in the horizontal well reduce or completely inhibit upward leakage. Leaky abandoned wells located far from horizontal wells exhibit smaller upward flows, but may experience greater cumulative leakage if the effects of production do not reach the leaky well.
- Natural upward flow, unrelated to hydraulic-fracturing operations, could occur through leaky wells either inside or outside of the SRV.
- Several factors are critical in controlling upward flow through leaky wells near horizontal wells including: (1) permeability and virgin pressure of the shale, (2) production at the horizontal well, and (3) abandonment method for the leaky well.

In summary, this paper examines a newly considered potential mechanism for upward flow to shallow aquifers overlying unconventional shale plays. The methods and results of this study are applicable to other unconventional shale plays where similar leaky abandoned wells exist.

Acknowledgement

Funding for this work was provided by the Evergreen Underground Water Conservation District, the Wintergarden Groundwater Conservation District, and the C. Gus Glasscock

Jr. Endowed Fund for Excellence in Environmental Sciences. The comments and suggestions from the four anonymous reviewers improved this paper significantly and were greatly appreciated.

CHAPTER THREE

Spatial Risk Analysis of Hydraulic Fracturing near Abandoned and Converted Oil and Gas Wells

This chapter was published as Brownlow, J.W., J.C. Yelderman, Jr., and S.C. James. 2016. Spatial risk analysis of hydraulic fracturing near abandoned and converted oil and gas wells. Groundwater. dx.doi.org/10.1111/gwat.12471

Abstract

Interaction between hydraulically generated fractures and existing wells (frac hits) could represent a potential risk to groundwater. In particular, frac hits on abandoned oil and gas wells could lead to upward leakage into overlying aquifers, provided migration pathways are present along the abandoned well. However, potential risk to groundwater is relatively unknown because few studies have investigated the probability of frac hits on abandoned wells. In this study, actual numbers of frac hits were not determined. Rather, the probability for abandoned wells to intersect hypothetical stimulated reservoir sizes of horizontal wells was investigated. Well data were compiled and analyzed for location and reservoir information, and sensitivity analyses were conducted by varying assumed sizes of stimulated reservoirs. This study used public and industry data for the Eagle Ford Shale play in south Texas, with specific attention paid to abandoned oil and gas wells converted into water wells (converted wells). In counties with Eagle Ford Shale activity, well-data analysis identified 55,720 abandoned wells with a median age of 1983, and 2,400 converted wells with a median age of 1954. The most aggressive scenario resulted in 823 abandoned wells and 184 converted wells intersecting the largest assumed stimulated reservoir size. Analysis showed abandoned wells have the potential to be

intersected by multiple stimulated reservoirs, and risks for intersection would increase if currently permitted horizontal wells in the Eagle Ford Shale are actually completed. Results underscore the need to evaluate historical oil and gas activities in areas with modern unconventional oil and gas activities.

Introduction

Hydraulic fracturing of shale has generated concern regarding risks to groundwater. Natural and anthropogenic features have been suggested as potential transport pathways from shale to overlying (shallower) aquifers (Vengosh et al. 2014). Compared to natural features, anthropogenic features such as abandoned oil and gas wells are more likely to act as continuous pathways to overlying aquifers and could facilitate upward migration of fluids over shorter timescales (Dusseault and Jackson 2014). Numerical models have considered the potential for abandoned wells to act as leakage pathways to shallower aquifers (Reagan et al. 2015; Brownlow et al. 2016). However, risks of potential groundwater impacts are not well understood because few studies have investigated the probability for such an event.

Hydraulic fracturing could pose a risk to groundwater if hydraulic-fracturing fluids or formation fluids (e.g., oil, gas, brine) migrate upward into shallower aquifers. One concern over hydraulic fracturing is the potential for a “frac hit” on abandoned oil and gas wells (Figure 3.1). Frac hits occur when hydraulically generated fractures intersect an existing well or a pathway intersecting an existing well. Following a frac hit on an abandoned well, upward leakage to an overlying aquifer may or may not occur depending on the hydraulic characteristics of the abandoned well. Fluid migration to

overlying aquifers requires the presence of both a driving force and a pathway along the abandoned well (Flewelling and Sharma 2014). Frac hits are not uncommon between two producing horizontal wells, and are predicted to increase as infill drilling proceeds (Lawal et al. 2013). Increased abundance or density of pre-existing discontinuities (e.g., fractures) that intersect abandoned wells could increase the probability of a frac hit, and may be natural or the result of previous hydraulic-fracturing treatments. If upward leakage along an abandoned well does occur after a frac hit, leakage may be reduced or stop over time due to production from the horizontal well (Reagan et al. 2015; Brownlow et al. 2016). However, fracture width decreases as a function of fracture length during hydraulic fracturing, and can result in poorly producing fractures further away. This effect is commonly referred to as fracture decay (Tran et al. 2013) and could diminish the potential beneficial effect of production following a frac hit on an abandoned well.

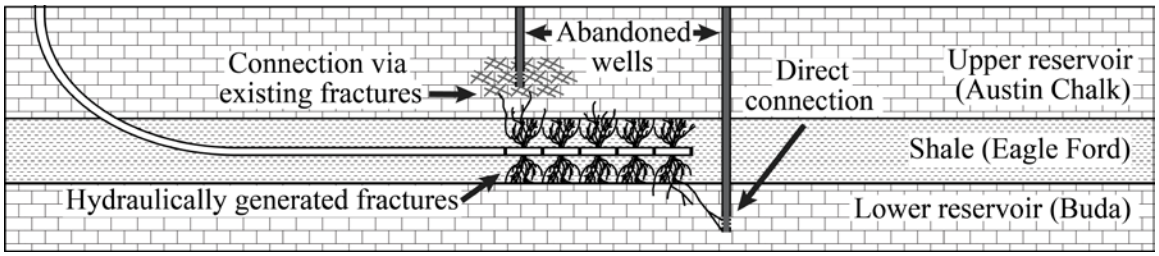

Figure 3.1. Schematic of frac hits on abandoned wells.

Although hydraulic fracturing has the potential to interact with abandoned oil and gas wells, assessing the risk of upward leakage following a frac hit is a complex task due to variable field practices, regulatory requirements, materials, and subsurface conditions; often unique to each well (Nordbotten et al. 2005). Because these issues have evolved over time, the risk of leakage depends on the age and abandonment technique associated with a particular well. The risk for potential leakage is highest in mature sedimentary

basins where historical oil and gas exploration and production have resulted in a high spatial density of abandoned wells (Gasda et al. 2004; Nordbotten et al. 2005). For example, in mature basins considered for geologic carbon storage, abandoned wells are thought to represent the single largest risk for CO_2 leakage (Gasda et al. 2004; Nordbotten et al. 2004; Nordbotten et al. 2005). Because geographic areas of oil and gas activity often overlap, abandoned oil and gas wells can be in close horizontal and vertical proximity to modern hydraulic-fracturing operations. Continued hydraulic fracturing in mature basins could result in increased numbers of frac hits on abandoned oil and gas wells over time as the spatial density of both horizontal and abandoned wells increases.

The probability of hydraulic fracturing interacting with an abandoned oil and gas well depends upon well location as well as the depth of the horizontal well, length of hydraulic fractures, depth of the abandoned well, and presence of pre-existing discontinuities (e.g., faults) (Montague and Pinder 2015). Thus, practical assessment of frac hits on abandoned wells, and potential upward leakage along an abandoned well after a frac hit, requires assessment of spatial and hydraulic information for both horizontal and abandoned wells. Proper assessment of spatial information requires a high-quality database and appropriate measures to quantify spatial distributions and patterns (Gasda et al. 2004). Hydraulic information can be unique to each well, and proper assessment requires extensive analysis of multiple factors such as the age, materials, and practices associated with a particular well (Gasda et al. 2004). Evaluation of spatial and hydraulic characteristics for certain abandoned oil and gas wells, such as those converted into water wells (converted wells) is cause for increased concern because converted wells can be

perforated in both the hydrocarbon reservoir and the overlying aquifer (Brownlow et al. 2016).

This study used historical data and spatial modeling to characterize potential risk for frac hits on abandoned and converted oil and gas wells. The potential for frac hits was characterized by investigating the probability that abandoned or converted oil and gas wells intersect an assumed stimulated reservoir size surrounding hydraulically fractured horizontal wells. The intersection of an abandoned oil and gas well with the assumed stimulated reservoir does not mean that the abandoned well has definitely experienced a frac hit, but does indicate the potential. Public and industry data for wells were collected, classified, and integrated using a Geographic Information System (GIS). Well data were analyzed for spatial location and reservoir information to develop spatial distributions in three-dimensions. Sensitivity analyses for the number and locations of potential frac hits were conducted by varying the assumed horizontal extent of the stimulated reservoir area (SRA) assigned to horizontal wells. A simple statistical analysis estimated the potential number and locations of abandoned and converted oil and gas wells that intersect the assumed SRA of horizontal wells. The study focused on the unconventional Eagle Ford Shale play in south Texas because it is exemplary of a mature sedimentary basin with data available for both abandoned and converted oil and gas wells.

Problem Background

Historical practices are important to consider when evaluating frac hits on abandoned oil and gas wells from hydraulic fracturing of shale. Historical oil and gas exploration practices may have resulted in abandoned wells completed in shale or

reservoirs adjacent to shale, within proximity to modern hydraulically generated fractures (Figure 3.2). Historical oil and gas exploration practices may also have resulted in abandoned wells completed in zones with natural discontinuities (e.g., fractures), which may increase susceptibility to frac hits. Similarly, historical oil and gas well-completion practices such as hydraulic fracturing may also result in increased susceptibility to frac hits.

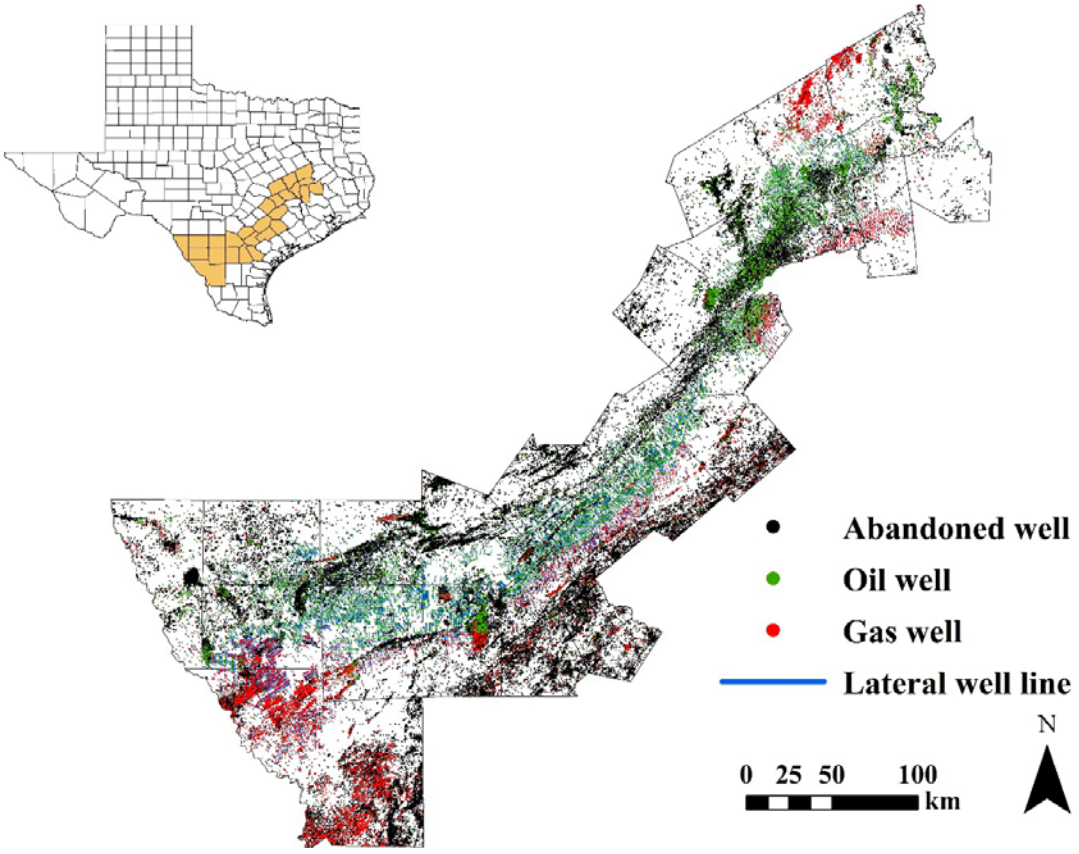

Figure 3.2. Abandoned and producing oil and gas wells across 26 Texas Counties with existing and permitted Eagle Ford Shale horizontal wells.

Following a frac hit, potential upward leakage along abandoned oil and gas wells is governed by the hydraulic characteristics of the abandoned well. Arguably, the most important control on hydraulic characteristics of abandoned oil and gas wells are plugging operations. Modern regulatory requirements for plugging abandoned oil and gas

wells are strict and typically require multiple plugs of recirculated cement (e.g., RRC 2000). Hydraulic characteristics of wells abandoned prior to modern regulations can vary broadly. Prior to current requirements, plugging materials sometimes consisted of brush, wood, paper sacks, or any other material that could be pushed into a well (Ide et al. 2006; Arthur and Hochheiser 2011). Historically, the most common material used to plug abandoned wells in the United States is drilling mud, whose weight and gel strength inhibit upward flow of reservoir fluids (Arthur and Hochheiser 2011). Other practices, such as conversion of abandoned oil and gas wells into water wells, are cause for increased concern regarding potential leakage to overlying aquifers. In the modern era of hydraulic fracturing, the abandonment technique can be a critical component when evaluating potential for upward leakage to an overlying aquifer potentially associated with frac hits.

Example: Eagle Ford Shale Play

The first modern unconventional Eagle Ford Shale (EFS) well was drilled in 2008 and the play has since expanded to include 52,000 km^2 across 26 Texas counties. Stratigraphically, the EFS is bound disconformably above by the Austin Chalk Group, and disconformably below by the Buda Formation or Woodbine Group. Economic production from the EFS requires a combination of laterally extensive (>1,500 m) horizontal wells and (15 to 20) multi-stage hydraulic fracturing runs (Martin et al. 2011). By 2015, approximately 11,460 EFS oil and gas wells had been completed (RRC 2016a). The potential number of EFS horizontal wells has been estimated from 20,000 to 100,000 in a fully mature play (Brownlow 2010; Nicot et al. 2011).

Since at least the 1920s, conventional wells have been drilled into the EFS and adjacent reservoirs (Stapp 1977). The overlying Austin Chalk reservoir is historically a prolific oil and gas play and has been drilled since the 1930s. Production from the Austin Chalk play has primarily occurred in 19 Texas counties, most of which overlap geographically with the modern EFS play (Scott 1977; Stapp 1977). Early exploration strategies (1930s to mid-1970s) involved targeting fracture-rich zones with vertical boreholes (Scott 1977; Stapp 1977). In the late-1970s, completion of vertical Austin Chalk wells with hydraulic fracturing significantly increased productivity, and by 1991 over 7,000 vertical wells had been drilled into the Austin Chalk (EIA 1993). Historical records suggest that vertical Austin Chalk wells were typically drilled to the base of the formation, and some were drilled deeper into the underlying EFS and Buda Formation. Similarly, advancements in logging-while-drilling systems combined with horizontal drilling in the 1980s allowed operators to connect multiple fracture systems with a single wellbore, resulting in drainage of larger areas and higher production rates (Shelkholeslami et al. 1991). By 1991, more horizontal wells (~5,000) had been drilled in the Austin Chalk than the rest of the world combined (Shelkholeslami et al. 1991). Economical long-term production has been a challenge for Austin Chalk production, and many thousands of wells have been abandoned over the years (Haymond 1991; EIA 1993).

Regulatory Environment

Oil and gas activity in Texas is regulated by the Texas Railroad Commission (RRC) according to “field” rules. Oil and gas fields consist of single or multiple

reservoirs related to the same individual geological condition (EIA 2016). Oil and gas fields may be subject to field-specific rules (e.g., well density, well-well spacing) that vary depending on reservoir pressure and production characteristics.

The RRC approves proposed oil and gas wells if they pass an administrative review of whether they meet applicable oil and gas field rules. Well-well regulatory spacing requirements typically only consider active wells completed in the same oil and gas reservoir as the proposed well. Abandoned wells completed in the same reservoir as a proposed well, or active wells completed in different reservoirs, are generally not considered from a regulatory perspective. These rules were not designed to consider potential frac hits on abandoned oil and gas wells or on wells completed in a deep hydrocarbon reservoir that have been converted into a water well. Hydraulic fracturing is allowed to take place in close areal and vertical proximity to abandoned wells, even with similar completion depths or depths greater than the shale reservoir. In addition, leakage factors such as age, abandonment technique, or conversion of an abandoned well into a water well are not considered. Historical and regulatory well-abandonment practices should be considered when evaluating the potential for leakage in the context of modern hydraulic-fracturing operations.

Methods

Data Collection

Available records for existing and permitted wells within the EFS play (26 counties) were collected from the RRC Digital Map Data and API Well Database (RRC

2015b). The 26 counties selected for this study include: Atascosa, Bastrop, Bee, Brazos, Burleson, DeWitt, Dimmit, Fayette, Frio, Gonzales, Grimes, Karnes, La Salle, Lavaca, Lee, Leon, Live Oak, Madison, Maverick, McMullen, Milam, Robertson, Walker, Webb, and Zavala. Digital Map Data include information for over 1.1 million wells across Texas, such as surface location, location reliability, and well type (e.g., oil, gas). The API Well Database provides additional information such as field (reservoir), depth, and plugging date. Data for converted wells were collected from online RRC databases (RRC 2016b, 2016c), the Texas Water Development Board (TWDB) online well database (TWDB 2016), and from local groundwater conservation districts (GCDs). Identification of converted wells in the RRC database required review of online records to determine if relevant forms (Form P-13: Application to Condition an Abandoned Well for Fresh Water Production) were electronically filed. The absence of an electronically filed P-13 form does not necessarily indicate that a conversion was not performed.

The following information was compiled from databases for each well depending upon availability: API well number, surface coordinates, bottom-hole coordinates, well type, field, depth, completion date, and plugging date. Unfortunately, information is often sparse and in many cases only surface location is documented (Nicot 2009). Wells with missing information were reviewed individually by cross-referencing API well numbers in available online records in an attempt to fill in missing information (RRC 2016b, 2016c). Wells with multiple sources of information were joined into a master record.

Data Classification

The review of individual well records indicated that well-depth data were sparse and unreliable. For example, some well depths were recorded significantly shallower than the listed depth of the reservoir produced by the well. Field data were more reliable and used as a proxy for well depth. Each field refers to a specific reservoir(s), located at the completion depth for the well. Reservoirs were determined for each abandoned well using field names from the Energy Information Administration oil and gas field master list (EIA 2016) and RRC records (RRC 2015b, RRC 2016b, 2016c). Reservoirs for converted wells were estimated by history matching with nearby abandoned oil and gas wells. When multiple field names existed for a well, multiple reservoirs were listed.

Six well groups were defined using well-type information: (1) existing EFS wells, (2) permitted EFS wells, (3) abandoned wells, (4) deep abandoned wells, (5) converted wells, and (6) deep converted wells. The abandoned well group consisted of dry wells, plugged oil, gas, and oil/gas wells. Other well types (e.g., shut-in, injection, storage, observation) were excluded from the abandoned well group unless records indicated that the well was plugged. The deep abandoned well group is a subset of the abandoned well group and consisted of abandoned wells with reservoirs listed as Austin Chalk or deeper. The converted well group consisted of oil and gas wells converted into water wells. The deep converted well group is a subset of the converted well group and consisted of converted wells interpreted to penetrate the Austin Chalk or deeper reservoirs.

GIS Analysis

A GIS managed, manipulated, and analyzed all data for each well group. Well surface and bottom-hole locations were entered into the GIS as points. Vertical wells are assumed straight. Horizontal and directional wells were mapped as lines connecting surface and bottom-hole locations.

Stimulated Reservoir Area

The horizontal extent of the fracture network generated during hydraulic fracturing in two-dimensions is defined as the SRA, which is approximated using an analytical solution for pore pressure diffusion in a homogenous anisotropic poroelastic medium (Shapiro et al. 1997; Yu and Aguilera 2012). The pressure-propagation distance is assumed to represent the hypothetical maximum horizontal extent of hydraulically generated fractures. In practice, hydraulic fractures rarely exceed and are often shorter than calculated pressure-propagation distances (Yu and Aguilera 2012). The analytical estimate of the symmetric hydraulic-fracture half-length in the horizontal is (Yu and Aguilera 2012):

$$L_{\mathrm{f}} = \mathrm{erfc}^{-1}\left(\frac{\Delta P_{\mathrm{trg}}}{\Delta P_{\mathrm{inj}}}\right)\sqrt{4\eta_x t}\,, \qquad \text{(Eq. 3.1)}$$

where ΔP_{trg} [MPa] is the minimum pressure difference required to trigger microseismic events, ΔP_{inj} [MPa] is the overall pressure difference induced by fluid injection, η_x [m^2/s] is the x-component of hydraulic diffusivity, and t [s] is injection time. Both ΔP_{inj} and η_x are estimated from hydraulic-fracturing pressures and microseismic data for the EFS (Bazan et al. 2010; Basu et al. 2012; Suliman et al. 2013; RRC 2016c). Estimation of

ΔP_{trg} requires detailed geomechanical analyses, but previous studies suggest a range of between 3 and 50 kPa (Ferreira et al. 1995; Shapiro et al. 1997). Here, we assume ΔP_{trg} = 0.03 MPa, ΔP_{inj} = 15 MPa, η_x = 1.3 m^2/s, and t = 4 h, which yields L_f = 600 m, an acceptable value for the upper limit of the horizontal extent of a hydraulic fracture or microseismic event based on previous studies (Bazan et al. 2010; Mayerhofer et al. 2010; Zimmer 2011; Basu et al. 2012; Yu and Aguilera 2012; Suliman et al. 2013).

Potential Frac-hit Density

If the reservoir is known, the intersection between a vertical well and a stimulated reservoir can be estimated with a two-dimensional approach. This approach was implemented in GIS by defining a rectangular area around each horizontal well to represent the SRA (Figure 3.3). Sensitivity analyses were conducted by varying L_f from 30 to 600 m in 30-m increments around horizontal wells. Potentially affected wells are defined as the number of abandoned or converted wells that intersect an SRA. Potential frac hits are defined as the number of SRAs that intersect abandoned or converted wells. Potential frac-hit density was computed using a kernel density estimation method. In this method, a circular area defined by a kernel function is placed over each potentially affected well resulting in a smooth and continuous density surface. A grid of 1-km^2 cells is overlain onto the study area and the density in each cell is estimated by summing the overlapping density surface from each potentially affected well. With x_j being a location vector over the study area and $x_1 ... x_n$ the location vectors of the n sampling points, the density estimation in x_j is (Silverman 1986):

$$\hat{f}_h(x_j) = \sum_{i=1}^{n} \frac{1}{h^2} W_i K\left[\frac{\left(x_j - x_i\right)}{h}\right], \qquad \text{(Eq. 3.2)}$$

where K is the kernel function, h is a smoothing parameter commonly referred to as the bandwidth, W_i is the weight, and $d_{ij} = x_j - x_i$ is the distance between point x_j and the event n_i. Here, we assume h = 10 km. Abandoned wells could be affected by multiple hydraulic-fracturing events, depending on whether the well intersects multiple SRAs, or if more than one stage in an SRA interacts with the well. Therefore, each observation is weighted (W_i) by the number of SRAs that intersect an abandoned well. This weighting approach assumes only one hydraulic-fracturing stage from each SRA can interact with an abandoned well. The kernel function was specified as the quartic function (Silverman 1986):

$$K(x_i) = \begin{cases} \frac{1}{3\pi}(1-t^2)^2 & t^2 < 1 \\ 0 & t^2 \geq 1 \end{cases}, \qquad \text{(Eq. 3.3)}$$

where $t = d_{ij}/h$. The value at each grid point j a distance d_{ij} from the event n_i is the sum of the individual kernel functions, $K(x_i)$, of the point belonging to bandwidth h (Produit et al. 2010).

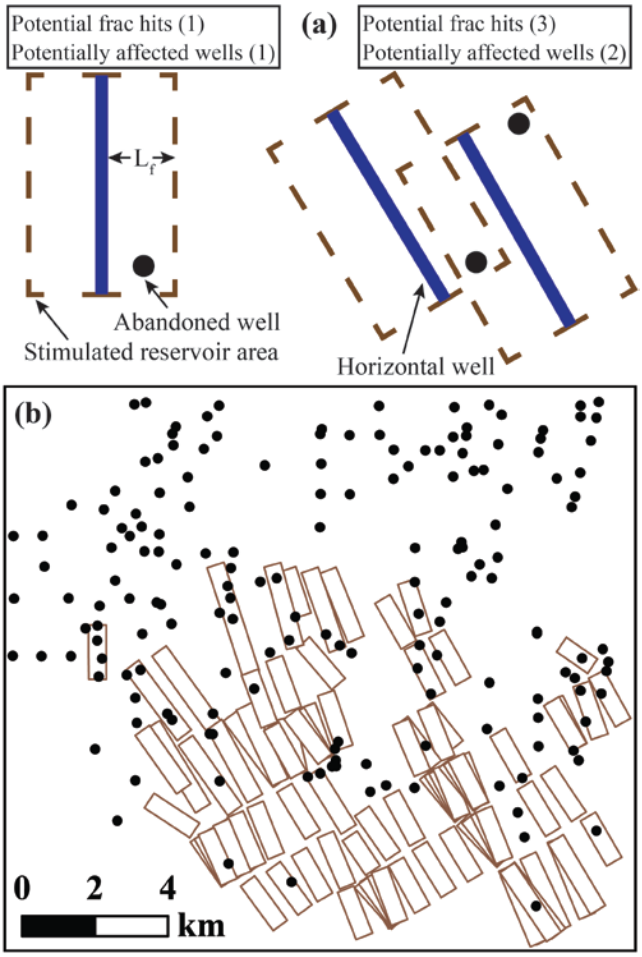

Figure 3.3. Conceptual model showing (a) potentially affected wells and potential frac hits (intersection) and (b) example application of methodology using well data for EFS horizontal wells and deep abandoned wells.

Results and Discussion

Eagle Ford Shale Horizontal Wells

The preceding analysis identified 12,145 existing EFS horizontal wells (Table 3.1). Completion-year data were available for all EFS horizontals, and ranged from 1978 to 2015, with a median completion year of 2013. Completion years prior to 2008 (i.e., the EFS discovery year) are recompletions of older wells. Nine of the 26 counties account for the largest proportion (92%) and greatest spatial density of EFS horizontals: Atascosa,

DeWitt, Dimmit, Gonzales, Karnes, La Salle, Live Oak, McMullen, and Webb (Figure 3.4a). The EFS wellbores are preferentially oriented in a NW-SE direction, the optimal direction for lateral propagation of hydraulic fractures due to the regional stress regime of the sedimentary basin (Heidbach et al. 2008). The average surface-expression length of EFS wellbores is 1,770 m, but this does not necessarily represent the length of the hydraulically fractured interval in the shale.

Table 3.1

Well Data Summary for Active EFS Area†

Well group	Well count	Reservoir(s) undetermined	Missing plug date	Plug year		Missing comp. date	Comp. year	
				Range	*Median*		*Range*	*Median*
EFS horizontals‡	12,145	-	-	-	-	-	1978-2015	2013
Abandoned	55,720	28,253	21,754	1908 - 2014	1993	34,205	1902-2014	1983
Deep abandoned	10,081	-	279	1950 - 2014	1994	1,096	1944-2014	1983
Converted	2,400	21	2,392	1983 - 2013	1996	623	1923-2014	1954
Deep converted	1,109	-	1,109	-	-	379	1930-2014	1953

†Well databases accessed April 1, 2015.

‡Existing EFS horizontal wells only. There are 6,707 permitted EFS horizontal wells.

There are 6,707 EFS horizontal wells permitted but not yet drilled, and some of these may never be drilled. Some of these EFS horizontal wells are located in areas without existing EFS activity, such as the northeastern portion of the play (Figure 3.4b). The nine counties with significant existing EFS activity account for 86% of permitted EFS horizontal wells. The average surface-expression length of permitted EFS horizontal wells is 1,900 m. Drilling trends for EFS horizontal wells have been toward increasing lateral lengths and hydraulic fracturing stages. County-level well data are available in Appendix C.1.

Abandoned Wells

Well-data interrogation assigned 55,720 wells to the abandoned well group (Table 3.1). Within the 26-county area (70,000 km^2), well density was ~0.8 abandoned wells/km^2. The abandoned well group comprised 50.2% dry wells, 49.5% abandoned production wells, and 0.3% other. The majority (61%) of abandoned wells listed no completion year. Abandoned wells with completion-year data ranged in dates from 1902 to 2014, with a median completion year of 1983. Abandoned wells are both abundant and spatially dense across all counties with EFS activity (Figure 3.4c). About 50% of abandoned wells across the study area are located in the nine counties with significant existing EFS activity.

In the context of unconventional activity, the lack of information for abandoned wells, especially older abandoned wells, complicates potential leakage assessments. The total number of abandoned wells, and deep abandoned wells, is an underestimate. Further, this analysis does not consider temporarily abandoned ("shut-in") oil and gas wells. The relatively recent median completion year is biased by missing data for older abandoned wells. For example, just seven wells are recorded with completion dates prior to 1935. In a survey of oil and gas wells in the Gulf Coast region of Texas, Nicot (2009) found few records for wells drilled before the 1930s and noted that hundreds to thousands of wells could have been drilled without being recorded, although they are probably shallow (< 600 m).

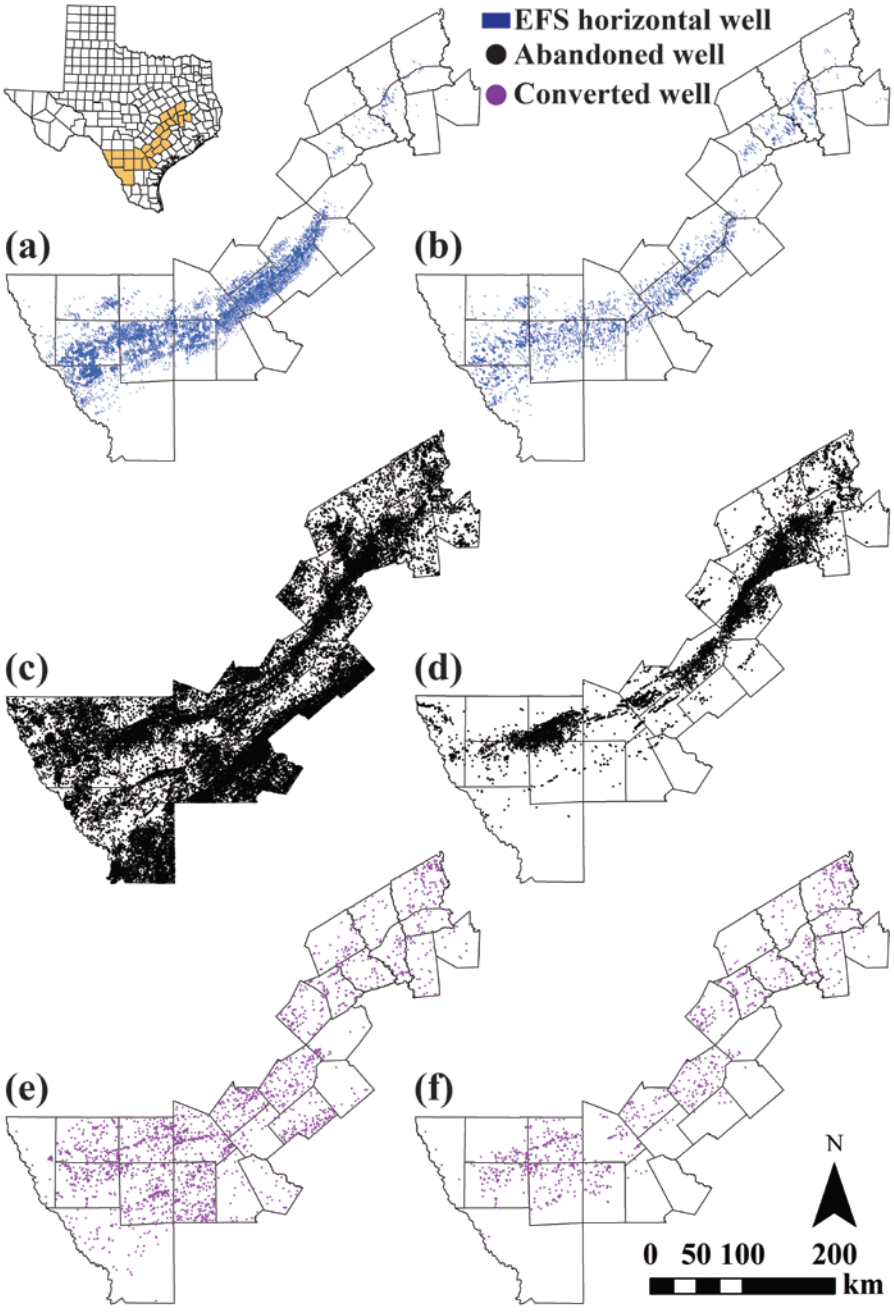

Figure 3.4. Maps of (a) existing horizontal wells, (b) permitted horizontal wells, (c) abandoned wells, (d) deep abandoned wells, (e) converted wells, and (f) deep converted wells.

The scarcity of records and information for abandoned oil and gas wells is not unique to the Eagle Ford Shale play. For example, the number of abandoned wells in Pennsylvania is estimated to range from 300,000 to 500,000 based on oil and gas

production data, yet the Pennsylvania Department of Environmental Protection only has records for ~12,000 abandoned wells (Kang et al. 2014). The number of abandoned oil and gas wells across the United States is uncertain, but estimates range from at least 2.3 million up to 3.0 million (Brandt et al. 2014; Townsend-Small et al. 2016).

The hydraulic characteristics of abandoned wells are also difficult to assess due to lack of information. Older abandoned wells pose a greater risk for leakage because well construction and abandonment materials are subject to degradation and have improved over time (Ide et al. 2006). Leakage potential for older wells also varies depending on whether the abandoned well was successful. Unsuccessful wells, which do not have production casing, can experience borehole closure over time from natural processes that reduce or inhibit leakage. However, the majority (>90%) of deep abandoned wells in this study are production wells, which are likely to have production casing present. Natural borehole closure may be inhibited by the presence of production casing, although corrosion of well materials over time can spur the borehole-closure process.

Abandonment requirements in Texas have increasingly focused on aquifer protection, and current rules require multiple zones (plugs) of recirculated cement in the wellbore (RRC 2000). The first specific plugging rules in Texas were promulgated in 1934, which required the producing formation to be plugged with recirculated cement, although plugging with mud-laden fluid remained common practice until at least 1967 (Nicot 2009). Some studies suggest 1967 as the demarcation after which abandoned wells were properly plugged (Johnston and Knape 1986; Warner et al. 1996; Warner et al. 1997). However even after 1967, there is evidence of improperly abandoned wells based on missing, incomplete, or inaccurate plugging reports (Warner et al. 1996; Warner et al.

1997; Warner 2001). Although 1967 has been suggested as a demarcation regarding plugging quality, using plugging dates to interpret hydraulic characteristics in this study is difficult because ~39% of abandoned wells have no plugging date and only 0.005% with records have a plugging date prior to 1967.

Converted Wells

Converted wells exist across all counties with EFS activity (Figure 3.4e). There are 2,400 converted wells in counties with EFS activity (Table 3.1). Most (74%) converted well records include the completion year, which ranged from 1923 to 2014, with a median of 1954. The majority (55%) of converted wells are located in the nine counties with the greatest density of EFS horizontal wells. Fewer converted wells exist in counties without GCDs, even though there may be more abandoned wells. Webb County, which does not have a GCD and has the most abandoned oil and gas wells (7,538), has 62 converted wells. Comparatively, La Salle County has a GCD and 1,481 abandoned oil and gas wells, but the most converted wells (264). The reason for these differences is not immediately clear, but may be related to factors like improved record keeping with the presence of a GCD or agricultural water demand.

There are an estimated 1,109 deep converted wells that were originally drilled to the Austin Chalk or a deeper reservoir. Deep converted wells show a NE-SW spatial trend across the central portion of the EFS play (Figure 3.4f) and 39% are located in counties with significant existing EFS activity (Figures 3.4a, 3.4f).

Converted wells tend to have earlier completion dates compared to abandoned wells, most likely an artifact of missing age data and records for abandoned wells.

Discussions with GCD staff suggest that the converted wells in this study may represent only a small fraction of the actual number of converted wells because the median age (1954) of converted wells predates the incorporation of most GCDs. The median age of converted wells also predates improved plugging requirements (~1967), and 99% are missing plugging data, which suggests that the majority of converted wells may be improperly abandoned according to current plugging standards. Harris (1965) noted a number of abandoned oil and gas wells had been converted into water wells, with no information on plugging practices. Older converted wells abandoned with drilling mud may represent increased risk for leakage because the gel strength can decrease over time due to dehydration (Johnston and Knape 1986). All converted wells with well-type information were abandoned production wells, but the majority (97%) of converted wells are missing this information.

Potential Frac-hits

After analysis, reservoirs were unable to be determined for 51% of abandoned and 1% of converted wells. Abandoned and converted wells could be affected by hydraulic fracturing if the borehole extends near or through the EFS, but insufficient data preclude a comprehensive analysis. Therefore, potential frac-hit results are based on the deep abandoned and deep converted well groups. County-level results are available in Table C.2.

Abandoned Wells

Potential frac hits on deep abandoned wells occur in almost every county with existing EFS activity (Figure 3.5a). The areas with the highest density of potential frac hits are the southwest, central, and northeast portions of the play (Figure 3.5a). Figure 3.6 plots the cumulative number of potentially affected wells and potential frac hits versus hydraulic-fracture half-length. The number of potentially affected wells is less than the number of potential frac hits, which suggests that abandoned wells are at risk for multiple frac hits. Differences between numbers of potential frac hits and affected wells are minimal at shorter hydraulic-fracture half lengths (<100 m), but become significant with increased hydraulic-fracture half-lengths (Figure 3.6a). At a 30-m hydraulic-fracture half-length, there are 127 potential frac hits and 112 potentially affected abandoned wells (Table 3.2). Thus, if all hydraulic fractures extend to at least 30 m there is a 1.3% probability that a deep abandoned well will intersect an SRA, and 1.1% of deep abandoned wells could be affected. At a 600-m hydraulic-fracture half-length, there are 1,527 potential frac hits and 823 potentially affected wells (Table 3.2). If hydraulic fractures extend to 600 m, there is a 15.1% probability that a deep abandoned well will intersect an SRA, and 8.2% of deep abandoned wells could be affected. Similarly, the probability that the SRA of one of the 12,145 EFS horizontal wells will intersect an abandoned well increases from 1.0 to 12.6% with the increased hydraulic-fracture half-length.

Table 3.2

Select Data for Well Groups that Intersect EFS Horizontal Well SRAs[†]

Fracture half-length (m)	Deep abandoned well group (n = 10,081)				Deep converted well group (n = 1,109)			
	No. frac hits	*% group*	*No. wells*	*% group*	*No. frac hits*	*% group*	*No. wells*	*% group*
30	127	1.3%	112	1.1%	23	2.1%	20	1.8%
600	1,527	15.1%	823	8.2%	425	38.3%	184	16.6%
30-P[‡]	205	2.0%	185	1.8%	40	3.6%	33	3.0%
600-P[‡]	3,175	31.5%	1,366	13.6%	725	65.4%	238	21.5%

[†]Well databases accessed April 1, 2015.

[‡]Analysis includes both existing and permitted EFS horizontal wells.

Including permitted EFS horizontal wells in the analysis reveals additional risk regions (Figure 3.5b). Potential frac-hit density increased in the southwestern and central portions of the play and additional counties are affected in the northeastern portion of the play (Figure 3.5b). Including permitted wells showed that as the hydraulic-fracture half-length increases from 30 to 600 m, the probability that an abandoned well will intersect an SRA increases from 2.0 to 31.5%, and the number of potentially affected wells increases from 1.8 to 13.6% (Figure 3.6b, Table 3.2). Thus, the probability that one of the 18,852 permitted or existing EFS horizontal wells will have its SRA intersect an abandoned well increased from 1.1 to 16.8% with the increased hydraulic-fracture half-length. The potential for frac hits increased at a greater rate with inclusion of permitted EFS horizontals (Figure 3.6b) than for existing EFS horizontals only (Figure 3.6a). This increased rate of potential frac hits is primarily due to infill drilling. Most drilling locations for permitted horizontal wells are located near existing horizontal wells and nearby abandoned wells already intersected by existing SRAs are multiply affected by these additional SRAs.

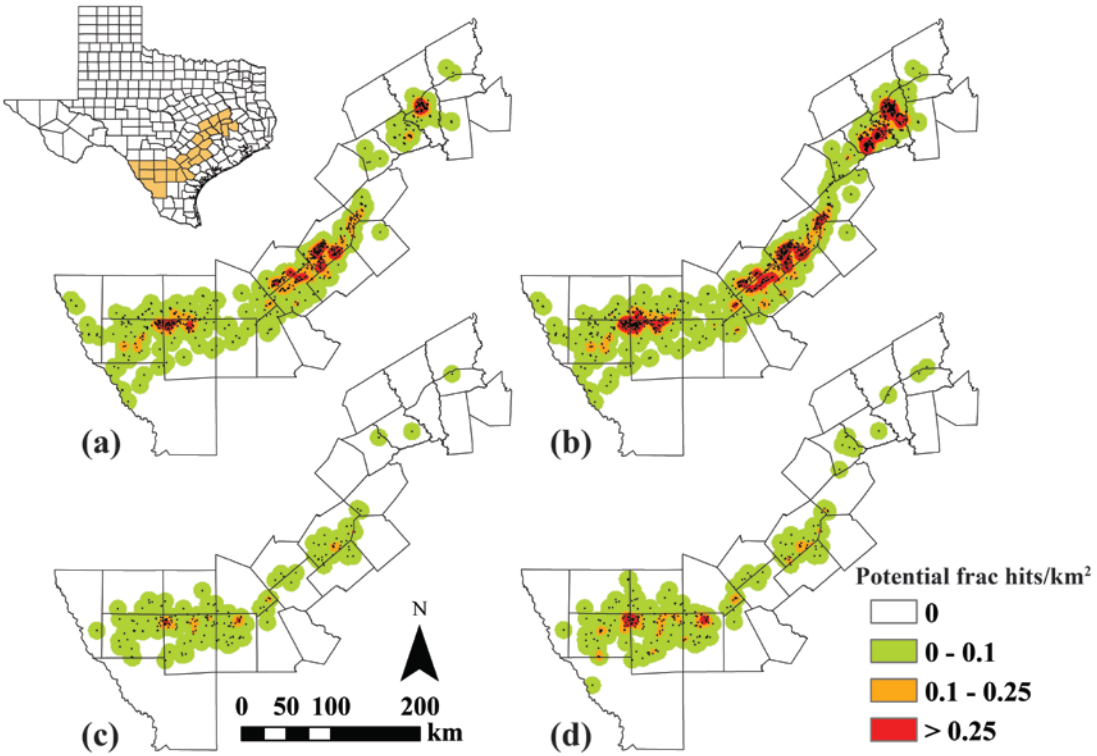

Figure 3.5. Heat map of potential frac-hit (intersection) density where the horizontal extent of the hydraulic-fracture half-length is 600 m for (a) abandoned wells and existing horizontal wells, (b) abandoned wells and existing/permitted horizontal wells, (c) converted wells and existing horizontal wells, (d) converted wells and existing/permitted horizontal wells. Only abandoned and converted wells that penetrate the Austin Chalk or deeper reservoirs are included in this analysis.

The intersection of an abandoned well with the SRA certainly does not mean that the abandoned well has experienced a frac hit, but does indicate the potential. Potential interaction between hydraulically generated fractures and abandoned wells is governed by several factors. The extent of hydraulic fractures is controlled by the stratigraphy and in situ stress states of the media. Microseismic data indicate that the horizontal extent of hydraulic-fracture half-lengths in the EFS commonly range from 100 to 300 m and microseismic events have been documented greater than 600 m (Bazan et al. 2010; Basu et al. 2012; Inamdar et al. 2010; Suliman et al. 2013). Microseismic data are typically used to characterize hydraulic-fracturing treatments, but do not necessarily indicate the

presence of a hydraulic fracture. Microseismic events can also represent reactivation of faults or fractures, or ductile rock failure.

There is potential for frac hits on abandoned oil and gas wells in shale plays across the United States. In the United States, hydraulic fracturing of shale primarily occurs in nine sedimentary basins (Flewelling and Sharma 2014). Oil and gas activity has occurred in most of these sedimentary basins since the 1950s, and many were drilled even earlier (late-1800s). Upward leakage along an abandoned oil and gas well following a frac hit requires a pathway and a failure of the abandoned well. Data for well barriers and failure rates of abandoned oil and gas wells in the United States show significant variability (~1.9 to 75%) and are often poorly documented (Davies et al. 2014).

If upward leakage does occur after a frac hit, it is limited by several factors (Flewelling and Sharma 2014). The low permeability of shale (1 to 1,000 nD) essentially precludes matrix flow. Low water saturation and high capillary forces in shale also limit fluid flow outside of hydraulic fractures, and the majority of hydraulic-fracturing fluids remain imbibed in the shale near hydraulic fractures (Engelder 2012; Engelder et al. 2014). Nonlinear pressure diffusion associated with fluid-rock interactions shows sharp pressure-diffusion fronts with little pressure propagation beyond hydraulically stimulated fractures (Shapiro and Dinske 2009a, 2009b). Upward leakage may also be reduced or even cease over time due to production of the horizontal well (Reagan et al. 2015; Brownlow et al. 2016), although these effects may not occur depending on the extent of fracture decay.

Converted Wells

Potential frac hits on converted wells occur in almost every county with existing EFS activity (Figure 3.5c). The largest density of potential frac hits is located in the southwestern portion of the play (Figure 3.5c). For a 30-m hydraulic-fracture half-length there are 23 potential frac hits and 20 potentially affected deep converted wells (Figure 3.6c, Table 3.2). At a 600-m hydraulic-fracture half-length, there are 425 potential frac hits and 184 potentially affected deep converted wells (Figure 3.6c, Table 3.2). Increasing the hydraulic-fracture half-length from 30 to 600 m increases the probability that a deep converted well will intersect an SRA from 2.1 to 38.3%, and the number of potentially affected deep converted wells increases from 1.8 to 16.6%. The probability that one of the 12,145 EFS horizontal wells will have an SRA that intersects a converted well varies from 0.2 to 3.5% with the hydraulic-fracture half-length.

Adding permitted EFS horizontal wells to the analysis reveals additional areas of risk and potential frac-hit density increased in the southwestern and northeastern portions of the play (Figure 3.5d). Increasing the hydraulic-fracture half-length from 30 to 600 m increases the probability that a deep converted well will intersect an SRA from 3.6 to 65.4%, and the number of potentially affected deep converted wells increases from 3.0 to 21.4% (Figure 3.6d, Table 3.2). Thus, the probability that one of the 18,852 permitted or existing EFS horizontal wells will have an SRA that intersects a converted well varies from 0.2 to 3.8% depending on hydraulic-fracture half-length. Similar to the cases with deep abandoned wells, the potential for frac hits increased at a greater rate with inclusion of permitted EFS horizontals (Figure 3.6d) than for existing EFS horizontals (Figure 3.6c) only.

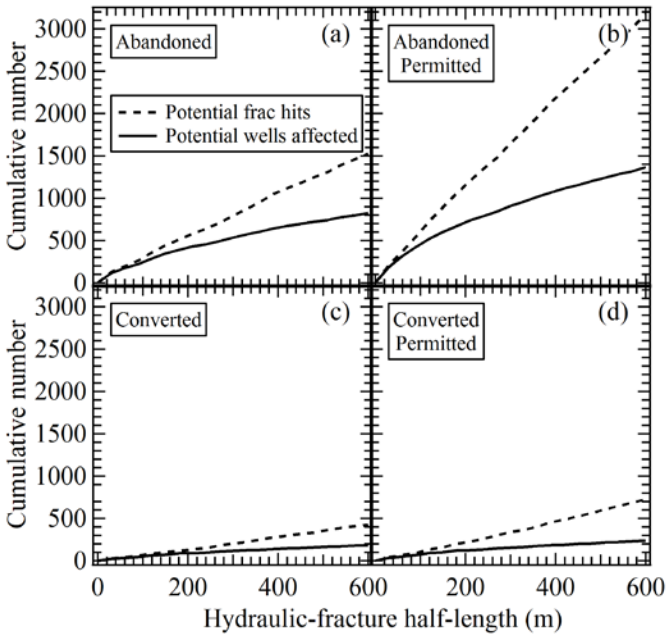

Figure 3.6. Number of potentially affected wells that intersect an SRA and number of potential frac hits (intersection) as a function of the horizontal extent of hydraulic-fracture half-length for (a) abandoned wells and existing horizontal wells, (b) abandoned wells and existing/permitted horizontal wells, (c) converted wells and existing horizontal wells, (d) converted wells and existing/permitted horizontal wells. Only abandoned and converted wells that penetrate the Austin Chalk or deeper reservoirs are included in this analysis.

Montague and Pinder (2015) found that the average probability of an encounter between hydraulic fracturing and abandoned wells in the Marcellus Shale region of New York to be about 0.025%. Frac hits documented from 2009 – 2012 in Alberta identified 20 incidents, resulting in an average probability of 0.4% (Kim 2012). In this study, the probability of an actual encounter was not determined, rather the probability that hydraulic fracturing would occur near an abandoned or converted well was estimated using an SRA method and existing and permitted well locations. If permitted and existing horizontal wells are considered, the average probabilities that the SRA of a horizontal well will intersect an existing well range from 1.1 to 16.8% for deep abandoned wells and 0.2 to 3.8% for deep converted wells. The spatial characteristics of these abandoned and

converted wells are known, and could be used to prioritize investigations of hydraulic characteristics such as field permeability tests (Gasda et al. 2013) or water-quality monitoring. Converted wells, if intersected by a horizontal well SRA, could represent additional risk to overlying aquifers and additional care may be required when selecting drilling locations for horizontal wells near them.

Conclusions

Abandoned and converted wells can intersect the SRA of a hydraulically fractured horizontal well. Such an intersection does not conclusively demonstrate that a frac hit has or will occur, however the potential for a frac hit exists. Similarly, a frac hit on an abandoned well does not necessarily imply that leakage to an overlying aquifer will occur, but the potential is there, too. Continued drilling and abandonment of oil and gas wells increases the likelihood of frac hits. The highest density for potential frac hits is not necessarily in areas with the greatest horizontal well density, it primarily depends upon the depth of abandoned wells. Each abandoned well is unique, and assessment of leakage potential requires critical review of historical oil and gas activities. An investigation of abandoned and converted wells near hydraulically fractured horizontal wells in the EFS revealed the following:

- The median completion year for converted wells is 1954, which suggests these wells have a higher risk for upward leakage than abandoned wells due to poorer plugging techniques in the past.
- Potential frac hits can occur in any county with Eagle Ford Shale activity. Depending on hydraulic-fracture half-length, up to 823 abandoned and 184

converted wells could intersect the stimulated reservoir of existing Eagle Ford Shale horizontal wells.

- Abandoned and converted wells have the potential to be multiply affected by hydraulic fracturing, and the risk of an encounter increases as permitted horizontal wells are drilled.
- Current TWDB and RRC records are insufficient to effectively protect groundwater resources. To mitigate concerns, well data need to be enhanced and reviewed. With respect to certain converted wells, regulatory well-spacing requirements should be reconsidered.

In summary, this paper examines the potential for abandoned and converted wells to be within frac-hit range (intersect the SRAs) of existing and permitted horizontal wells. The methods developed for this study are applicable to other unconventional shale plays with abandoned and converted wells.

Acknowledgements

Funding for this work was provided by the Evergreen Underground Water Conservation District, the Wintergarden Groundwater Conservation District, and the C. Gus Glasscock Jr. Endowed Fund for Excellence in Environmental Sciences. The comments and suggestions from the three anonymous reviewers improved this paper significantly and were greatly appreciated.

CHAPTER FOUR

Uncertainty Analysis: Influence of Hydraulic Fracturing on Overlying Aquifers in the Presence of Leaky Abandoned Wells

This chapter was submitted as Brownlow, J.W., S.C. James, and J.C. Yelderman, Jr. 2016. Uncertainty analysis: influence of hydraulic fracturing on overlying aquifers in the presence of leaky abandoned wells.

Abstract

The usefulness of a model uncertainty analysis can be reduced if the calibration dataset does not appropriately inform parameter estimates and model predictions. Model simplicity can improve its usefulness in cases where observations are unavailable, but further insight may be gleaned by developing a calibration dataset to explore and minimize uncertainty. This study applies a series of techniques to investigate uncertainty in a simple numerical model of upward flow (leakage) through an abandoned oil and gas well converted into a water well in hydraulically fractured shale. Model calibration was achieved by developing a limited calibration dataset from well-specific measurements at a horizontal well in the Eagle Ford Shale play. Uncertainty in the calibrated model was interrogated using sensitivity, linear, and nonlinear analyses available in the PEST suite. Sensitivity analysis suggests that flowback after hydraulic fracturing could be crucial in reducing leakage. Linear analyses indicate horizontal-well production rates and long-term reservoir pressures are valuable measurements to collect when evaluating potential leakage. Nonlinear analyses emphasize the range in predictive uncertainty of potential leakage. The results underscore the need to evaluate and include additional types of well data in public records, such as flowback and co-produced water volumes. Overall, the

results of this study illustrate the utility of uncertainty analysis with a limited calibration dataset applied to a simple model.

Introduction

Uncertainty analysis of models is a fundamental step in the modeling process, especially if model predictions are to be considered in decision making (Jakeman and Letcher 2003; Pappenberger and Beven 2006). Uncertainty in a model prediction is related to uncertainty in model input data, model parameter values, and model structure (Refsgaard et al. 2006). In complex models, uncertainty analyses can be computationally demanding and limited by the availability of a sufficiently large and relevant calibration dataset. In contrast to complex models, uncertainty analyses of simple models are computationally frugal and can benefit from a relatively smaller calibration dataset. Neither a simple nor complex model can guarantee predictive accuracy due to the intrinsic heuristic nature of a model (Konikow and Bredehoeft 1992). However, certain efforts can be made to explore and minimize predictive uncertainty.

Improvement of a model is an iterative process, of which simplicity is a cornerstone during early model construction. Model complexity is measured by the number of model parameters used to define system properties among other aspects (Hill 2006). Simple models have few parameters defined based on hydrogeologic knowledge or hypotheses, and model solutions tend to be dominated by model structure (Hill and Tiedeman 2007; Foglia et al. 2013; La Vigna et al. 2016). In addition, models with few parameters risk bias during calibration to achieve optimal model-measurement fit, although such bias may still achieve a tangible reduction in model predictive uncertainty

(Moore and Doherty 2005). The tradeoffs between simplicity and complexity approaches in modeling have been the subject of numerous debates and research (e.g., Gómez-Hernández 2006; Hill 2006; Hunt et al. 2007; Engelhardt et al. 2014; Hill et al. 2016). Regardless of the level of model complexity, a useful model can be defined as one that (James et al. 2009):

1. Provides predictions.

2. Reports predictions within quantified uncertainty bounds.

3. Mathematically reduces uncertainty bounds to their minimum.

The additional value from a model gained during quantification and reduction of uncertainty bounds is often provided by incorporation of appropriate parameter-estimation and uncertainty analysis software, and a range of methods and codes have been developed for such purposes (Poeter and Hill 1999; Hill and Tiedeman 2007; Adams et al. 2014; Doherty 2016; Vrugt 2016). Ultimately, the objective of most uncertainty analysis exercises is interrogation and reduction of model predictive uncertainty. In concert with this objective, additional value from a model can be gleaned such as valuation of different types of data to collect based on their ability to constrain predictive uncertainty (Dausman et al. 2010).

Ideally, observations of system behavior are available to build a calibration dataset that can be used to quantify and constrain uncertainty bounds of model parameters through the calibration process. Invariably the availability, quantity, and quality of observations varies depending upon the model and system considered. In models where observations are not available (i.e., an “uncalibrated model”), model predictive uncertainty encompasses the probability range of model parameters, and level

of uncertainty in model structure (Gallagher and Doherty 2006). Thus, uncertainty in uncalibrated models is often difficult to determine because incorrect estimates of parameter uncertainty influence estimates of uncertainty in model structure (Refsgaard et al. 2006). That is not to say that an uncalibrated model is not useful; it may provide reasonable predictions or be used as an interpretive model of system processes (e.g., Myers 2012).

If at least a few observations become available, parameter uncertainty bounds may be reduced dependent upon parameter sensitivity to the calibration dataset (Moore and Doherty 2005). However, the value of a particular observation in the calibration dataset toward reducing parameter uncertainty bounds is somewhat tenuous with respect to the level of trustworthiness and associated noise with that observation. Similarly, the propensity of an observation to reduce uncertainty in a model prediction coincides with the noise and ability of that observation to constrain parameters that affect the prediction. Therefore, calibration datasets with fewer observations than model parameters often prompt acquisition of additional types and numbers of observations in an effort to further constrain uncertainty (Hunt et al. 2006; Sun et al. 2012; Delsman et al. 2016). In the case that observations are not available, a limited calibration dataset can be developed using indirect measurements to spur the uncertainty analysis component for model improvement.

In this study a series of uncertainty analyses are conducted on a simple model of upward flow through an abandoned oil and gas well in the stimulated reservoir of hydraulically fractured shale (Figure 4.1a). The model focused on leaky abandoned oil and gas wells converted into water wells (converted wells) in the Eagle Ford Shale study

area, and is described by Brownlow et al. (2016a). The analysis is structured as follows: first, a sensitivity analysis of the uncalibrated model is performed. Second, the model was calibrated with a limited dataset of observations calculated from measurements from well records. Finally, predictive uncertainty of the model is quantified using linear and nonlinear analyses. The software used for these analyses is part of the publically available PEST suite, which is extensively documented (Doherty 2016). The study provides an exploratory evaluation of major contributing factors to model uncertainty in leakage and assessment of data needed for development of more complex models that evaluate leakage.

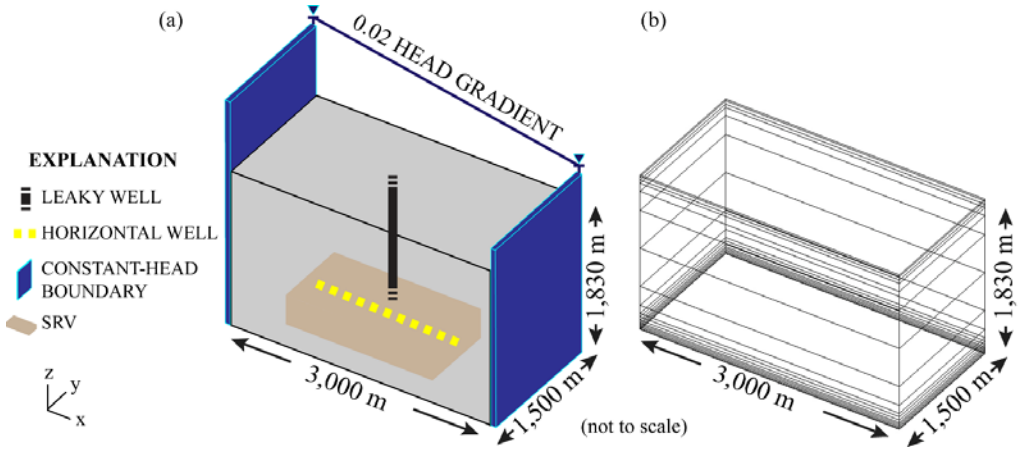

Figure 4.1. (a) Conceptual model of a leaky well in the SRV of a horizontal well, and (b) model vertical discretization used by Brownlow et al. (2016a).

The Model

A full description of the model is available (Brownlow et al. 2016a), and a brief summary of aspects pertinent to the current analysis is presented. The study area encompassed the Eagle Ford Shale play in south Texas. The stratigraphy of the model is based on well records for the liquid-producing region of the Eagle Ford Shale play (RRC 2016a). The conceptual model consists of a three-dimensional layered sedimentary basin

comprising sixteen layers with five distinct hydrostratigraphic units from the oil and gas reservoirs to the overlying aquifer: (1) confined aquifer, (2) interburden, (3) upper reservoir, (4) shale, and (5) lower reservoir (Figure 4.1b). Each hydrostratigraphic unit is homogenous and vertically anisotropic.

The model domain is constructed as a rectangular prism with dimensions 3,000 m long by 1,500 m wide by 1,830 m thick. Horizontal discretization was 5×5 m^2 and the vertical discretization varied by layer. Constant-head boundary conditions are applied as a gradient along the sides of the model, and no-flow boundary conditions are imposed at the base and top of the domain. Flow across the model is simulated by applying a uniform horizontal gradient of 0.02. The MODFLOW-2005 (Harbaugh 2005) code was used to build the flow model. Steady-state flow conditions are assumed for calibration purposes, and were established using the MODFLOW-2005 Link-AMG solver (Mehl and Hill 2001).

Hydraulic fracturing is implemented using a 1,500-m MODFLOW-2005 WELL boundary centered vertically and laterally in the shale, and a stimulated reservoir volume (SRV) approach. For the SRV approach, injection at the horizontal well coincides with an instantaneous and uniform increase in horizontal permeability and decrease in vertical anisotropy within a defined volume surrounding the well. The size of the SRV is established using pressure-diffusion equations and measurements from typical hydraulic-fracturing treatments for horizontal wells in the Eagle Ford shale. The calculated SRV used in the model comprised an area of 420,000 m^2 and height of 60 m (thickness of the shale) centered on the horizontal well. After injection ceases, a period of flowback is simulated at the horizontal well with a head-controlled flux (MODFLOW-2005 DRAIN)

boundary, which removes a specified fluid volume at surface elevation. Following flowback, production of the horizontal well is simulated with a period of high-rate pumping followed by a period of low-rate pumping.

The leaky converted well is simulated using the Multi-Node Well 2 (MODFLOW-2005 MNW2) Package (Konikow et al. 2009) as a vertical well that extends from the shale to the overlying confined aquifer. Two types of borehole conditions for leaky converted wells were considered: (1) open, and (2) mud-filled. Open converted wells were simulated as nonpumping vertical wells, screened in the confined aquifer layer and a reservoir layer. Mud-filled converted wells were simulated as pumping wells in the shale with drawdown limited by a computed head at the base of the mud-filled borehole.

The original model considered a variety of hydraulic-fracturing and leaky well scenarios, such as cases of injection-only and injection with flowback only. Here, only one scenario is simulated: injection with flowback and production at the horizontal well and a leaky mud-filled converted well offset 30 m from the injection location. It is assumed that any barriers (e.g., packer) to flow present in the wellbore have failed when the simulation begins.

Methods

Parameters

There are eighteen hydraulic-property model parameters for hydraulic conductivity, vertical anisotropy, and storativity. Model parameters with precalibration

values and uncertainties are listed in Table 4.1. Hydraulic-property constancy is assumed for the five hydrostratigraphic units and SRV. Precalibration values were derived in the original model using common analytical solutions from depth-dependent pore-fluid relationships and literature values for the study area. References for all precalibration parameter values and uncertainty bounds are provided in Appendix D.1.

There are eight hydraulic fracturing model parameters: (1) injection rate, (2) injection time, (3) flowback rate, (4) flowback time, (5) early-stage production rate, (6) early-stage production time, (7) late-stage production rate, and (8) late-stage production time. Precalibration parameter values were established using literature values, and most parameter uncertainty bounds were defined from available well records (RRC 2016c). For example, well records indicate the well was hydraulically fractured in twenty stages. Typical lengths of time for each stage range from 20 min to 2 hours (Martin et al. 2011), and time of injection was allowed to vary from 0.28 to 1.67 d. Time of flowback was established by taking the difference between recorded dates of hydraulic fracturing and initial production of the well. Flowback rate is dependent on conductivity of DRAIN boundaries, and was allowed to vary one order of magnitude from the precalibration value. Well records show that production at the horizontal well significantly declined after 450 days. Therefore, the time of early-stage production was set to 450 d. The average oil production rate over the first 450 days plus a possible range in water production (0 to 30%) was used as the early-stage production rate. Similarly, the rate for late-stage production is based on the average oil production rate over the remaining 2,200 days plus a possible range in produced water production (0 to 30%).

Twelve hydraulic and six well parameters were deemed adjustable for linear analyses. The number of adjustable parameters was decreased from eighteen to four for the nonlinear analyses as listed in Table 4.1.

Table 4.1
Description of Parameters used in Uncertainty Analysis

Parameter	Description	Adjustable[1]	Unit	Precalibrated value
hk_aq	Aquifer hydraulic conductivity	-	m/d	8.6×10^{-1}
hk_int	Interburden hydraulic conductivity	-	m/d	7.7×10^{-9}
hk_ac	Austin Chalk hydraulic conductivity	S/L	m/d	1.7×10^{-7}
hk_ef	Eagle Ford hydraulic conductivity	S/L	m/d	1.2×10^{-8}
hk_bd	Buda hydraulic conductivity	S/L	m/d	1.8×10^{-7}
hk_srv	SRV hydraulic conductivity	S/L/N	m/d	7.1×10^{-6}
vani_aq	Aquifer anisotropy	-	-	10
vani_int	Interburden anisotropy	-	-	100
vani_ac	Austin Chalk anisotropy	S/L	-	100
vani_ef	Eagle Ford anisotropy	S/L	-	1000
vani_bd	Buda anisotropy	S/L	-	100
vani_srv	SRV anisotropy	S/L	-	10
ss_aq	Aquifer specific storage	-	1/m	2.6×10^{-6}
ss_int	Interburden specific storage	-	1/m	1.0×10^{-5}
ss_ac	Austin Chalk specific storage	S/L	1/m	1.2×10^{-6}
ss_ef	Eagle Ford specific storage	S/L	1/m	5.0×10^{-5}
ss_bd	Buda specific storage	S/L	1/m	1.1×10^{-6}
ss_srv	SRV specific storage	S/L/N	1/m	5.0×10^{-5}
r_inj	Injection rate	S/L	m^3/d	45.43
t_inj	Period of injection	S/L	d	0.833
r_fb	Flowback rate	S/L	m^2/d	2.9×10^{-4}
t_fb	Period of flowback	S/L	d	7
r_prd1	Early-stage production rate	S/L/N	m^3/d	−0.053
t_prd1	Period of early-stage production	-	d	450
r_prd2	Late-stage production rate	S/L/N	m^3/d	−0.0106
t_prd2	Period of late-stage production	-	d	5049
h_mud	Hydraulic head at base of mud column	S	m	2510

[1] S/L/N = parameter adjustable during sensitivitiy, linear and nonlinear analyses, respectivel

Observations

A total of six observations, one hard and five soft, were used in the calibration dataset (Table 4.2). Soft observations rely on transformation of measurements available

in most well records. The five soft observations included total volume of flowback, and hydraulic head at the horizontal well upon ceasing: (1) injection, (2) flowback, (3) early-stage production, and (4) late-stage production. Hard observations are those directly transferrable from well records to the model. In this case, the total volume injected during hydraulic fracturing (~14,000 m^3) is used. Appendix D.2 provides a detailed summary of measurements from the well records used as input values for generating the calibration dataset. The methodology to generate the soft observations from measurements in well records is described below.

Table 4.2
Description of Observations used in Uncertainty Analysis

Observation	Value	Unit	Description
h_inj	3600	m	Hydraulic head at horizontal well after injection ceases
h_fb	3430	m	Hydraulic head at horizontal well after flowback ceases
h_prd1	2400	m	Hydraulic head at horizontal well after early-stage production ceases
h_prd2	525	m	Hydraulic head at horizontal well after late-stage production ceases
sum_inj	14000	m^3	Total fluid volume injected during hydraulic fracturing
sum_fb	2300	m^3	Total fluid volume removed during flowback

The total fluid volume removed during flowback is the sum of water and oil removed after injection but prior to production. Hydrocarbon volumes produced prior to injection are typically reported in well records, but water volumes are not. Here, the *sum_fb* observation is the volume of oil removed at the horizontal well prior to production (300 m^3), plus an acceptable volume of water (15% of injected fluid volume, see [Boschee 2014]).

The formation of fracture openings requires pressures following injection to exceed the minimum in-situ horizontal stress of the shale. In the absence of tectonic stress, the minimum horizontal stress is approximated as (Eaton 1969):

$$\sigma_{hmin} = \frac{\nu}{1-\nu}(\sigma_v - \alpha P_p) + \alpha P_p, \qquad \text{(Eq. 4.1)}$$

where ν is Poisson's ratio, σ_v is the overburden stress [m], α is Biot's constant, and P_p is the reservoir fluid pressure [m]. Typical ranges used for Poisson's ratio in Eagle Ford Shale are between 0.25 and 0.27 (Mullen et al. 2010; Manchanda et al. 2012; Roussel et al. 2012) and a value of 0.26 was used here. Biot's constant is assumed to have a value of 1. Overburden stress is approximated using a pressure gradient of 22.6 MPa/km and a depth of 2,350 m. Reservoir fluid pressure (2,535 m) was calculated using a pressure gradient of 10.5 MPa/km based on well location and pressure gradient maps (Cander 2012; Burke et al. 2013). Collectively, these values yield an estimated minimum horizontal stress of 34.6 MPa.

Net pressure required to maintain the fracture opening above the minimum horizontal stress can be approximated using the analytical solution for a semi-infinite fracture (Sneddon 1946):

$$P_{net} = \frac{wE}{4(1-\nu^2)h_f}, \qquad \text{(Eq. 4.2)}$$

where w is the maximum width of the hydraulic fracture [m], E is Young's modulus [GPa], and h_f is the half-height of the hydraulic fracture [m]. Typical values used for Young's modulus in Eagle Ford Shale are between 10 to 30 GPa (Mullen et al. 2010; Manchanda et al. 2012; Roussel et al. 2012). Here, the following values are used: w = 0.075 m, E = 10 GPa, ν = 0.26, and h_f = 30, which yields P_{net} = 0.70 MPa. The calculated value is appropriate based on observed and modeled net pressures for Eagle Ford Shale hydraulic-fracturing treatments (Manchanda et al. 2012; Roussel et al. 2012). The sum of computed in-situ minimum horizontal stress and net pressure represent the

h_inj observation (3600 m), or hydraulic head in the shale immediately after injection ceases.

Well-potential tests are conducted after flowback and prior to production. The measurements recorded during well-potential tests of the horizontal well were used to estimate bottomhole pressure. Calculated bottomhole pressure was used for the head observation after flowback ceases (*h_fb*). Total pressure drop across the wellbore is the sum of pressure drops due to elevation, friction, and acceleration:

$$\frac{\mathrm{d}p}{\mathrm{d}h} = \left(\frac{\mathrm{d}p}{\mathrm{d}h}\right)_{elev} + \left(\frac{\mathrm{d}p}{\mathrm{d}h}\right)_{fric} + \left(\frac{\mathrm{d}p}{\mathrm{d}h}\right)_{accl}. \qquad \text{(Eq. 4.3)}$$

Here, the empirical multiphase flow correlation developed by Poettmann and Carpenter (1952) was solved for bottomhole pressure using an iterative procedure and measurements made during the well-potential test as inputs.

Most horizontal wells in shale plays are subject to rapid declines in initial production and reservoir fluid pressure as hydraulic fractures are drained (Lane and Chokshi 2014). When bottomhole pressures decline to hydrostatic conditions, fluids cease to naturally flow to the surface and maintaining production requires implementation of an artificial lift system. The inflection point at the horizontal well between high- and low-rate production (t = 450 d) is assumed to represent the transition from overpressure to roughly hydrostatic pressure (*h_prd1* = 2400 m)

If possible, bottomhole pressures are maintained above the bubblepoint pressure of the reservoir fluid to avoid fluid loss from two-phase flow (Hinchman and Barree 1985; Economides et al. 1989). Therefore, the bubble point pressure of the reservoir fluid represents the head observation (*h_prd2*) at the end of late-stage production (t = 15 yr). Numerous correlations have been developed for estimating the bubblepoint pressure of a

reservoir fluid, here we use the generally applicable correlation (Vasquez and Beggs 1980):

$$P_{bp} = \left[\frac{56.060 R_s}{\gamma_g} 10^{\frac{-10.393 \gamma_{API}}{(T+460)}} \right]^{\frac{1}{1.187}}, \qquad \text{(Eq. 4.4)}$$

where T is reservoir temperature [°F], R_s is the solution gas-oil ratio [scf/STB], γ_g is the gas specific gravity [-], and γ_{API} is the oil API gravity [-]. Note the correlation was developed using imperial units, and here we use: T = 230°F, R_s = 71, γ_{API} = 33, and γ_g = 0.65, which yields P_{bp} = 420 m. Head observations used over the production period (*h_prd1*, *h_prd2*) in the calibration dataset are consistent with expected pressure declines for horizontal wells (Ilk et al. 2012; Portis et al. 2013; Cherian et al. 2015).

Prediction

The prediction of interest is the cumulative volume of fluid that flowed from the shale into the overlying aquifer through the 30-m leaky mud-filled well over the 15-year simulation time, hereafter referred to as leakage.

Uncertainty Analysis

Uncertainty analyses comprised three approaches: (1) sensitivity analysis, (2) calibration and linear analysis, and (3) nonlinear analysis. Full description of the theory behind each approach is available in the PEST documentation (Doherty 2016). For brevity, each approach is briefly described below.

Sensitivity Analysis

Sensitivity analysis aims to evaluate changes in model outputs due to changes in model inputs. Local sensitivity analysis methods test the effect of varying a single parameter on model results (Hou et al. 2015). Here, a local method is applied using the model-independent SENSAN program from the PEST suite. SENSAN allows a user to automate the local sensitivity analysis process with continuous model runs of different prepared parameter sets, recording model outputs from each run. Parameter sets were constructed for each model scenario to allow a single parameter to increasingly vary from nominal by a factor of 10%. The normalized sensitivity coefficient was used to evaluate relative sensitivity of corresponding model output with respect to variation of a particular model parameter (Doherty 2016):

$$NSC = \frac{|(o - o_0)/o_0|}{|(p - p_0)/p_0|}, \qquad \text{(Eq. 4.5)}$$

where o and p are model output and parameter values from a particular model run, and o_0 and p_0 are model output and parameter nominal values.

Model Calibration and Linear Analysis

Model calibration and parameter estimation is achieved by minimization of the objective function that characterizes model-to-measurement misfit:

$$\Phi = (\mathbf{Xp} - \mathbf{h})^t \mathbf{Q} (\mathbf{Xp} - \mathbf{h}), \qquad \text{(Eq. 4.6)}$$

where **h** is a vector of observations in the calibration dataset, **p** is a vector of model parameters, **X** is a matrix describing the action of the model as it operates on parameters, and **Q** is the weight matrix. Automated model calibration and parameter estimation were

carried out using singular value decomposition (Moore and Doherty 2005; Moore and Doherty 2006; Doherty et al. 2010).

Analyses that assume model linearity provide insights into parameter contributions to predictive uncertainty, and contributions of observations to reductions in predictive uncertainty (James et al. 2009; Dausman et al. 2010). Contributions to predictive uncertainty from model parameters and observations were evaluated using the GENLINPRED utility in PEST that applies techniques outlined by Moore and Doherty (2005). The ability of each parameter to be estimable based on the calibration dataset ("identifiability") was evaluated using the IDENTPAR utility in PEST that applies the techniques outlined by Doherty and Hunt (2009).

Nonlinear Analysis

Two nonlinear analyses were applied to the calibrated model: (1) calibration-constrained maximization/minimization, and (2) calibration-constrained null-space Monte Carlo (NSMC). Predictive maximization/minimization is employed by constraining the objective function to a specified limit that describes the confidence level of the prediction. The methodology behind predictive maximization/minimization is detailed by Vecchia and Cooley (1987). For this analysis, predictions were maximized and minimized according to the computed objective function constraint (Christensen and Cooley 1999):

$$\Phi_0 = \Phi_{\min}\left[\frac{t^2_{\alpha/2}(n-m)}{(n-m)}+1\right], \qquad \text{(Eq. 4.7)}$$

where Φ_{min} is the value of the objective function calculated during calibration, t is Student's t distribution, α is confidence level, n is number of observations, and m is

number of adjustable parameters. Here, α = 0.0005 (99.9% confidence level), n = 6, and m = 4.

Calibration-constrained NSMC provides a mechanism to assess model predictive capabilities and distributions under nonlinear model assumptions (viz., James et al. 2009; Herckenrath et al. 2011), and the methodology is well-documented (Tonkin et al. 2007; Tonkin and Doherty 2009). The advantage behind the NSMC method is the ability to generate predictions from a computed series of calibration-constrained parameter sets. Calibration-constrained parameters sets were developed by optimization of randomly generated parameter sets to a level defined by the previously computed target objective function constraint. The optimization process was limited to a maximum of three nonlinear iterations. Each calibration-constrained parameter set was subjected to a single model run to analyze leakage, and individual model runs were aggregated to construct the probability distribution for leakage.

Results and Discussion

Sensitivity Analysis

Results for the sensitivity analysis are displayed as a sensitivity matrix in Figure 4.2. Selected parameters are ranked in order of their respective sensitivity to a particular observation. Head (*h*) observations were most sensitive to storativity of the SRV (*ss_srv*), and least sensitive to changes in head (*h_mud*) at the base of the leaky mud-filled well. Variation of horizontal-well parameters showed head observations were most sensitive to the rate of flowback (*r_fb*), and least sensitive to injection rate (*r_inj*). Simulated heads

were more sensitive to variation of late-stage production rates (*r_prd2*) than early-stage production rate (*r_prd1*).

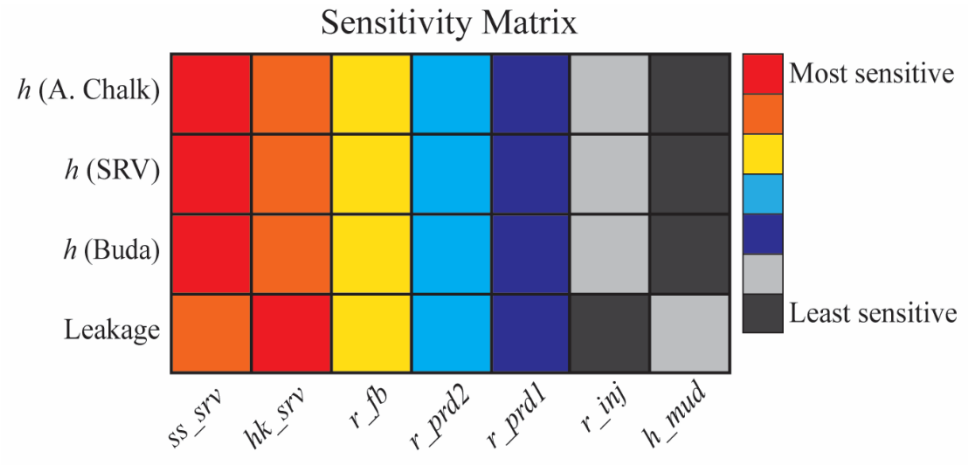

Figure 4.2. Sensitivity matrix for the mud-filled leaky well 30 m from the horizontal well. Parameters (defined in Table 1) shown are ranked in order of sensitivity to a respective observation.

Sensitivity rankings of horizontal-well parameters for leakage share similar trends to those seen in head observations. For example, of the horizontal-well parameters, leakage was most sensitive to *r_fb*, and more sensitive to *r_prd2* than *r_prd1*. However, one difference from sensitivities of head is that leakage is more sensitive to variations in hydraulic conductivity in the SRV (*hk_srv*) and least sensitive to *r_inj*. Leakage is also more sensitive to *h_mud* than *r_inj* compared to observations of head.

The sensitivity of head and leakage to flowback rate is notable because the original model did not show a significant effect in reducing head at the horizontal well or leakage from the addition of flowback. The lack of an appreciable effect on leakage with the addition of flowback in the original model is attributed to the small volume removed over the flowback period (~8% of injected fluid). The high sensitivity of head and leakage to flowback rates suggests both volume of fluid removed and duration of flowback affect potential upward leakage after hydraulic fracturing. Shale plays that

remove less volume during flowback have a larger potential to maintain higher heads after hydraulic fracturing. For example, up to 40% of injected fluid can be returned over the flowback period in the Marcellus Shale play (Boschee 2014). Unfortunately, the duration of flowback is not always reported. Accurate times for flowback duration can be difficult to determine because fluids may not be continuously removed over the period between hydraulic fracturing and first production at the horizontal well.

Heads and leakage are more sensitive to late-stage production than early-stage production simply due to the longer time period over which late-stage production occurs. Similarly, the sensitivity of heads and leakage to injection rate is relatively less, due to the shorter period of time over which injection occurs. These observations are not unexpected given that leakage is represented as the cumulative volume of upward flow through the leaky well over the 15-year simulation time. If potential upward leakage during or immediately following injection were of interest, leakage would certainly be more sensitive to injection volumes and rates. The effects of early-stage production at the horizontal well can be beneficial in rapidly reducing or inhibiting potential leakage. Maintaining a high production rate over the long term may be equally as important in reducing leakage as high early-stage production rates because pressures in the shale tend to decline rapidly and plateau over the production period at the horizontal well.

The sensitivity of head and leakage to hydraulic parameters of the SRV suggest that both virgin shale permeability and shale permeability after hydraulic fracturing are important factors in potential upward leakage. Although leakage is less sensitive to *h_mud* than other parameters, the potential for long-term upward leakage depends upon

pore-fluid properties of the shale and the presence of a vertically upward hydraulic gradient along the mud in the borehole.

Linear Analysis

Parameter Contributions to Predictive Uncertainty

Model calibration to the limited calibration dataset predicted a leakage of 2.7 m^3. The calibration process resulted in a decrease of predictive uncertainty in leakage. Precalibration and postcalibration uncertainty variance were 52.5 and 2.6 $(m^3)^2$, respectively.

Figure 4.3 details precalibration and postcalibration contributions to predictive uncertainty variance from parameters used in the linear predictive uncertainty analysis. Calculation of a particular parameter's contribution to predictive uncertainty variance assumes the value of that parameter is perfectly known. The *hk_srv* parameter makes up the single largest contribution to precalibration uncertainty variance. The calibration process showed a decrease of predictive uncertainty variance in *hk_srv*, but increased uncertainty variance for parameters *ss_srv*, *t_fb*, *r_prd1*, and *r_prd2*.

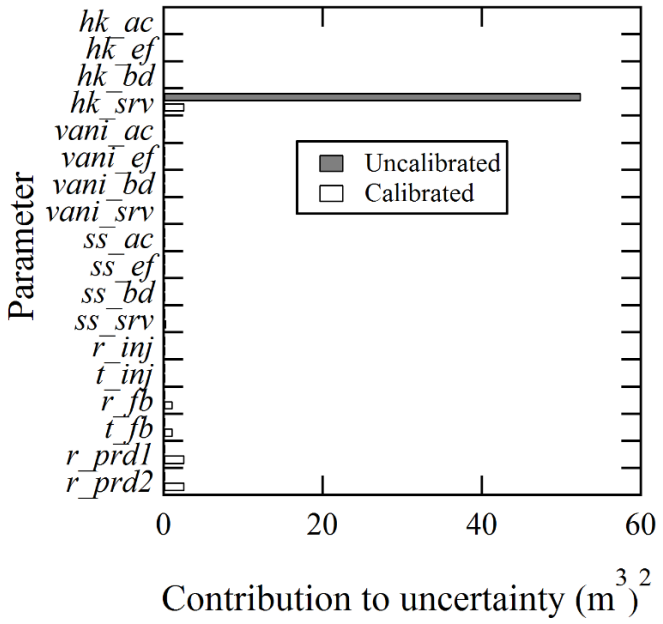

Figure 4.3. Precalibration (grey) and postcalibration (white) parameter contributions to uncertainty of cumulative leakage through the mud-filled leaky well 30 m from the horizontal well.

Parameter uncertainty bounds for the hydraulic conductivity of the SRV are significantly wider than those used for other parameters in the analysis, related to the large range in possible shale permeability after hydraulic fracturing occurs. The sensitivity analysis showed leakage was highly sensitive to *hk_srv* (Figure 4.2), and it is not surprising that the parameter significantly contributes to precalibration uncertainty. The decrease in postcalibration uncertainty contribution of *hk_srv* suggest at least some information is available in the calibration dataset to constrain the prediction. Minor postcalibration rises in uncertainty variance of *ss_srv*, *r_fb*, *t_fb*, *r_prd1*, and *r_prd2* are the result of correlation with other parameters during the calibration process that yielded improved reductions in predictive uncertainty. Increases in postcalibration parameter contributions to predictive uncertainty relative to their respective precalibration levels is not uncommon (Gallagher and Doherty 2007; James et al. 2009).

Observation Contributions to Predictive Uncertainty

Figure 4.4 details the effects of different observations on predictive uncertainty. The increase in predictive uncertainty variance of leakage due to removing a particular observation from the calibration dataset is shown in Figure 4.4a. The level of predictive uncertainty variance represents the exclusivity of information that resides in each observation for reducing uncertainty of leakage. Observations *h_inj*, *h_fb*, *sum_inj*, and *sum_fb* have a level of information that is not repeated in other observations that make up the calibration dataset. In contrast, some information from observations *h_2y* and *h_15y* is redundant with other observations.

Although a limited calibration dataset is applied to this model, the information content of each observation is fairly compartmentalized. However, the premise of the generated observations was to provide a set of observations relevant to each major phase (i.e., injection, flowback, production) at the horizontal well. Because few observations are used, the low exclusivity content of observations *h_2y* and *h_15y* is explained by these observations containing information about heads in the reservoir over the production period at the horizontal well.

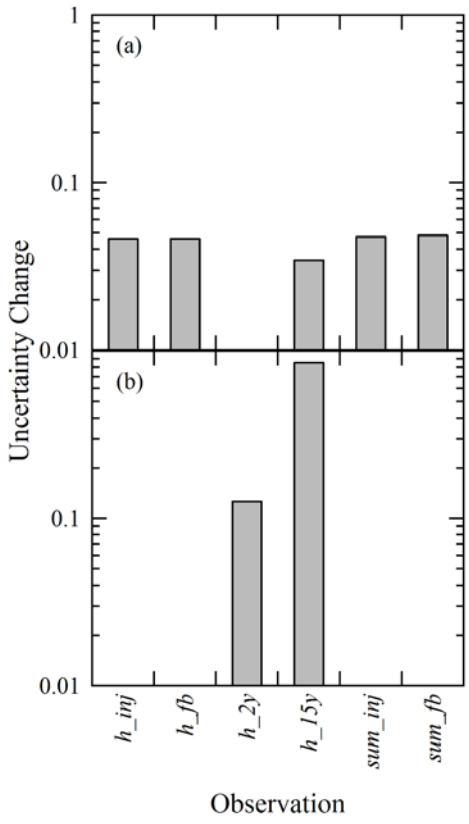

Figure 4.4. (a) increase in postcalibration predictive uncertainty variance with omission of each observation for the mud-filled leaky well 30 m from the horizontal well. (b) decrease in postcalibration predictive uncertainty variance with inclusion of each observation for the mud-filled leaky well 30 m from the horizontal well.

Figure 4.4b shows the decrease in precalibration predictive uncertainty variance if a particular observation is used as the sole member of the calibration dataset. Resulting decreases in precalibration predictive uncertainty variance are an indicator of the information content of each observation in reducing uncertainty in leakage. Head observations at the horizontal well over the production period, *h_2y* and *h_15y*, have the highest information content toward reducing predictive uncertainty.

The higher information content of observation *h_15y* shows that although information between observations in the calibration dataset is somewhat exclusive (Figure 4.4a), head observations at the horizontal well over longer time periods are most

valuable in reducing predictive uncertainty of leakage (Figure 4.4b). Clearly, accurate measurements of production rates and pressures within the shale are crucial to properly assess potential long-term effects of hydraulic fracturing on upward leakage along abandoned wells. If predictions of leakage over shorter time periods are of interest, accurate measurements of injection and flowback rates and volumes would likely become more valuable in reducing predictive uncertainty. For example, abandoned and converted oil and gas wells can be in close proximity to horizontal wells (Brownlow et al. 2016b), and leakage could occur during or immediately following hydraulic fracturing if a hydraulic fracture intersects a pathway to an abandoned oil and gas well.

Parameter Identifiability and Uncertainty Reduction

The capability of the model to constrain parameters was computed on the basis of truncation of six singular values (Figure 4.5). Three parameters are highly (~1.0) identifiable: *ss_srv*, *r_prd1*, and *r_prd2*. Five parameters, *hk_srv*, *r_inj*, *t_inj*, *r_fb*, and *t_fb* are moderately identifiable. The remaining ten parameters have little to no identifiability. Parameters with little identifiability are associated with a lack of relevant information in the calibration dataset to constrain that parameter. If leakage is sensitive to a parameter that lacks identifiability, the calibration process will not achieve a reduction in uncertainty of leakage with the existing calibration dataset.

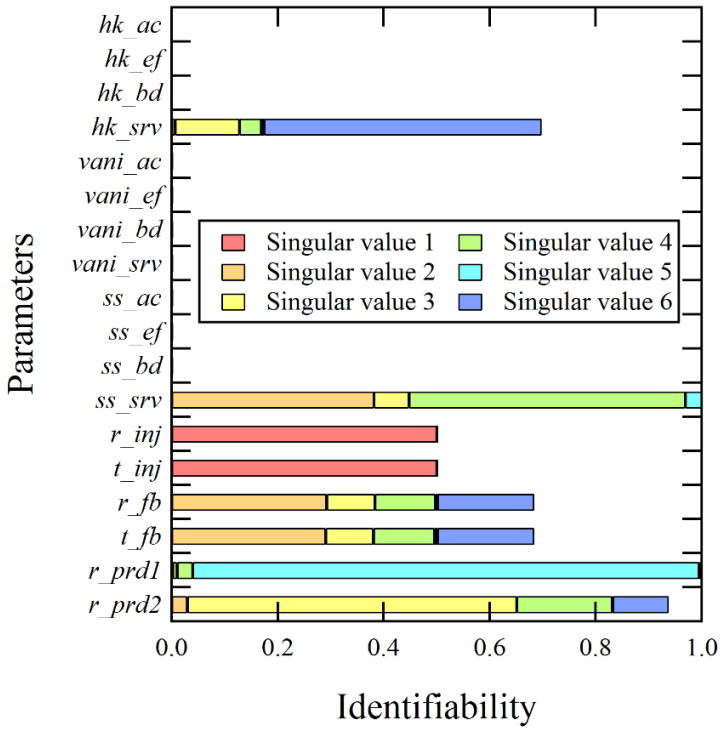

Figure 4.5. Identifiability, or estimability, of parameters used in the analysis of the mud-filled leaky well at 30 m from horizontal well. Parameter identifiability is shown as a stacked bar representing the sum of contribution from each singular value.

The high identifiability of parameter *ss_srv* is mostly related to the inclusion of injection volume (*sum_inj*) and head after injection (*h_inj*) observations in the calibration dataset. Although parameter *ss_srv* does not greatly contribute to predictive uncertainty (Figure 4.3), leakage is sensitive it (Figure 4.2). Therefore, there is at least some benefit to including injection-related data in the analysis. Unfortunately, leakage is more sensitive to parameter *hk_srv* than *ss_srv* (Figure 4.2), and *hk_srv* has only moderate identifiability (~0.7). Further constraints on parameter *hk_srv* could be imposed if additional information relevant to the parameter were added to the calibration dataset, but current observations do not carry sufficient data for an accurate estimation of *hk_srv*. In contrast to *hk_srv*, parameters *r_prd1* and *r_prd2* are highly identifiable due to the

inclusion of head observations over the production period in the calibration dataset. Because leakage is sensitive to early and late-stage production rates at the horizontal well, the model can impose reliable constraints on parameters *r_prd1* and *r_prd2*.

Figure 4.6 depicts relative parameter uncertainty variance reduction for each parameter. Trends in relative parameter uncertainty variance are similar to those expressed by the parameter identifiability plot (Figure 4.5). There is little to no reduction in parameter uncertainty variance for ten parameters due to a lack of relevant available information in the calibration dataset. However, parameters without visible reductions in parameter uncertainty variance also tend to contribute little to predictive uncertainty in leakage (Figure 4.3). The *r_prd2* parameter is highly identifiable (~1.0), but has a comparatively lower level (~0.8) of parameter uncertainty variance reduction. Larger reductions in parameter uncertainty variance for *r_prd2* might be achieved with additional long-term pressure measurements in the calibration dataset.

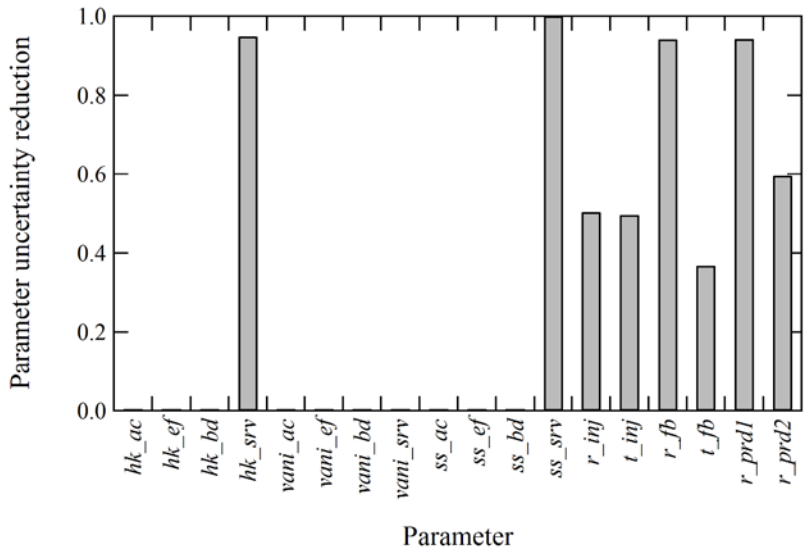

Figure 4.6. Relative uncertainty variance reduction from precalibration level for each parameter used in the analysis of the mud-filled leaky well 30 m from the horizontal well.

Nonlinear Analysis

Calibration-constrained Minimization and Maximization

Nonlinear analyses used four adjustable parameters: *hk_srv*, *ss_srv*, *r_prd1*, and *r_prd2*. Nonlinear analysis of the model using the limited calibration dataset resulted in a minimized leakage of 0.08 m^3, and maximized leakage of 2.85 m^3. The minimized leakage prediction is close to two standard deviations less than that of the calibrated model. The maximized leakage prediction is only slightly larger than the reported 2.7 m^3 value in the calibrated model. Typically, it is expected that minimized and maximized values would approach three standard deviations of predictive uncertainty. The minimized leakage approaches zero because three standard deviations would result in negative leakage. The maximized leakage is expected to approach a value close to 7.5 m^3, based on an uncertainty standard deviation of 1.6 m^3. The minor increase in the maximized leakage relative to the leakage value in the calibrated model could be attributed to parameters *r_inj*, *t_inj*, *r_fb*, and *t_fb* not being included in the nonlinear analysis. Linear analysis showed that these parameters contribute a measure of predictive uncertainty to the analysis (Figure 4.3).

Calibration-constrained NSMC

In total, 500 parameter sets were generated for the NSMC analysis. Each set parameter set comprised 20 fixed parameters, in addition to the four adjustable parameters used in the constrained minimization/maximization analysis. After the optimization process, all of the parameter sets resulted in objective functions below the

target measurement objective function. The frequency distribution for leakage from model parameterization with the 500 modified parameter sets is shown in Figure 4.7. The NSMC analysis yields leakages within bounds predicted by the constrained minimization/maximization process of 0.08 to 2.8 m^3. The probability distribution of leakage from the 500 modified parameter sets show the majority of realizations fall near the calibrated leakage (2.7 m^3), and tail off towards near-zero leakage. The distribution of leakage suggest that in some cases leaky wells may leak exceptionally small volumes (< 1 m^3). The possibility of relatively small volumes of leakage suggests that small variations in hydraulic properties of the shale (e.g., permeability) and mud-filled leaky well (e.g., mud density) could lead to cases where upward leakage simply does not occur.

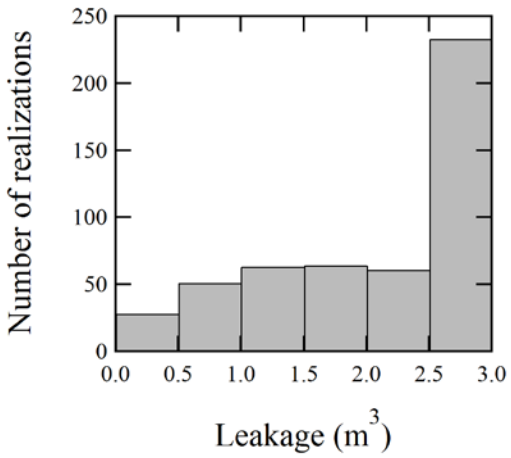

Figure 4.7. Histogram of calibration-constrained cumulative leakage volumes after 15 years of simulation time through a mud-filled leaky well 30 m from the horizontal well.

Conclusions

This study provides an analysis of uncertainty for a simple hypothetical model of upward leakage along an abandoned and converted oil and gas well in the stimulated reservoir of hydraulically fractured shale. The numerical model was calibrated by

developing a series of observations from analytical solutions and measurements for a horizontal well. The development of the calibration dataset permitted model interrogation using common methods for sensitivity, linear, and nonlinear uncertainty analyses. The results of the analysis emphasize the additional insight that can be gleaned from a simple numerical model with the addition of relatively few observations. The analysis revealed the following points concerning model predictive capabilities and future leakage assessments:

- The range in shale permeability after hydraulic fracturing contributes the most to predictive uncertainty in leakage.
- Rate and duration of flowback after hydraulic fracturing plays a significant role in the potential for upward flow along leaky wells.
- Horizontal-well production rates and reservoir-pressure measurements in the shale are crucial observations for evaluating potential long-term leakage.
- Improved reporting of certain well measurements in public records would improve characterization of risk for leakage. In particular, well-specific data regarding flowback volumes and rates, and volumes of water co-produced with hydrocarbons are highly beneficial data for leakage assessments.

In summary, this paper demonstrates the utility of exploratory uncertainty assessments given a simple hypothetical model and limited calibration dataset. Such analyses provide an important first step for assessing potentially “new” environmental risks with numerical models when few measurements are available for model calibration. The results of this study should be considered in the development of similar models with increased complexity.

Acknowledgements

Funding for this work was provided by the Evergreen Underground Water Conservation District, the Wintergarden Groundwater Conservation District, and the C. Gus Glasscock Jr. Endowed Fund for Excellence in Environmental Sciences.

CHAPTER FIVE

Conclusions

This study evaluated potential risks associated with hydraulic fracturing near abandoned oil and gas wells, with attention to abandoned oil and gas wells converted into water wells. Four investigations were conducted: (1) development of a numerical model to assess magnitude of upward leakage along a leaky abandoned well in proximity of hydraulic fracturing, (2) characterization of abandoned and converted oil and gas wells and probability of their intersection with stimulated areas surrounding horizontal wells, (3) interrogation of model uncertainty and evaluation of data crucial for future investigations, and (4) preliminary assessment of an organic geochemical fingerprint to identify potential groundwater quality impacts.

Leaky wells near hydraulic fracturing could facilitate upward migration of fluids over shorter timescales compared to natural geological pathways. Each sedimentary basin is unique, and evaluation of leaky wells as potential pathways for contaminants requires critical review of historical oil and gas activities. Certain abandoned wells, such as leaky converted wells, represent potential conduits for upward flow to aquifers because they are open to both a deep formation and an overlying aquifer. However, upward flow to an overlying aquifer due to hydraulic fracturing of shale requires a unique series of circumstances. The four investigations revealed the following about potential groundwater risks from hydraulic fracturing near leaky abandoned oil and gas wells:

1. Hydraulic fracturing of shale could pose a risk to groundwater if certain spatial and hydraulic conditions exist. The largest potential for upward

leakage into an overlying aquifer is posed by a frac hit on an abandoned oil and gas well converted into a water well.

2. The probability of a frac hit can be approximated by establishing the intersection of an abandoned oil and gas well with stimulated reservoir volume of a horizontal well. Such an intersection does not conclusively demonstrate that a frac hit has or will occur, nor imply that leakage to an overlying aquifer will occur, but the potential exists.
3. Predictive uncertainty in potential upward leakage could be reduced if certain measurements are available. These measurements include: (1) rate and duration of flowback at the horizontal well, (2) long-term production rates at the horizontal well, (3) permeability and pressures in the hydraulically fractured shale, and (4) hydraulic characteristics of the abandoned oil and gas well.
4. Evidence for a frac hit may manifest as a rapid drop in treatment pressure at a horizontal well or rapid rise in water level at a nearby converted well during hydraulic fracturing. Upward fluid leakage following a frac hit could be identified by site-specific organic geochemical fingerprints of reservoir pore-fluids and correlation with organic composition of groundwater.

In summary, this work examines a newly considered potential mechanism for upward flow to shallow aquifers overlying unconventional shale plays. The methods applied in this study are applicable to other unconventional shale plays where similar leaky abandoned wells exist. Overall, results underscore the need to evaluate historical oil

and gas activities in areas with modern unconventional oil and gas activities, and improve historical and future data contained in public records.

APPENDICES

APPENDIX A

Copyright Permissions

Permission granted for Brownlow, J.W., S.C. James, and J.C. Yelderman, Jr. 2016. Influence of hydraulic fracturing on overlying aquifers in the presence of leaky abandoned wells. Groundwater. dx.doi.org/10.1111/gwat.12431

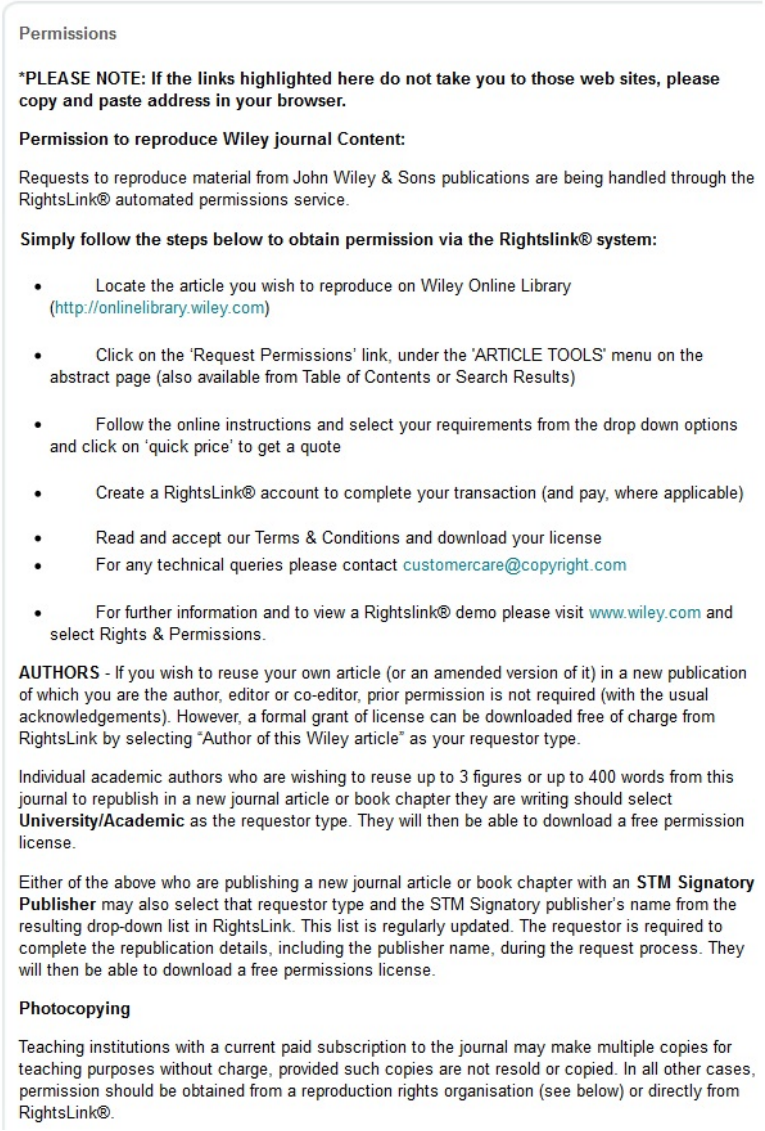

Permissions

***PLEASE NOTE: If the links highlighted here do not take you to those web sites, please copy and paste address in your browser.**

Permission to reproduce Wiley journal Content:

Requests to reproduce material from John Wiley & Sons publications are being handled through the RightsLink® automated permissions service.

Simply follow the steps below to obtain permission via the Rightslink® system:

- Locate the article you wish to reproduce on Wiley Online Library (http://onlinelibrary.wiley.com)
- Click on the 'Request Permissions' link, under the 'ARTICLE TOOLS' menu on the abstract page (also available from Table of Contents or Search Results)
- Follow the online instructions and select your requirements from the drop down options and click on 'quick price' to get a quote
- Create a RightsLink® account to complete your transaction (and pay, where applicable)
- Read and accept our Terms & Conditions and download your license
- For any technical queries please contact customercare@copyright.com
- For further information and to view a Rightslink® demo please visit www.wiley.com and select Rights & Permissions.

AUTHORS - If you wish to reuse your own article (or an amended version of it) in a new publication of which you are the author, editor or co-editor, prior permission is not required (with the usual acknowledgements). However, a formal grant of license can be downloaded free of charge from RightsLink by selecting "Author of this Wiley article" as your requestor type.

Individual academic authors who are wishing to reuse up to 3 figures or up to 400 words from this journal to republish in a new journal article or book chapter they are writing should select **University/Academic** as the requestor type. They will then be able to download a free permission license.

Either of the above who are publishing a new journal article or book chapter with an **STM Signatory Publisher** may also select that requestor type and the STM Signatory publisher's name from the resulting drop-down list in RightsLink. This list is regularly updated. The requestor is required to complete the republication details, including the publisher name, during the request process. They will then be able to download a free permissions license.

Photocopying

Teaching institutions with a current paid subscription to the journal may make multiple copies for teaching purposes without charge, provided such copies are not resold or copied. In all other cases, permission should be obtained from a reproduction rights organisation (see below) or directly from RightsLink®.

Copyright Permissions

Permission granted for Brownlow, J.W., J.C. Yelderman, Jr., and S.C. James. 2016. Spatial risk analysis of hydraulic fracturing near abandoned and converted oil and gas wells. Groundwater. dx.doi.org/10.1111/gwat.12471

Permissions

***PLEASE NOTE: If the links highlighted here do not take you to those web sites, please copy and paste address in your browser.**

Permission to reproduce Wiley journal Content:

Requests to reproduce material from John Wiley & Sons publications are being handled through the RightsLink® automated permissions service.

Simply follow the steps below to obtain permission via the Rightslink® system:

- Locate the article you wish to reproduce on Wiley Online Library (http://onlinelibrary.wiley.com)
- Click on the 'Request Permissions' link, under the 'ARTICLE TOOLS' menu on the abstract page (also available from Table of Contents or Search Results)
- Follow the online instructions and select your requirements from the drop down options and click on 'quick price' to get a quote
- Create a RightsLink® account to complete your transaction (and pay, where applicable)
- Read and accept our Terms & Conditions and download your license
- For any technical queries please contact customercare@copyright.com
- For further information and to view a Rightslink® demo please visit www.wiley.com and select Rights & Permissions.

AUTHORS - If you wish to reuse your own article (or an amended version of it) in a new publication of which you are the author, editor or co-editor, prior permission is not required (with the usual acknowledgements). However, a formal grant of license can be downloaded free of charge from RightsLink by selecting "Author of this Wiley article" as your requestor type.

Individual academic authors who are wishing to reuse up to 3 figures or up to 400 words from this journal to republish in a new journal article or book chapter they are writing should select **University/Academic** as the requestor type. They will then be able to download a free permission license.

Either of the above who are publishing a new journal article or book chapter with an **STM Signatory Publisher** may also select that requestor type and the STM Signatory publisher's name from the resulting drop-down list in RightsLink. This list is regularly updated. The requestor is required to complete the republication details, including the publisher name, during the request process. They will then be able to download a free permissions license.

Photocopying

Teaching institutions with a current paid subscription to the journal may make multiple copies for teaching purposes without charge, provided such copies are not resold or copied. In all other cases, permission should be obtained from a reproduction rights organisation (see below) or directly from RightsLink®.

Copyright Licensing Agency

Institutions based in the UK with a valid photocopying and/or digital license with the Copyright Licensing Agency may copy excerpts from Wiley books and journals under the terms of their license. For further information go to CLA.

Copyright Clearance Center

Institutions based in the US with a valid photocopying and/or digital license with the Copyright Clearance Center may copy excerpts from Wiley books and journals under the terms of their license, please go to CCC.

Other Territories: Please contact your local reproduction rights organisation.

For further information please visit www.wiley.com and select Rights & Permissions.

If you have any questions about the permitted uses of a specific article, please contact us.

Permissions Department
John Wiley & Sons Ltd.
The Atrium,
Southern Gate,
Chichester
West Sussex, PO19 8SQ
UK
Email: Permissions@wiley.com
Fax: 44 (0) 1243 770620

or

Permissions Department
John Wiley & Sons Inc.
111 River Street MS 4-02
Hoboken, NJ 07030-5774
USA
Email: Permissions@wiley.com
Fax: (201) 748-6008

APPENDIX B.1

Derivation of Model Parameters

Reservoir Parameters

Depth-dependence was applied to certain properties (temperature, pressure, and salinity) to *in-situ* reservoir pore fluid (fluid density and dynamic viscosity), which are and used when calculating hydrogeologic parameters (storativity, hydraulic conductivity, and hydraulic head). Salinity data were obtained from the U.S. Geological Survey National Produced Waters Geochemical Database (Blondes et al. 2015). Reservoir salinity was at 50,000 mg/l at the top of the upper reservoir and increased to 60,500 mg/l at the base of the lower reservoir, yielding a salinity gradient of approximately 50 mg/l · m. Reservoir temperature was calculated using a geothermal gradient of 36.5°C/km and average annual surface temperature of 26.7°C (Loucks et al. 1984). Reservoir pressures were calculated using a pressure gradient of 10.5 MPa/km (Burke et al. 2013). Hydrostatic conditions are not applied because the Eagle Ford Shale is overpressured within the play area, and pressure gradients range from 10.5 to 18.1 MPa/km (Burke et al. 2013).

Reservoir pore fluid density and dynamic viscosity were calculated after Batzle and Wang (1992).Calculated fluid densities assume sodium chloride is the dominant dissolved component based on chemical composition data of formation waters in south Texas (Blondes et al. 2015).

Hydraulic heads were computed by dividing reservoir pressures by the specific weights (ρg) of the pore fluid. The elevation term, z [m], was taken as depth relative to

the base of the model. Hydraulic head (h_{hyd}) was calculated for each reservoir as described by (Hubbert 1940):

$$h_{hyd} = \frac{P_f}{\rho g} + z\,, \qquad \text{(Eq. B1.1)}$$

where P_f [Pa] is calculated fluid pressure, g [m/s^2] is gravitational acceleration, and ρ [kg/m^3] is fluid density. The hydraulic head in the confined aquifer layer is known from water-level measurements (2310 to 2250 m). Hydraulic head in the interburden layer interpolated between head in the aquifer and computed heads in the reservoirs.

Ranges and averages for intrinsic permeability for conventional reservoirs were obtained from literature (Stapp 1977; Dawson et al. 1995; Martin et al. 2011). In this model, the intrinsic permeability of both conventional reservoirs was specified as 10^{-17} m^2. Mean matrix permeabilities for the Eagle Ford Shale range from 10^{-18} to 10^{-21} m^2 (Chaudhary et al. 2011; Martin et al. 2011; McKeon 2011). Here, the updip (shallower) portion of the Eagle Ford Shale play is modeled, and permeability is 7×10^{-19} m^2 for the unfractured shale. Intrinsic permeability of the interburden was set to 10^{-20} m^2 (Harrison and Summa 1991). Permeability anisotropy (k_h:k_v = 100) in the interburden was selected based on values from previous studies (Bethke 1989; Harrison and Summa 1991). Interburden and reservoir permeabilities are reasonable, based on comparison to pressure seals analyses (Downey 1984; Deming 1994).

Hydraulic conductivities were calculated as (Freeze and Cherry 1979):

$$K = \frac{k_i \rho g}{\mu}\,, \qquad \text{(Eq. B1.2)}$$

where k_i [m^2] is intrinsic permeability, ρ is fluid density, and μ [kg/m · s] is fluid dynamic viscosity. The presence of multiple fluid phases reduces K and water saturation in the

reservoirs ranges from 15 to 85% (Stapp 1977; Dawson et al. 1995). All reservoir hydraulic conductivities were therefore reduced by ~2.5 orders of magnitude after Morel-Seytoux et al. (1996) using a water saturation of 35% (where the fitted parameter, n, = 2.5). Multiphase fluids are also present throughout the interburden, and the calculated interburden K was also reduced (assuming a water saturation of 85% and n = 2.5, see Morel-Seytoux et al. 1996).

Storativity was estimated as (Cooper 1966):

$$S = S_s b\,, \qquad \text{(Eq. B1.3)}$$

$$S_s = \rho_w g(c_r + \varphi\beta)\,, \qquad \text{(Eq. B1.4)}$$

where S_s [1/m] is the specific storage, ρ_w [kg/m^3] is water density, φ [-] is porosity, c_r [m^2/N] is rock compressibility, β [m^2/N] is water compressibility, and b [m] is reservoir thickness. Water compressibility ranges from 4.4×10^{-10} to 4.8×10^{-10} m^2/N (Domenico and Schwartz 1998; Freeze and Cherry 1979), and the average of these values was used. Rock compressibility for the Austin Chalk and Buda was set to 10^{-10} m^2/N (Domenico and Schwartz 1998; Donnez 2007). Rock compressibilities for the Eagle Ford Shale are typically higher than for conventional reservoirs based on high percent of smectite in the clay minerals (Hsu and Nelson 2002; McKeon 2011). Eagle Ford Shale reservoir simulations use rock compressibilities between 10^{-8} and 10^{-9} m^2/N, and the average value of 5×10^{-9} m^2/N is sometimes used (Medeiros et al. 2008; Bazan et al. 2010; Chaudhary et al. 2011; Sheng and Chen 2013; Suliman et al. 2013). Here, we use this average.

APPENDIX B.2

Approximation of SRV Extent and Effective Reservoir Permeability

Stimulated Reservoir Permeability and Volume

Hydraulic fracturing in the model occurs along a 1,500-m horizontal well in twenty separate 75-m stages. Each treatment stage typically has 4 to 8 perforation clusters (Bazan et al. 2010; Inamdar et al. 2010; Stegent et al. 2010; McKeon 2011; Syfan et al. 2013). For this model, the fracture growth in each stage is assumed to interact and propagate within the same overall fracture network, so that one large fracture network is developed along the perforated interval length (e.g., Bazan et al. 2010). The dimensionless fracture density for the model is:

$$N_{\mathrm{f}} = \frac{w_{\mathrm{f}}}{x_{\mathrm{f}}}, \qquad \text{(Eq. B2.1)}$$

where w_{f} [m] is the hydraulic fracture width and x_{f} [m] is the average spacing of hydraulic fractures. Hydraulic fracture width varies between 3 and 10 mm (Economides and Nolte 2000). Here, we assume two fractures are generated per stage and: w_{f} = 7.5 mm; x_{f} = 37.5 m. This yields an approximate dimensionless fracture density of 2×10^{-4}. The effective permeability of the stimulated reservoir is generalized as:

$$k_{\mathrm{eff}} = k_{\mathrm{f}} N_{\mathrm{f}} + k_{\xi}(1 - N_{\mathrm{f}}), \qquad \text{(Eq. B2.2)}$$

where k_{ξ} [m^2] is the matrix permeability of the reservoir and k_{f} [m^2] is the permeability of the hydraulic fractures. The matrix permeability can be difficult to quantify, and core measurements are typically orders of magnitude lower than the effective shale permeability (Chaudhary et al. 2011; Tian et al. 2013; Alotaibi et al. 2015). Mean matrix

permeabilities for the Eagle Ford Shale range from 10^{-18} to 10^{-21} m^2 (Chaudhary et al. 2011; Martin et al. 2011; McKeon 2011). Hydraulic fracture permeabilities are higher, and can range as high as 8×10^{-11} m^2 (Bazan et al. 2010; Chaudhary et al. 2011). Here, the following values are used: $k_f = 2 \times 10^{-12}$ m^2 and $k_\xi = 7 \times 10^{-19}$ m^2 resulting in $k_{eff} = 4 \times 10^{-16}$ m^2. The estimated value is consistent with previous studies that documented average permeabilities for the stimulated reservoir ranging from 2×10^{-19} to 8×10^{-14} m^2 (Medeiros et al. 2008; Bazan et al. 2010; Suliman et al. 2013; Alotaibi et al. 2015).

To approximate the SRV, hydraulic fractures are assumed to be a straight, planar, height-fixed fractures confined by reservoir layers. This two-dimensional fracture geometry is known as the PKN (Perkins-Kern-Nordgren) model (Economides and Nolte 2000). The half-length of the (symmetric) hydraulic fracture (L_f) can be described as a function of the injection time (Economides and Nolte 2000; Shapiro and Dinske 2009a; Shapiro and Dinske 2009b):

$$L_f(t) = \frac{Qt}{4h_f C_L \sqrt{2t} + 2h_f w_f}, \qquad \text{(Eq. B2.3)}$$

and

$$C_L \approx \sqrt{\frac{k_{eff}\varphi c_f}{\pi\mu}} \cdot \Delta P_{inj}, \qquad \text{(Eq. B2.4)}$$

where Q [m^3/s] is the average injection rate, t [s] is time, h [m] is the average fracture height, w [m] is the average fracture width, and C_L [m/s$^{1/2}$] is the fluid-loss coefficient. The injection rate for this model is 0.158 m^3/s, a typical rate for Eagle Ford stimulation (Martin et al. 2011). The fluid-loss coefficient is estimated using k_{eff}, φ, c_f [1/Pa] the compressibility of the reservoir fluid, μ, and ΔP_{inj} [Pa] the pressure difference between the fracture and the far-field reservoir. Here, we use the following values: $k_{eff} = 4 \times 10^{-16}$ m^2;

$\varphi = 0.1$; $c_f = 5 \times 10^{-9}$ Pa^{-1}; $\mu = 3.5 \times 10^{-4}$ Pa · s; $\Delta P_{inj} = 15$ MPa. The estimated leakage coefficient is $C_L = 2 \times 10^{-4}$ m/s$^{1/2}$, which falls within the range reported by Economides and Nolte (2003) of 2×10^{-3} and 2×10^{-5} m/s$^{1/2}$, and is similar to leakage coefficients estimated by Shapiro et al. (2006).

Use of the estimated leak-off coefficient in (B2.4) yields an estimated fracture half-length ($t = 1$ hr) of $L_f = 140$ m. Hydraulic fracture half-lengths in the Eagle Ford are reported between 100 and 300 m, therefore our calculated value is realistic (Bazan et al. 2010; Chaudhary et al. 2011; Jaripatke et al. 2014). Using L_f, the SRV in the model is calculated assuming a 60-m-thick shale reservoir and a 1,500-m horizontal well for total SRV = 2.5×10^7 m^3, an acceptable volume based on previous studies (Bazan et al. 2010; Mayerhofer et al. 2010; Zimmer 2011; Basu et al. 2012; Suliman et al. 2013).

Hydraulic Diffusivity

In the limit of a long-term injection, the apparent hydraulic diffusivity of the fractured domain is calculated as (Shapiro et al. 2006):

$$D_{ap} = \frac{Q^2}{128\pi h_f^2 C_L^2}. \qquad \text{(Eq. B2.5)}$$

Hydraulic diffusivities within the SRV vary between 0.3 and 4.0 m^2/s (Shapiro et al. 1997; Shapiro et al. 2006; Shapiro and Dinske 2009b; Yu et al. 2012). Here, a value of $D_{ap} = 0.42$ m^2/s is given. To estimate the hypothetical maximum extent of hydraulic fracturing (microseismic triggering front), the known triggering front equation was used (Shapiro et al. 1997):

$$L = \sqrt{4\pi D_{ap} t}. \qquad \text{(Eq. B2.6)}$$

At t = 1 hr, the triggering front is 140 m. The hydraulic diffusivity of the hypothetical hydraulic fracture is also calculated as (Shapiro et al. 2006):

$$D_{\mathrm{f}} = \frac{k_{\mathrm{f}}}{c_{\mathrm{t}}\mu_{\mathrm{t}}\varphi_{\mathrm{f}}}, \qquad \text{(Eq. B2.7)}$$

where φ_{f} is the porosity of the proppant pack, and c_{t} and μ_{t} are the compressibility and viscosity of the treatment fluid, respectively. The viscosity of the treatment fluid, which can vary by orders of magnitude, significantly influences D_{f}. Eagle Ford Shale operators typically apply slickwater treatments (μ_{f} ranges from 2×10^{-3} to 3×10^{-3} Pa · s), although some operators use higher viscosity fluids (e.g., hybrids and cross-link types) with μ_{f} ranging from 0.01 to 1.0 Pa · s (Martin et al. 2011; Boschee 2014; Jaripatke et al. 2014). Here, we assume $c_{\mathrm{f}} \approx 4.44 \times 10^{-10}$ 1/Pa (assuming the compressibility of the treatment fluid is similar to that of water), $\mu_{\mathrm{f}} = 3 \times 10^{-3}$ Pa · s (viscosity of slickwater), and φ_{f} = 0.35. This yields D_{f} = 4.2 m^2/s, similar to values reported by Shapiro et al. (2006) for hydraulic fractures.

Fracture Conductivity

To compare the selected fracture permeability and width, we compute the fracture conductivity which is considered a key parameter in hydraulic-fracture treatment design:

$$C_{\mathrm{f}} = k_{\mathrm{f}} w_{\mathrm{f}}. \qquad \text{(Eq. B2.8)}$$

Fracture conductivity in the Eagle Ford Shale ranges from 1.4×10^{-16} to 8.4×10^{-14} m^3 with an average value of 2.5×10^{-14} m^3 sometimes used in simulations of hydraulically fractured shale (Bazan et al. 2010; Chaudhary et al. 2011; Morsy et al. 2013; Sheng and Chen 2014). For $k_{\mathrm{f}} = 2 \times 10^{-12}$ m^2 and w_{f} = 7.5 mm, $C_{\mathrm{f}} = 1.5 \times 10^{-14}$ m^3.

To evaluate if L_f and selected the hydraulic-fracture permeability are compatible, we compute the dimensionless fracture conductivity, which is another key parameter for hydraulic fracturing design (Economides and Nolte, 2000):

$$C_{fD} = \frac{k_f w_f}{k_\xi L_f}. \qquad \text{(Eq. B2.9)}$$

Note that the term in the numerator is C_f from (B2.8). For L_f = 140 m, C_{fD} = 150. Typical values for C_{fD} range from 25 to 1,600 in the Eagle Ford Shale (Bazan et al. 2010; Chaudhary et al. 2011; Syfan et al. 2013), with higher values associated with lower matrix permeabilities (Economides and Nolte 2000).

APPENDIX B.3

Hydraulic Heads for Upper and Lower Shale Layers

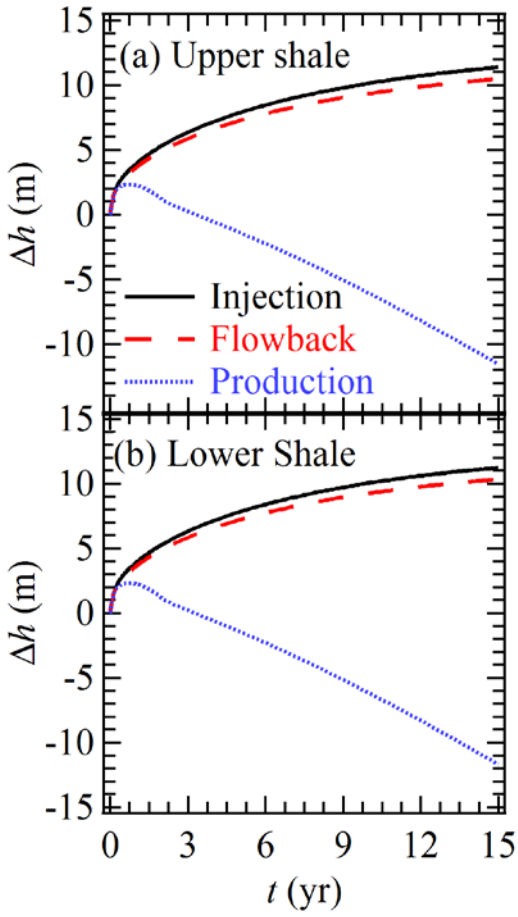

Figure B.3. Simulated changes in hydraulic head for each hydraulic-fracturing scenario (i.e., injection, injection with flowback, and injection with flowback and production): (a) in shale layer 12 above the horizontal well; and (b) in shale layer 14 below the horizontal well.

APPENDIX B.4

Flow through Leaky Wells without Hydraulic Fracturing

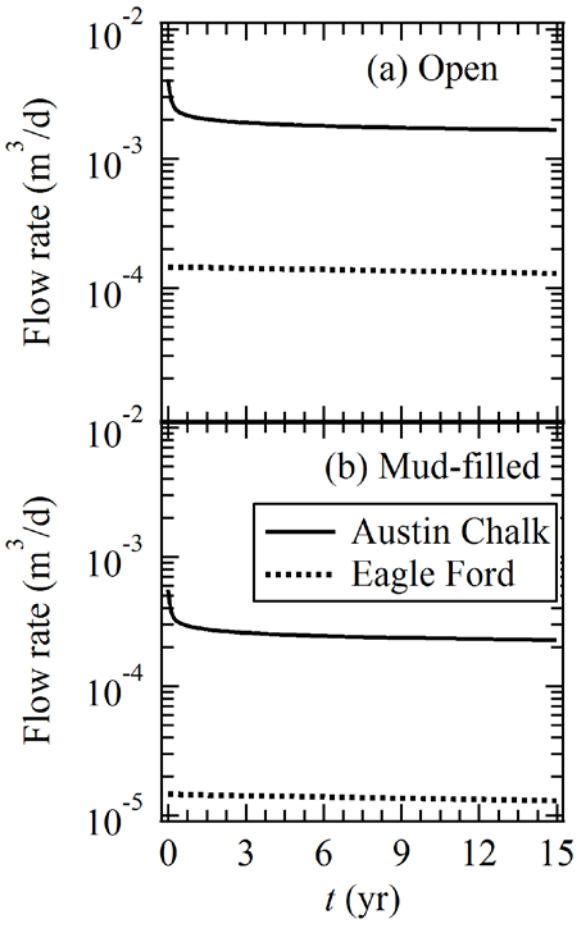

Figure B.4. Simulated discharge through a leaky well screened in the Austin Chalk or Eagle Ford Shale into the overlying aquifer without hydraulic fracturing: (a) open leaky well, and (b) mud-filled leaky well. Barriers to upward flow through the borehole are assumed to have failed at the beginning of the simulation.

APPENDIX B.5

Steady-state Flow between Layers

Table B.5
Steady-state Flow between Layers

Layer No.	Flow to Above (m^3/d)	Flow from Above (m^3/d)	Flow to Below (m^3/d)	Flow from Below (m^3/d)	Total Flow In (m^3/d)	Total Flow Out (m^3/d)
1	-	-	5.2×10^{-7}	1.9×10^{-5}	1.0×10^{3}	1.0×10^{3}
2	1.9×10^{-5}	5.2×10^{-7}	2.1×10^{-7}	3.6×10^{-5}	1.0×10^{3}	1.0×10^{3}
3	3.6×10^{-5}	2.1×10^{-7}	-	5.6×10^{-5}	1.0×10^{3}	1.0×10^{3}
4	5.6×10^{-5}	-	-	5.8×10^{-5}	9.2×10^{-5}	9.2×10^{-5}
5	5.8×10^{-5}	-	-	5.7×10^{-5}	1.3×10^{-4}	1.3×10^{-4}
6	5.7×10^{-5}	-	-	5.7×10^{-5}	2.0×10^{-4}	2.0×10^{-4}
7	5.7×10^{-5}	-	-	6.0×10^{-5}	1.3×10^{-4}	1.3×10^{-4}
8	6.0×10^{-5}	-	-	7.8×10^{-5}	1.0×10^{-4}	1.0×10^{-4}
9	7.8×10^{-5}	-	-	1.2×10^{-4}	3.0×10^{-4}	3.0×10^{-4}
10	1.2×10^{-4}	-	-	4.0×10^{-5}	2.8×10^{-4}	2.8×10^{-4}
11	4.0×10^{-5}	-	-	1.7×10^{-6}	2.2×10^{-4}	2.2×10^{-4}
12	1.7×10^{-6}	-	-	8.7×10^{-7}	8.5×10^{-6}	8.5×10^{-6}
13	8.7×10^{-7}	-	-	5.2×10^{-7}	7.9×10^{-6}	7.9×10^{-6}
14	5.2×10^{-7}	-	-	4.1×10^{-7}	7.7×10^{-6}	7.7×10^{-6}
15	4.1×10^{-7}	-	-	2.0×10^{-7}	8.1×10^{-5}	8.1×10^{-5}
16	2.0×10^{-7}	-	-	-	8.1×10^{-5}	8.1×10^{-5}

APPENDIX C.1

County-level Well Data Summary for Active EFS Area

Table C.1

County-level Well Data Summary for Active EFS Area[†]

County	EFS horizontal wells		Abandoned wells		Converted wells		GCD
	Completed	Permitted	All	Deep	All	Deep	
Atascosa[‡]	565	326	3810	286	252	48	Yes
Bastrop	0	1	1384	190	94	72	Yes
Bee	25	6	3932	10	22	0	Yes
Brazos	54	178	1091	922	44	44	Yes
Burleson	26	147	1888	1377	42	32	Yes
DeWitt[‡]	1032	634	2006	25	124	7	Yes
Dimmit[‡]	1917	1086	2293	300	179	89	Yes
Fayette	87	46	1952	1157	28	10	Yes
Frio	145	151	2958	1586	193	127	Yes
Gonzales[‡]	1006	389	1661	803	139	108	Yes
Grimes	4	3	401	156	31	28	Yes
Karnes[‡]	1834	850	1678	142	29	4	Yes
La Salle[‡]	1864	1035	1481	217	264	115	Yes
Lavaca	145	159	2383	33	11	2	No
Lee	23	63	1151	738	69	69	Yes
Leon	9	9	1006	491	109	109	Yes
Live Oak[‡]	507	213	3992	16	25	5	Yes
Madison	11	11	560	310	25	25	Yes
Maverick	50	8	2187	262	21	6	No
McMullen[‡]	1190	683	3172	32	247	56	Yes
Milam	3	1	1805	56	40	15	Yes
Robertson	11	14	344	165	26	19	Yes
Walker	1	4	282	21	15	12	Yes
Webb[‡]	1290	525	7538	20	62	3	No
Wilson	148	43	2653	543	134	50	Yes
Zavala	198	122	2112	223	175	54	Yes
Total	12145	6707	55720	10081	2400	1109	

[†]Well databases accessed April 1, 2015.

[‡]County with significant (>500) existing EFS horizontal wells.

APPENDIX C.2

County-level Data for Wells that Intersect Existing EFS Horizontal Well SRAs

Table C.2

County-level Data for Wells that Intersect Existing EFS Horizontal Well SRAs[†]

County	Deep abandoned well group		Deep converted well group	
	No. wells (L_f = 30 m)[¶*]	No. wells (L_f = 600 m)	No. wells (L_f = 30 m)	No. wells (L_f = 600 m)
Atascosa[‡]	1 (1)	17 (35)	1 (1)	8 (22)
Bastrop	-	-	-	-
Bee	-	-	-	-
Brazos	16 (18)	105 (152)	-	-
Burleson	3 (3)	37 (41)	-	1 (1)
DeWitt[‡]	7 (8)	11 (42)	1 (1)	5 (15)
Dimmit[‡]	13 (14)	79 (157)	2 (1)	33 (63)
Fayette	1 (1)	19 (34)	1 (1)	2 (7)
Frio	3 (4)	54 (67)	-	7 (11)
Gonzales[‡]	17 (21)	187 (409)	2 (1)	25 (61)
Grimes	1 (1)	5 (5)	-	-
Karnes[‡]	11 (11)	72 (170)	-	2 (6)
La Salle[‡]	14 (14)	96 (175)	5 (1)	53 (132)
Lavaca	2 (5)	4 (14)	1 (4)	1 (10)
Lee	1 (1)	4 (5)	-	1 (1)
Leon	1 (1)	2 (2)	-	-
Live Oak[‡]	2 (2)	9 (23)	-	2 (6)
Madison	-	-	-	1 (1)
Maverick	7 (8)	13 (14)	-	2 (2)
McMullen[‡]	4 (5)	9 (18)	6 (1)	31 (74)
Milam	-	-	-	-
Robertson	-	9 (17)	-	-
Walker	-	-	-	-
Webb[‡]	3 (3)	11 (16)	-	-
Wilson	4 (5)	59 (108)	1 (1)	3 (3)
Zavala	1 (1)	21 (23)	-	7 (10)
Total	112 (127)	823 (1527)	20 (23)	184 (425)

[†]Well databases accessed April 1, 2015.

*Potential number of frac hits shown in parentheses.

[¶]L_f is the half-length of a symmetrical hydraulic fracture

[‡]County with significant (>500) existing EFS horizontal wells.

APPENDIX D.1

Description of Parameter Uncertainty Bounds and Calibrated Values

Table D.1
Description of Parameter Uncertainty Bounds and Calibrated Values

Parameter	Adjustable[1]	Unit	Lower Bound	Upper Bound	[2]Calibrated value	References	Notes
hk_aq	-	m/d	-	-	-	Thorkildsen and Price 1991; Mace 1999	Fixed
hk_int	-	m/d	-	-	-	Downey 1984; Thorkildsen and Price 1991; Deming 1994	Fixed
hk_ac	S/L	m/d	1.7×10^{-9}	3.7×10^{-4}	1.7×10^{-7}	Scott 1977; Snyder and Craft 1977; Guéguen and Palciauskas, 1994; Dawson et al. 1995; Martin et al. 2011	Range in *k*
hk_ef	S/L	m/d	1.0×10^{-11}	1.2×10^{-7}	1.2×10^{-8}	Scott 1977; Snyder and Craft 1977; Martin et al. 2011; Walls and Sinclair 2011	Range in *k*
hk_bd	S/L	m/d	2.6×10^{-10}	1.6×10^{-4}	1.8×10^{-7}	Scott 1977; Snyder 1977; Guéguen and Palciauskas, 1994	Range in *k*
hk_srv	S/L/N	m/d	9.0×10^{-10}	4.0×10^{-4}	6.7×10^{-7}	Medeiros et al. 2008; Bazan et al. 2010; Suliman et al. 2013; Tian et al. 2013; Alotaibi et al. 2015	Range in *k*
vani_aq	-	-	-	-	-	Thorkildsen 1991; Mace 1999	Fixed
vani_int	-	-	-	-	-	Harrison and Summa 1991	Fixed
vani_ac	S/L	-	10	120	100	Yeh et al. 1986; Mace 1998	Range in literature values
vani_ef	S/L	-	10	10000	1000	Begg and King 1985; Fogg 1986; Begg et al. 1987; Bethke 1989	Range in literature values for shales
vani_bd	S/L	-	10	120	100	Yeh et al. 1986; Mace 1998	Similar or lower than vani_ac
vani_srv	S/L	-	5	200	12.5	Economides and Nolte 2000	Range of decrease after injection
ss_aq	-	1/m	-	-	-	Thorkildsen and Price 1991; Mace 1999	Fixed
ss_int	-	1/m	-	-	-	Thorkildsen and Price 1991; Mace 1999	Fixed
ss_ac	S/L	1/m	1.1×10^{-6}	1.9×10^{-6}	1.2×10^{-6}	Dawson et al. 1995; Dawson 2000; Dawson and Almon 2010	Porosity ranges
ss_ef	S/L	1/m	1.0×10^{-5}	1.0×10^{-4}	5.0×10^{-5}	Dawson 2000; Dawson and Almon 2010; Martin et al. 2011; Walls and Sinclair 2011	Compressibility and porosity ranges
ss_bd	S/L	1/m	1.0×10^{-6}	1.2×10^{-6}	1.1×10^{-6}	Scott 1977; Snyder and Craft 1977	Porosity ranges
ss_srv	S/L/N	1/m	1.0×10^{-5}	1.0×10^{-4}	8.7×10^{-5}	Dawson 2000; Hsu and Nelson 2002; Dawson and Almon 2010; Martin et al. 2011; McKeon 2011; Walls and Sinclair 2011	Compressibility/porosity ranges
r_inj	S/L	m^3/d	15	92	50	Stegent et al. 2010; Martin et al. 2011; Stegent et al. 2011; Gomaa et al. 2014; Gu et al. 2015; Lecampion et al. 2015	Range in EFS injection rates
t_inj	S/L	d	0.28	1.67	0.93	Stegent et al. 2010; Martin et al. 2011; Stegent et al. 2011; Gomaa et al. 2014; Gu et al. 2015; Lecampion et al. 2015	Range in EFS injection times
r_fb	S/L	m^2/d	2.9×10^{-5}	2.9×10^{-3}	5.1×10^{-4}	Boschee 2014; RRC 2016	Order of magnitude range in flowback rates
t_fb	S/L	d	1	33	13.7	RRC 2016	Time between injection and production
r_prd1	S/L/N	m^3/d	−0.04	−0.1	−0.096	Inamdar et al. 2010; Ilk et al. 2012; Alotaibi et al. 2015; RRC 2016	Range in early-stage production rates
t_prd1	-	d	-	-	-	RRC 2016	Production decline inflection point
r_prd2	S/L/N	m^3/d	−0.005	−0.04	−0.039	Inamdar et al. 2010; Ilk et al. 2012; Alotaibi et al. 2015; RRC 2016	Range in late-stage production rates
t_prd2	-	d	-	-	-	RRC 2016	Production decline inflection point
h_mud	S	m	-	-	-	-	Mud column extends to aquifer base

[1]S/L/N = parameter adjustable during sensitivitiy, linear and nonlinear analyses, respectively

[2]Calibrated values are shown for scenario of mud-filled leaky well at 30 m from horizontal well

APPENDIX D.2

Description of Parameter Uncertainty Bounds and Calibrated Values

Table D.2
Well Measurements Used to Develop Observations

Measurement	Value	Unit[1]
Tubing inside diameter	1.9	inches
Tubing flowing pressure	1200	PSI
Oil production rate	700	STB/d
Water production rate	300	STB/d
Gas production rate	65	Mscf/d
Producing gas-liquid ratio	65	scf/STB
Solution gas-oil ratio	93	scf/STB
Water cut	30	%
Oil gravity	33	API
Water specific gravity	1.05	[-]
Gas specific gravity	0.65	[-]
Wellhead temperature	100	°F
Depth	7700	ft
Bottomhole temperature	230	°F

[1]Well measurements recorded in customary units

APPENDIX E

Geochemical Fingerprinting of Eagle Ford Shale Crude Oil and Produced Water

Introduction

Hydraulic fracturing could pose a risk to groundwater if hydraulic-fracturing fluids or formation fluids (e.g., oil, gas, brine) migrate upward into shallower aquifers. A major concern associated with the potential for upward migration of contaminants into shallower aquifers is the propensity to detect and attribute a specific source if a groundwater impact occurs. Organic compositions of crude oils and formation waters in hydraulically fractured shales are a central component in forensic investigations of potential changes in groundwater quality. For example, site-specific characterization of organic compounds in shale pore-fluids provides a geochemical fingerprint that can be used to distinguish and identify hydrocarbons in groundwater. The development of a fingerprint is possible due to the variety and abundance of hydrocarbon compounds found in crude oil and formation water, often unique to each horizontal well.

Characterization of organic substances are an important step in forensic groundwater investigations of environmental impacts from oil and gas activity (Wang et al. 2006; Morrison and Murphy 2010). Organic substances found in hydrocarbon-producing shales show significant variation in substance type and abundance (Orem et al. 2007; 2014). Organic substances in shale pore fluid may originate naturally from the shale, or from organic chemicals added during completion and production practices (Orem et al. 2014). The range of natural organic substances in crude oil are attributed to variability in source organisms, depositional environments, thermal maturity of the

sediment, and post-depositional alteration (Peters et al. 2005). Perhaps the most consistent means for differentiation of crude oil are biomarkers. Biomarkers are complex molecules derived from formerly living organisms, and particularly useful for geochemical fingerprinting because they are often unique to local depositional environments (Wang et al. 2006). In addition, biomarkers are useful for establishment of hydrocarbon sources because they: (1) can be detected in low quantities, (2) are degradation-resistant in the environment.

Extractable hydrocarbons in formation waters or organic-rich shales are highly variable (Orem et al. 2007; 2014). Hydrocarbon compounds in produced waters include polycyclic aromatic hydrocarbons (PAHs), heterocyclic compounds, other aromatics (e.g., alkyl benzenes), phenols, and long chain fatty acids. Low octanol/water partition coefficients (K_{ow}) of organic compounds suggest low partition of shale hydrocarbons co-produced waters. However, high reservoir temperatures (> 100°C) and pressures (> 20 MPa) can increase the K_{ow} of hydrocarbons and increase partitioning in produced waters. In the case of high temperature produced waters, organic geochemical signatures may be similar to crude oils produced from the shale. The organic geochemical signature of hydrocarbons in produced water may be enhanced by the presence of emulsified crude oil, turbulent mixing, and incomplete treatment (phase separation) of produced water. Therefore, produced waters sampled at the surface may conserve diagnostic biomarker ratios found in crude oils in the reservoir.

This report details a preliminary assessment of potentially significant organic substances in Eagle Ford Shale crude oil and produced water. Column chromatography was used to separate the total lipid extract (TLE) from crude oil and produced water

samples into saturate, aromatic and polar fractions. Fractions were analyzed using gas chromatography/mass spectrometry (GC/MS). Individual organic compounds were identified and their mass spectral features used to determine diagnostic biomarker ratios: maximum carbon chain length (C_{max}), average chain length (ACL), carbon preference index (CPI), odd-even preference (OEP), and pristane/phytane (Pr/Ph). The methods and results of this study could be applied at the site-level to aid in the development of an organic geochemical fingerprint used to detect, correlate, or differentiate potential groundwater impacts associated with hydraulic fracturing.

Investigations of the organic geochemistry for the Eagle Ford Shale have documented substantial variability in total organic carbon (TOC) and kerogen types (Dawson 2000; Edman and Pitman 2010). Organic analyses have identified heavy *n*-paraffins (C_{23} to C_{34}), fatty acids (C_{14} to C_{34}), and normal and isoprenoid fatty alcohols (C_{12} to C_{26}). Organic compounds in Eagle Ford Shale crude oil are probably attributed to catagenesis of autochthonous algal biomass (Longbottom et al. 2016). Catagenesis of marine algae biomass suggests that shorter (*n*-C_{12} to *n*-C_{18}) aliphatic and branched hydrocarbons dominate the bulk organic composition of Eagle Ford Shale crude oils, resulting in low ACL (*n*-C_{12} to *n*-C_{18}) and C_{max} values (Eglinton and Eglinton 2008). Pristane/phytane (Pr/Ph) is commonly employed as paleoredox biomarker, and may be useful in organic fingerprinting because they are environmental persistent.

Sample Collection

One crude oil (CRD-1) and one produced water (PRW-1) were obtained from an Eagle Ford Shale horizontal well. Sample collection followed methods after Orem et al.

(2007), and are briefly described here. Samples were collected at the well from a storage tanks using a stainless-steel dipper to carefully fill a new, pre-cleaned glass jar (CRD-1) and amber jug (PRW-1). Immediately after collection, samples were cooled to 4° C and prepared for transport. Samples were transported to the laboratory within 24 hours. Prior to storage, sample-container headspace was filled with a gentle stream of N_2 and sealed ith Parafilm M.

Column Chromatography

Approximately 1 mL of crude oil and 10 mL of HPLC-grade hexane were placed together in a 10-mL Erlenmeyer flask. The solution was then placed in an ultrasonic water bath for 2 minutes for mixing. Asphaltenes were removed by passing the mixture through a Pasteur pipette containing glass wool to retain the asphaltene fraction. The concentrated solution was transferred to a 3-g silica gel chromatographic column for cleanup and fractionation. Columns were preconditioned using 5 mL of hexane, followed by addition of the concentrated solution. Saturated fraction was eluted with four successive 1-mL aliquots of hexane; aromatic fraction was eluted with four successive 1 mL aliquots of hexane/DCM (1:1, v/v); and the polar fraction was eluted with four successive 1 mL aliquots of DCM/MeOH (1:1, v/v). The final extract for each fraction was evaporated under a gentle stream of dry nitrogen to a final volume of approximately 3 mL. Aliquots of aromatic and polar extract fractions were converted to trimethylsilyl derivatives by reaction with N, O-bis(trimethylsilyl)trifluoroacetamide (BSTFA) and pyridine in sealed vials for 30 minutes at 60 °C.

Isolation of organic compounds in produced water consisted of liquid/liquid extraction with four sequential volumes of 50 mL DCM. The combined extract of 200 mL was then concentrated to a volume of 5 mL under a gentle stream of dry nitrogen. Asphaltenes were removed by passing the mixture through a Pasteur pipette containing glass wool to retain the asphaltene fraction. The concentrated solution was transferred to a 3-g silica gel chromatographic column for cleanup and fractionation following previous methods.

GC/MS Analysis

GC/MS analyses of extract fractions were performed on a Thermo DSQII. Separation was achieved on a 30 m x 250 µm x 0.25 µm fused silica capillary column coated with DB5 (i.e., 95% dimethyl siloxane and 5% phenyl siloxane). The following conditions were used for the GC/MS run: 1.0 µL splitless injection, constant flow of 1.5 mL/min, solvent delay of 2.5 min, ion source of 250 °C, temperature program of 60–100 °C at 15 °C/min, 100–300 °C at 3 °C/min, and a hold at 300 °C for 10 min. The mass spectrometer was operated in the electron impact mode (EI) at 70 eV ionization energy and scanned from 50 to 1000 (3.04 scans per second). Data were acquired and processed using Xcalibur software. Individual organic compounds in chromatograms were identified by comparison of mass spectral features to libraries of mass spectral data (NIST08 and Wiley), and by comparison to an alkane standard. Identification of the organic compounds was carried out by computer matching against the mass spectral databases, and visual interpretation of each individual peak.

Results and Discussion

Major biomarker groups and characteristic signals for crude oil/produced water saturate fractions are reported in Table E.1. A summary of diagnostic biomarker ratios is reported in Table E.2. Major biomarker observations of saturate fractions for both samples include n-alkanes, isoalkanes, isoprenoids, steranes, diasteranes, and methyl steranes. Saturate hydrocarbon data are listed in Table E.3.

Table E.1
Major Biomarker Distributions (Saturate Fraction)

Biomarker	MS fragment ions (*m/z*)	Tentatively identified	
		CRD-1	PRW-1
n-alkanes	57	X	X
alkyl-cyclohexanes	83	-	-
methyl-alkyl-cyclohexanes	97	-	-
isoalkanes and isoprenoids	113, 183	X	X
sesquiterpanes	123	-	-
adamantanes	135, 136, 149, 163, 177, 191	-	-
diamantanes	187, 188, 201, 215, 229	-	-
tri-, tetra-, penta-cyclic terpanes	191	-	-
25-norhopanes	177	-	-
28,30-bisnorhopanes	163, 191	-	-
steranes	217, 218	X	X
5α(H)-steranes	149, 217, 218	-	-
5β(H)-steranes	151, 217, 218	-	-
diasteranes	217, 218, 259	X	X
methyl-steranes	217, 218, 231, 232	X	X
monoaromatic steranes	253	-	-
triaromatic steranes	231	-	-

Table E.2
Diagnostic Biomarker Ratios (Saturate Fraction)

Sample	C_{max}	ACL	CPI	OEP	Pr/Ph	Pr/*n*-C_{17}	Ph/*n*-C_{18}
CRD-1	*n*-C_{17}	26.8	0.9	0.7	0.5	0.20	0.60
PRW-1	*n*-C_{17}	29.3	0.9	0.7	0.6	0.26	0.63

Saturate fraction GC/MS traces for produced water are shown in Figures E.1a and E.2a. Major peaks are observed for the *n*-alkane series (*n*-C_{11} to *n*-C_{36}), and acyclic isoprenoids. One difference is a Gaussian distribution of *n*-alkanes (*n*-C_{15} to *n*-C_{22}), compared to the linear distribution observed for crude oil. This difference could be

explained by the preferential loss of shorter-chain *n*-alkanes (e.g., *n*-C_6 to *n*-C_{14}) due to biodegradation or preferential separation during the on-site treatment process prior to storage.

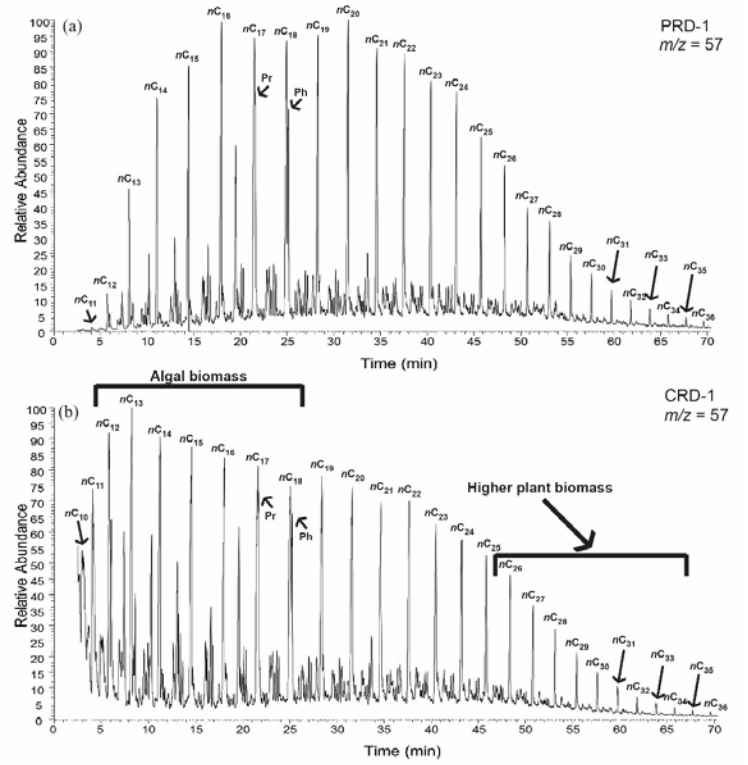

Figure E.1. Comparison of select ion chromatogram (*m*/*z* [mass/charge] = 57) for Eagle Ford Shale (a) crude oil and (b) produced water saturate fractions. GC/MS traces show the distribution of the homologous *n*-alkane series (*n*-C_{10} to *n*-C_{36}). EFS crude oil is dominated by shorter (*n*-C_{11} to *n*-C_{24}) carbon chains. EFS produced water shows bulk *n*-alkane distribution from *n*-C_{15} to *n*-C_{22}.

Diagnostic biomarker ratios matched reasonably well with crude oil (Table E.2). Produced water values for C_{max}, CPI, and OEP were nearly identical to those observed in crude oil, but ACL, Pr/Ph, Pr/*n*-C_{17} and Ph/*n*-C_{18} values were elevated. The preferential separation or degradation of shorter-chain *n*-alkanes would account for trends observed in biomarker ratios. The C_{max} value did not change as *n*-C_{17} remained the most abundant n-alkane. CPI and OEP values were conserved because the ratios are computed with longer-chain n-alkanes more resistant to degradation and separation. Increased ratios of Pr/*n*-C_{17}

and Ph/*n*-C_{18} are diagnostic of crude oil biodegradation because loss of n-alkanes precedes the relatively resistant acyclic isoprenoids (Peters et al. 2005). Further evidence for biodegradation may be supported by polar and aromatic fraction analyses. Aromatic components are relatively resistant and expected to increase as a function of biodegradation. In contrast, less resistant polar (NSO) components decrease with biodegradation.

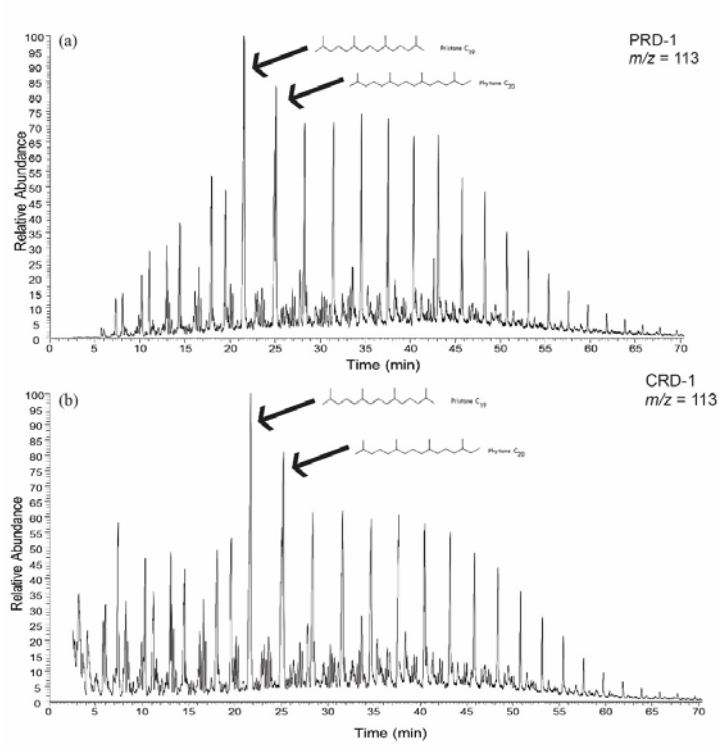

Figure E.2. Comparison of select ion chromatogram (*m*/*z* = 113) for Eagle Ford Shale (a) crude oil and (b) produced water saturate fractions. GC/MS traces show the distribution of isoalkanes and acyclic isoprenoids. Peaks for acyclic isoprenoids Pr and Ph are conspicuous.

Low CPI and Cmax (= *n*-C_{17}) values indicate that organic matter is predominately derived from algae, without input from higher plants (Eglinton and Eglinton 2008). The *n*-alkane ACL is the weight-averaged number of carbon atoms of higher plants and used to differentiate organic sources (Jeng 2006). The low ACL value (= 26.8) for CRD-1

indicates a lack of terrestrial organic-matter inputs. Acyclic isoprenoid compounds Pr and Ph were observed at high relative abundances and low ratio (Pr/Ph = 0.5). Low Pr/Ph ratios indicate organic matter deposition in a reducing paleoenvironment. Comparison between acyclic isoprenoids and n-alkanes (Pr/*n*-C_{17} and Ph/*n*-C_{18}) can indicate paleoredox conditions, organic matter maturity/source, and biodegradation (Peters et al. 2005). Pr/*n*-C_{17} (= 0.2) and Ph/*n*-C_{18} (= 0.6) values for EFS crude correspond to mature algal-sourced organic matter deposited in a marine reducing environment.

Table E.3
Saturate Fraction Data

Hydrocarbon Compound	Carbon Number	Retention Time (min)	
		CRD-1	PRD-1
Decane	*n*-C_{10}	2.95	-
Undecane	*n*-C_{11}	4.09	4.03
Dodecane	*n*-C_{12}	5.8	5.7
Tridecane	*n*-C_{13}	8.25	8.06
Tetradecane	*n*-C_{14}	11.2	11.06
Pentadecane	*n*-C_{15}	14.57	14.44
Hexadecane	*n*-C_{16}	18.07	17.95
Heptadecane	*n*-C_{17}	21.61	21.5
2,6,10,14-Tetramethylpentadecane	Pr	21.67	21.53
Octadecane	*n*-C_{18}	25.05	24.95
2,6,10,14-Tetramethylhexadecane	Ph	25.24	25.11
Nonadecane	*n*-C_{19}	28.4	28.29
Icosane	*n*-C_{20}	31.61	31.52
Heneicosane	*n*-C_{21}	34.7	34.6
Docosane	*n*-C_{22}	37.65	37.57
Tricosane	*n*-C_{23}	40.49	40.4
Tetracosane	*n*-C_{24}	43.22	43.14
Pentacosane	*n*-C_{25}	45.83	45.77
Hexacosane	*n*-C_{26}	48.36	48.29
Heptacosane	*n*-C_{27}	50.78	50.74
Octacosane	*n*-C_{28}	53.12	53.1
Nonacosane	*n*-C_{29}	55.39	55.38
Triacontane	*n*-C_{30}	57.59	57.58
Hentriacontane	*n*-C_{31}	59.73	59.72
Dotriacontane	*n*-C_{32}	61.81	61.81
Tritriacontane	*n*-C_{33}	63.83	63.83
Tetratriacontane	*n*-C_{34}	65.79	65.8
Pentratriacontane	*n*-C_{35}	67.71	67.72
Hexatriacontane	*n*-C_{36}	69.59	69.58

Summary

Organic substances in Eagle Ford Shale crude oil and produced water were fractionated (saturate, aromatic, polar) and saturate fractions were analyzed using GC/MS. Mass spectral data were used to identify biomarkers and determine diagnostic ratios. Crude oil saturate fractions are primarily composed of these compounds *n*-alkane series (*n*-C_{10} to *n*-C_{36}) and acyclic isoprenoids Pr and Ph. Diagnostic biomarker ratios indicate the crude oil

was generated from a mature source rock containing algal-sourced organic matter deposited in a marine reducing environment. Analysis of the produced-water saturate fraction shows similar organic compounds to those observed in the crude-oil saturate fraction. However, there was a decrease in the abundance of shorter-chain *n*-alkane compounds in the produced water compared to the crude oil. Diagnostic biomarker ratios indicate differences in abundance *n*-alkane compounds may be explained by biodegradation. The preliminary results of this study indicate that there is the potential to develop a site-specific geochemical fingerprint for certain hydrocarbon compounds sourced from the Eagle Ford Shale.

REFERENCES

Adams, B.M., L.E. Bauman, W.J. Bohnhoff, K.R. Dalbey, M.S. Ebeida, J.P. Eddy, M.S. Eldred, P.D. Hough, K.T. Hu, J.D. Jakeman, J.A. Stephens, L.P. Swiler, D.M. Vigil, and T.M. Wildey. 2014. Dakota, A Multilevel Parallel Object-Oriented Framework for Design Optimization, Parameter Estimation, Uncertainty Quantification, and Sensitivity Analysis: Version 6.0 User's Manual. Sandia Technical Report SAND2014-4633.

Alotaibi, B.Z., D.S. Schechter, and R.A. Wattenbarger. 2015. Production Forecast, Analysis and Simulation of Eagle Ford Shale Oil Wells. Paper 172929 *in SPE Middle East Unconventional Resources Conference and Exhibition*, January 26 – 28, Muscat, Oman.

Arthur, J.D., and H.W. Hochheiser. 2011. Plugging and Abandonment of Oil and Gas Wells. Working Document of the National Petroleum Council North American Resource Development Study, Washington, DC.

Avci, C.B. 1994. Evaluation of flow leakage through abandoned wells and boreholes. *Water Resources Research* 30, no. 9: 2565 – 2578.

Basu, N., G. Barzola, H. Bello, P. Clarke, and O. Viloria. 2012. Eagle Ford reservoir characterization from multisource data integration. Paper 80234 in *AAPG Annual Convention and Exhibition*, April 22 – 25, Long Beach, California.

Batzle, M. and Z. Wang. 1992. Seismic properties of pore fluids. *Geophysics* 57, no. 11: 1396 – 1408.

Bazan, L.W., S.D. Larkin, M.G. Lattibeaudiere, and T.T. Palisch. 2010. Improving Production in the Eagle Ford Shale with Fracture Modeling, Increased Fracture Conductivity, and Optimized Stage and Cluster Spacing Along the Horizontal Wellbore. Paper 138425 in *Tight Gas Completions Conference*, November 2 – 3, San Antonio, Texas.

Begg, S.H., P.R. King. 1985. Modelling the effects of shales on reservoir performance: calculation of effective vertical permeability. Paper 13529 in *SPE Reservoir Simulation Symposium*, February 10 – 13, Dallas, Texas.

Begg, S.H., R.R. Carter, and P. Dranfield. 1989. Assigning effective values to simulator gridblock parameters for heterogeneous reservoirs. *SPE Reservoir Engineering* 4, no. 4: 455 – 463.

Bethke, C.M. 1989. Modeling subsurface flow in sedimentary basins. *Geologische Rundschau* 78, no. 1: 129 – 154.

Blondes, M.S., K.D. Gans, J.J. Thordsen, M.E. Reidy, B. Thomas, M.A. Engle, Y.K. Kharaka, and E.L. Rowan. 2015. U.S. Geological Survey National Produced Waters Geochemical Database v2.1 (provisional): U.S. Geological Survey. http://eerscmap.usgs.gov/pwapp/ (accessed March 8, 2015).

Boschee, P. 2014. Produced and Flowback Water Recycling and Reuse: Economics, Limitations, and Technology. *Oil and Gas Facilities* 3, no. 01: 16 – 21.

Brandt, A.R., G.A. Heath, E.A. Kort, F. O'Sullivan, G. Pétron, S.M. Jordaan, P. Tans, J. Wilcox, A.M. Gopstein, D. Arent, S. Wofsy, N.J. Brown, R. Bradley, G.D. Stucky, D. Eardley, and R. Harriss. 2014. Methane leaks from North American natural gas systems. *Science* 343, no. 6172: 733–735.

Brownlow, D.T. 2010. Eagle Ford Shale Play and the Carrizo Aquifer. *Fountainhead* 4th Quarter.

Brownlow, J.W., S.C. James, and J.C. Yelderman, Jr. 2016a. Influence of hydraulic fracturing on overlying aquifers in the presence of leaky abandoned wells. *Groundwater*. dx.doi.org/10.1111/gwat.12431

Brownlow, J.W., J.C. Yelderman, Jr, and S.C. James. 2016b. Spatial risk analysis of hydraulic fracturing near abandoned and converted oil and gas wells. *Groundwater*. dx.doi.org/10.1111/gwat.12471

Burke, L.A., S.A. Kinney, R.F. Dubiel, and J.K. Pitman. 2013. Regional maps of subsurface geopressure gradients of the onshore and offshore Gulf of Mexico basin. U.S. Geological Survey Open File Report 2013-1058.

Cander, H. 2012. Sweet spots in shale gas and liquids plays: Prediction of fluid composition and reservoir pressure. Paper 40936 in *AAPG Annual Convention and Exhibition*, April 22 – 25, Long Beach, California.

Chaudhary, A.S., C.A. Ehlig-Economides, and R.A. Wattenbarger. 2011. Shale Oil Production Performance from a Stimulated Reservoir Volume. Paper 147596 in *SPE Annual Technical Conference and Exhibition*, October 30 – November 3, Denver, Colorado.

Cherian, B.V., M. McCleary, S. Fluckiger, N. Nieswiadomy, B. Bundy, S. Edwards, R. Rifia, K. Kublik, S. Narasimhan, J. Gray, O. Olaoye, and H. Shaikh. 2015. Production Performance in the In-Fill Development of Unconventional Resources. Paper 175963 in *SPE/CSUR Unconventional Resources Conference*, October 20 – 22, Calgary, Alberta.

Christensen, S., and R.L. Cooley. 1999. Evaluation of prediction intervals for expressing uncertainties in groundwater flow model predictions. *Water Resources Research* 35, no 9: 2627 – 2639.

Cooper, H.H. 1966. The equation of groundwater flow in fixed and deforming coordinates. *Journal of Geophysical Research* 71, no. 20: 4785 – 4790.

Curry, M., T. Maloney, R.A. Woodroof, and R.S. Leonard. 2010 Less Sand May Not Be Enough. Paper 131783 in *SPE Unconventional Gas Conference*, February 23 – 25, Pittsburgh, Pennsylvania.

Dausman, A.M., J. Doherty, C.D. Langevin, and M.C. Sukop. 2010. Quantifying data worth toward reducing predictive uncertainty. *Groundwater* 48, no. 5: 729 – 740.

Davies, R.J., S. Almond, R.S. Ward, R.B. Jackson, C. Adams, C., Worrall, F. Worrall, L.G. Herringshaw, J.G. Gluyas, and M.A. Whitehead. 2014. Oil and gas wells and their integrity: Implications for shale and unconventional resource exploitation. *Marine and Petroleum Geology* 56: 239 – 254.

Dawson, W.C., B. Katz, and V.D. Robison. 1995. Austin Chalk (!) petroleum system Upper Cretaceous, southeastern Texas: A case study. *Gulf Coast Association of Geological Societies Transactions* 45: 157 – 163.

Dawson, W.C. 1997. Limestone microfacies and sequence stratigraphy: Eagle Ford Group (Cenomanian-Turonian) north-central Texas outcrops: *Gulf Coast Association of Geological Societies Transactions* 47: 99 – 105.

Dawson, W.C. 2000. Shale microfacies-Eagle Ford Group (Cenomanian–Turonian) North-Central Texas outcrops and subsurface equivalents. *Gulf Coast Association of Geological Societies Transactions*: 50: 607 – 621

Dawson, W.C., and W.R. Almon. 2010. Eagle Ford Shale variability: Sedimentologic influences on source and reservoir character in an unconventional resource unit. *Gulf Coast Association of Geological Societies Transactions* 60: 181 – 190.

Delsman, J.R., P. Winters, A. Vandenbohede, G.H.P. Oude Essink, and L. Lebbe. 2016. Global sampling to assess the value of diverse observations in conditioning a real-world groundwater flow and transport model. *Water Resources Research* 52, 1652 – 1672.

Deming, D. 1994. Factors necessary to define a pressure seal. *AAPG Bulletin* 78, no. 6: 1005 – 1009.

Doherty, J. 2016. PEST: Model-Independent Parameter Estimation, Watermark Numerical Computing, Brisbane, Queensland, Australia.

Doherty, J., and R.J. Hunt. 2009. Two statistics for evaluating parameter identifiability and error reduction. *Journal of Hydrology* 366, no. 1: 119 – 127.

Doherty, J., and R.J. Hunt. 2010. Approaches to highly parameterized inversion: A guide to using PEST for groundwater-model calibration. U.S. Geological Survey Scientific Investigations Report 2010–5211. Reston, Virginia: USGS, 60 p.

Domenico, P.A., and F.W. Schwartz. 1998. *Physical and Chemical Hydrogeology*. New York City, New York: John Wiley & Sons Inc.

Donnez, P. 2007. *Essentials of Reservoir Engineering.* Paris, France: Editions Technip.

Downey, M.W. 1984. Evaluating seals for hydrocarbon accumulations. *AAPG Bulletin* 68, no. 11: 1752 – 1763.

Dusseault, M. and R. Jackson. 2014. Seepage pathway assessment for natural gas to shallow groundwater during well stimulation, in production, and after abandonment. *Environmental Geosciences* 21, no. 3: 107 – 126.

Eaton, B.A. 1969. Fracture gradient prediction and its application in oilfield operations. *Journal of Petroleum Technology* 21, no. 10: 1353 – 1360.

Economides, M.J., and K.G. Nolte. 2000. *Reservoir Stimulation*, Third Edition. Wiley, NY. 750 p.

Economides, M.J., M. Cikes, H. Pforter, T.H. Udick, and P. Uroda. 1989. The Stimulation of a Tight, Very-High-Temperature Gas-Condensate Well. *SPE Formation Evaluation* 4, no. 1: 63 – 72.

Edman, J.D., and J.K. Pitman. 2010. Geochemistry of Eagle Ford Group source rocks and oils from the First Shot field area, Texas. *Gulf Coast Association of Geological Societies Transactions* 60: 217 – 234.

Eglinton, T.I., and G. Eglinton. 2008. Molecular proxies for paleoclimatology. *Earth and Planetary Science Letters* 275, no. 1: 1 – 16.

Energy Information Administration (EIA). 1993. *Drilling Sideways – A Review of Horizontal Well Technology and Its Domestic Application*. Washington, DC: EIA.

Energy Information Administration (EIA). 2016. Oil and Gas Field Code Master List. Accessed from http://www.eia.gov/naturalgas/fieldcode/ (last accessed February 3, 2016)

Engelder, T. 2012. Capillary tension and imbibition sequester frack fluid in Marcellus gas shale. *Proceedings of the National Academy of Sciences* 109, no. 52: E3625 – E3625.

Engelder, T., L.M. Cathles, and L.T. Bryndzia. 2014. The fate of residual treatment water in gas shale. *Journal of Unconventional Oil Gas Resources* 7: 33 – 48.

Engelhardt, I., J.G. De Aguinaga, H. Mikat, C. Schüth, and R. Liedl. 2014. Complexity vs. simplicity: groundwater model ranking using information criteria. *Groundwater* 52, no. 4: 573 – 583.

Ferreira, J. M., R.T. De Oliveira, M. Assumpção, J.A. Moreira, R.G. Pearce, and M.K. Takeya. 1995. Correlation of seismicity and water level in the Açu reservoir – an example from northeast Brazil. *Bulletin of the Seismological Society of America* 85, no. 5: 1483 – 1489.

Fisher K. and N. Warpinski. 2011. Hydraulic fracture-height growth: real data. Paper 145949 in *SPE Annual Technical Conference and Exhibition*, October 30 – November 2, Denver, Colorado.

Fisher, K. 2014. Hydraulic fracture growth: Real data. Paper 41354 in *AAPG Eagle Ford plus Adjacent Plays and Extensions Workshop*, February 24-26, San Antonio, Texas.

Flewelling, S.A. and M. Sharma. 2014. Constraints on upward migration of hydraulic fracturing fluid and brine. *Groundwater* 52, no. 1: 9 – 19.

Flewelling, S.A., M.P. Tymchak, and N. Warpinski. 2013. Hydraulic fracture height limits and fault interactions in tight oil and gas formations. *Geophysical Research Letters* 40, no. 14: 3602 – 3606.

Fogg, G.E. 1986. Groundwater flow and sand body interconnectedness in a thick, multiple-aquifer system. *Water Resources Research* 22, no. 5: 679 – 694.

Foglia, L., S.W. Mehl, M.C. Hill, and P. Burlando. 2013. Evaluating model structure adequacy: The case of the Maggia Valley groundwater system, southern Switzerland. *Water Resources Research* 49, no. 1: 260 – 282.

Freeze, R.A., and J.A. Cherry. 1979. *Groundwate*r. Englewood Cliffs, New Jersey: Prentice Hall.

Gallagher, M., and J. Doherty. 2006. Parameter estimation and uncertainty analysis for a watershed model. *Environmental Modelling & Software* 22, no. 7: 1000 – 1020.

Gallagher, M., and J. Doherty. 2007. Predictive error analysis for a water resource management model. *Journal of Hydrology* 34, no. 3–4: 513 – 533.

Gasda, S.E., M.A. Celia, J.Z. Wang, and A. Duguid. 2013. Wellbore permeability estimates from vertical interference testing of existing wells. *Energy Procedia* 37: 5673 – 5680.

Gasda, S.E., S. Bachu, and M.A. Celia. 2004. Spatial characterization of the location of potentially leaky wells penetrating a deep saline aquifer in a mature sedimentary basin. *Environmental Geology* 46, no. 6-7: 707 – 720.

Gassiat C., T. Gleeson, R. Lefebvre, and J. McKenzie. 2013. Hydraulic fracturing in faulted sedimentary basins: Numerical simulation of potential contamination of shallow aquifers over long time scales. *Water Resources Research* 49, no. 12: WR014287

Gomaa, A.M., Q. Qu, R. Maharidge, S. Nelson, and T. Reed. 2014. New insights into hydraulic fracturing of shale formations. Paper 17594 in *International Petroleum Technology Conference*, January 20 – 22, Doha, Qatar.

Gómez-Hernandez, J.J. 2006. Complexity. *Groundwater* 44, no. 6: 782 – 785.

Gu, H., B. Lecerf, X. Weng, and O. Kresse, O. 2015. Effect of Fracture Breakdown Pressure on Multicluster Hydraulic Fracturing Treatments. Paper 15-126 in *49th US Rock Mechanics/Geomechanics Symposium*, June 28 – July 1, San Francisco, California.

Guéguen, Y., V. Palciauskas. 1994. *Introduction to the physics of rocks*. Princeton University Press.

Harbaugh, A.W. 2005. MODFLOW-2005, the U.S. Geological Survey Modular Ground-Water Model – The Ground-Water Flow Process. Reston, Virginia: USGS Techniques and Methods 6-A16.

Harris, H.B. 1965. Ground-water resources of La Salle and McMullen counties. *Texas Water Commission Bulletin* 6520, 59 pp.

Harrison, W.J. and L.L. Summa. 1991. Paleohydrology of the Gulf of Mexico basin. *American Journal of Science* 291, no. 2: 109 – 176.

Haymond, D. 1991. The Austin Chalk – An Overview. *Houston Geological Society Bulletin* 33, no. 8: 27 – 34.

Heidbach, O., M. Tingay, A. Barth, J. Reinecker, D. Kurfeß, and B. Müller. 2008. The World Stress Map database release 2008. doi:10.1594/GFZ.WSM.Rel2008

Herckenrath, D., C.D. Langevin, and J. Doherty. 2011. Predictive uncertainty analysis of a saltwater intrusion model using null-space Monte Carlo. *Water Resources Research* 47, no. 5.

Hill, M.C. 2006. The practical use of simplicity in developing ground water models. *Groundwater* 44, no. 6: 775 – 781.

Hill, M.C., and C.R. Tiedeman. 2007. *Effective Groundwater Model Calibrations, with Analysis of Data, Sensitivities, Predictions, and Uncertainty*. New York: Wiley.

Hill, M.C., D. Kavetski, M. Clark, M. Ye, M. Arabi, D. Lu, L. Foglia, and S. Mehl. 2016. Practical use of computationally frugal model analysis methods. *Groundwater* 54, no. 2: 159 – 170.

Hinchman, S.P., and R.D. Barree. 1985. Productivity Loss in Gas Condensate Reservoirs. Paper 14203 in *SPE Annual Technical Conference and Exhibition*, September 22 – 25, Las Vegas, Nevada.

Honarpour, M.M., N.R. Nagarajan, A. Orangi, F. Arasteh, and Z. Yao. 2012. Characterization of Critical Fluid PVT, Rock, and Rock-Fluid Properties – Impact on Reservoir Performance of Liquid Rich Shales. Paper 158042 in *SPE Annual Technical Conference and Exhibition*, October 8 – 10, San Antonio, Texas.

Hou, T., Y. Zhu, H. Lü, E. Sudicky, Z. Yu, and F. Ouyang. 2015. Parameter sensitivity analysis and optimization of Noah land surface model with field measurements from Huaihe River Basin, China. *Stochastic Environmental Research and Risk Assessment* 29, no. 5: 1383 – 1401.

Hsu, S.C. and P.P. Nelson. 2002. Characterization of eagle ford shale. *Engineering Geology* 67, no. 1: 169 – 183.

Hubbert, M.K. 1940. The theory of ground-water motion. *The Journal of Geology* 48, no. 8: 785 – 944.

Hunt, R.J., D.T. Feinstein, C.D. Pint, and M.P. Anderson. 2006. The importance of diverse data types to calibrate a watershed model of the Trout Lake Basin, Northern Wisconsin, USA. *Journal of Hydrology* 321, no. 1: 286 – 296.

Hunt, R.J., J. Doherty, and M.J. Tonkin. 2007. Are models too simple? Arguments for increased parameterization. *Groundwater* 45, no. 3: 254 – 262.

Ide, S., S. Friedmann, and H. Herzog. 2006. CO_2 Leakage through Existing Wells: Current Technology and Regulations. In *Proceedings of 8th Greenhouse Gas Technology Conference*, June 19 – 22, Trondjheim, Norway.

Ilk, D., N.J. Broussard, and T.A. Blasingame. 2012. Production Analysis in the Eagle Ford Shale – Best Practices for Diagnostic Interpretations, Analysis, and Modeling. Paper 160076 in *SPE Annual Technical Conference and Exhibition*, October 8 – 10, San Antonio, Texas.

Inamdar, A.A., T.M. Ogundare, R. Malpani, W.K. Atwood, K.E. Brook, A.M. Erwemi, and D. Purcell. 2010. Evaluation of Stimulation Techniques Using Microseismic Mapping in the Eagle Ford Shale. Paper 136873 in *Tight Gas Completions Conference,* November 2 – 3, San Antonio, Texas.

Independent Petroleum Association of America (IPAA). 2013. *2012-2013 IPAA Oil & Gas Producing Industry in Your State*. Washington, DC: IPAA.

Jakeman, A.J., and R.A. Letcher. 2003. Integrated assessment and modelling: features, principles and examples for catchment management. *Environmental Modelling & Software* 18, no. 6: 491 – 501.

James, S.C., J. Doherty, and A.A. Eddebbarh. 2009. Practical postcalibration uncertainty analysis: Yucca Mountain, Nevada. *Groundwater* 47, no. 6: 851 – 869.

Jaripatke, O.A., O. Samandarli, E. McDonald, and P.L. Richmond. 2014. Completion Optimization of an Unconventional Shale Play: Implementation of a Successful Completion Design Optimization Plan and the Results. Paper 170764 in *SPE Annual Technical Conference and Exhibition,* October 27 – 29, Amsterdam, The Netherlands.

Jeng, W.L. 2006. Higher plant n-alkane average chain length as an indicator of petrogenic hydrocarbon contamination in marine sediments. *Marine Chemistry* 102, no. 3: 242 – 251.

Johnston, O.C., and B.J. Knape. 1986. Pressure effects of the static mud column in abandoned wells. Texas Water Commission, Austin, TX, 99 pp.

Kang, M., C.M. Kanno, M.C. Reid, X. Zhang, D.L. Mauzerall, M.A. Celia, Y. Chen, and T.C. Onstott. 2014. Direct measurements of methane emissions from abandoned oil and gas wells in Pennsylvania. *Proceedings of the National Academy of Sciences* 111, no 51: 18173 – 18177.

Kim, T. 2012. Overview of interwellbore communication incidents: an ERCB perspective. In *Canadian Society for Unconventional Resources 14th Annual Conference,* October 3, Calgary, Alberta.

Kissinger, A., R. Helmig, A. Ebigbo, H. Class, T. Lange, M. Sauter, M. Heitfeld, J. Klunker and W. Jahnke. 2013. Hydraulic fracturing in unconventional gas reservoirs: risks in the geological system, part 2. *Environmental Earth Sciences* 70, no. 8: 3855 – 3873.

Konikow, L.F., and G.Z. Hornberger. 2006. Modeling effects of multinode wells on solute transport. *Groundwater* 44, no. 5: 648 – 660.

Konikow, L.F., and J.D. Bredehoeft. 1992. Ground-water models cannot be validated. *Advances in Water Resources* 15, no. 1: 75 – 83.

Konikow, L.F., G.Z. Hornberger, K.J. Halford, and R.T. Hanson. 2009. Revised multi-node well (MNW2) package for MODFLOW ground-water flow model. U.S. Geological Survey Techniques and Methods 6-A30. Reston, Virginia: USGS.

Kreitler, C.W. 1989. Hydrogeology of sedimentary basins. *Journal of Hydrology* 106, no. 1: 29 – 53.

La Vigna, F., M.C. Hill, R. Rossetto, and R. Mazza. 2016. Parameterization, sensitivity analysis, and inversion: an investigation using groundwater modeling of the surface-mined Tivoli-Guidonia basin (Metropolitan City of Rome, Italy). *Hydrogeology Journal*, 1 – 19.

Lacombe, S., E.A. Sudicky, S.K. Frape, and A.J.A. Unger. 1995. Influence of leaky boreholes on cross-formational groundwater flow and contaminant transport. *Water Resources Research* 31, no. 8: 1871 – 1882.

Lane, W., and R. Chokshi. 2014. Considerations for Optimizing Artificial Lift in Unconventionals. Paper 1921823 in *Unconventional Resources Technology Conference*, August 25 – 27, Denver, Colorado.

Lawal, H., G. Jackson, N. Abolo, and C. Flores. 2013. A Novel Approach to Modeling and Forecasting Frac Hits in Shale Gas Wells. Paper 164898 in *EAGE Annual Conference & Exhibition incorporating SPE Europec*, June 10 – 13, London, UK.

Lecampion, B., J. Desroches, X. Weng, J. Burghardt, and J.E. Brown. 2015. Can we engineer better multistage horizontal completions? Evidence of the importance of near-wellbore fracture geometry from theory, lab and field experiments. Paper 173363 in *SPE Hydraulic Fracturing Technology Conference*, February 3 – 5, The Woodlands, Texas.

Llewellyn, G.T. 2014. Evidence and mechanisms for Appalachian Basin brine migration into shallow aquifers in NE Pennsylvania, USA. *Hydrogeology Journal* 22, no. 5: 1055-1066.

Loucks, R.G., M.M. Dodge, and W.E. Galloway. 1984. Regional controls on diagenesis and reservoir quality in lower Tertiary sandstones along the Texas Gulf Coast. In *Clastic Diagenesis, AAPG Memoir 37*, ed. D.A. McDonald and R.C. Surdam, 15 – 45.

Longbottom, T.L., W.C. Hockaday, K.S. Boling, G. Li, Y. Letourmy, H. Dong, and S.I. Dworkin. 2016. Organic structural properties of kerogen as predictors of source rock type and hydrocarbon potential. *Fuel* 184: 792 – 798.

Mace, R.E. 1998. Ground-Water Flow and Solute Transport in a Fractured Chalk Outcrop, North-Central Texas. Unpublished dissertation, The University of Texas at Austin.

Mace, R.E., R.C. Smyth, L. Xu, J. Liang, and W.L. Fisher. 1999. Transmissivity, hydraulic conductivity, and storativity of the Carrizo-Wilcox Aquifer in Texas. Texas Bureau of Economic Geology, Austin, TX.

Magara, K. 1978. *Compaction and Fluid Migration, Practical Petroleum Geology*. New York City, New York: Elsevier.

Manchanda, R., N.P. Roussel, and M.M. Sharma. 2012. Factors influencing fracture trajectories and fracturing pressure data in a horizontal completion. Paper 12-633 in *46th US Rock Mechanics/Geomechanics Symposium*, June 24 – 27, Chicago, Illinois.

Martin, R., J.D. Baihly, R. Malpani, G.J. Lindsay, and W.K. Atwood. 2011. Understanding Production from Eagle Ford-Austin Chalk System. Paper 145117 in *SPE Annual Technical Conference and Exhibition*, October 30 – November 2, Denver, Colorado.

Mayerhofer, M.J., E. Lolon, N.R. Warpinski, C.L. Cipolla, D.W. Walser, and C.M. Rightmire. 2010. What is stimulated reservoir volume (SRV)?. *SPE Production & Operations* 25, no. 1: 89 – 98.

McKeon, M. 2011. Horizontal Fracturing in Shale Plays. In *PTTC Taking a Deeper Look at Shales: Geology and Potential of the Upper Ordovician Utica Shale in the Appalachian Basin*, June 21, New Philadelphia, Ohio.

Medeiros, F., E. Ozkan, and H. Kazemi. 2008. Productivity and Drainage Area of Fractured Horizontal Wells in Tight Gas Reservoirs. *SPE Reservoir Evaluation and Engineering* 11, no. 5: 902-911.

Mehl, S.W., and M.C. Hill. 2001. User guide to the Link-AMG (LMG) package for solving matrix equations using an algebraic multigrid solver. U.S. Geological Survey Open File Report 01-177. Reston, Virginia: USGS.

Montague, J.A., and G.F. Pinder. 2015. Potential of hydraulically induced fractures to communicate with existing wellbores. *Water Resources Research* 51, no. 10: WR016771.

Morrison, R.D., B.L. Murphy. 2010. Environmental forensics: contaminant specific guide. Academic Press.

Moore, C., and J. Doherty. 2005. Role of the calibration process in reducing model predictive error. *Water Resources Research* 41, no. 5.

Moore, C., and J. Doherty. 2006. The cost of uniqueness in groundwater model calibration. *Advances in Water Resources* 29, no. 4: 605 – 623.

Morel-Seytoux, H.J., P.D. Meyer, M. Nachabe, J. Touma, M.T. van Genuchten, and R.J. Lenhard. 1996. Parameter equivalence for the Brooks-Corey and van Genuchten soils characteristics: Preserving the effective capillary drive. *Water Resources Research* 32, no. 5: 1252 – 1258.

Morsy, S., J.J. Sheng, and M.Y. Soliman. 2013. Waterflooding in the Eagle Ford Shale Formation: Experimental and Simulation Study. Paper 167056 in *SPE Unconventional Resources Conference and Exhibition-Asia Pacific*, November 11 – 13, Brisbane, Australia.

Mullen, J. 2010. Petrophysical characterization of the Eagle Ford Shale in south Texas. Paper 138145 in *Canadian Unconventional Resources and International Petroleum Conference*, October 19 – 21, Calgary, Alberta.

Myers, T. 2012. Potential contaminant pathways from hydraulically fractured shale to aquifers. *Groundwater* 50, no. 6: 872 – 882.

Neuzil, C.E. 1994. How permeable are clays and shales? *Water Resources Research* 30, no. 2: WR0293.

Nicot, J.P. 2009. A survey of oil and gas wells in the Texas Gulf Coast, USA, and implications for geological sequestration of CO2. *Environmental geology* 57, no. 7: 1625 – 1638.

Nicot, J.P., A.K. Hebel, S.M. Ritter, S. Walden, R. Baier, P. Galusky, J. Beach, R. Kyle, L. Symank, and C. Breton. 2011. Draft Report: Current and projected water use in the Texas mining and oil and gas industry: report prepared by the Bureau of Economic Geology at The University of Texas, Austin, Texas, for the Texas Water Development Board.

Nordbotten, J.M., D. Kavetski, M.A. Celia, and S. Bachu. 2008. Model for CO2 leakage including multiple geological layers and multiple leaky wells. *Environmental Science & Technology* 43, no. 3: 743 – 749.

Nordbotten, J.M., M.A. Celia, and S. Bachu. 2004. Analytical solutions for leakage rates through abandoned wells. *Water Resources Research* 40, no. 4.

Nordbotten, J.M., M.A. Celia, S. Bachu, and H.K. Dahle. 2005. Semianalytical solution for CO2 leakage through an abandoned well. *Environmental Science & Technology* 39, no. 2: 602 – 611.

Orem, W.H., Tatu, C.A., Lerch, H.E., Rice, C.A., Bartos, T.T., Bates, A.L., Tewalt, S., and Corum, M.D., 2007, Organic compounds in produced waters from coalbed natural gas wells in the Powder River Basin, Wyoming, USA: *Applied Geochemistry* 22: 2240 – 2256.

Orem, W., C. Tatu, M. Varonka, H. Lerch, A. Bates, M. Engle, L. Crosby, and J. McIntosh. 2014. Organic substances in produced and formation water from unconventional natural gas extraction in coal and shale. International Journal of *Coal Geology* 126: 20 – 31.

Pappenberger, F., and K.J. Beven. 2006. Ignorance is bliss: Or seven reasons not to use uncertainty analysis. *Water Resources Research*, 42, no. 5.

Peters, K.E., C.C. Walters, and J.M. Moldowan. 2005. The Biomarker Guide, Volumes 1 and 2: Cambridge University Press, Cambridge, U.K., 1155 p.

Poeter, E.P., and M.C. Hill. 1999. UCODE, a computer code for universal inverse modeling. *Computers & Geosciences* 25, no. 4: 457 – 462.

Poettmann, F.H., and P.G. Carpenter. 1952. The multiphase flow of gas, oil, and water through vertical flow strings with application to the design of gas-lift installations. *Drilling and Production Practice*, 257 – 317.

Portis, D.H., H. Bello, M. Murray, B. Suliman, G. Barzola, and N. Basu 2013. A Comprehensive Well Look-Back; Analyzing Three Years' Worth of Drilling, Completing and Producing Eagle Ford Wells in Order to Understand Trend-Wide Performance Drivers and Variability. Paper 1581570 in *Unconventional Resources Technology Conference*, August 12 – 14, Denver, Colorado.

Produit, T., N. Lachance-Bernard, E. Strano, S. Porta, and S. Joost. 2010. A network based kernel density estimator applied to Barcelona economic activities. *Lecture Notes in Computer Science* 6106: 32 – 45.

Railroad Commission of Texas (RRC). 2000. *Well Plugging Primer*. Austin, Texas: RRC.

Railroad Commission of Texas (RRC). 2015a. Well data from Online Research Queries Database at RRC. http://www.rrc.state.tx.us/about-us/resource-center/research/online-research-queries/ (accessed February 22, 2015).

Railroad Commission of Texas (RRC). 2015b. Digital Map Data and API Data. http://www.rrc.state.tx.us/about-us/resource-center/research/data-sets-available-for-purchase/digital-map-data/ (last accessed April 10, 2015).

Railroad Commission of Texas (RRC). 2016a. Eagle Ford Information. http://www.rrc.state.tx.us/oil-gas/major-oil-gas-formations/eagle-ford-shale/ (last accessed February 3, 2016).

Railroad Commission of Texas (RRC). 2016b. Neubus Online Database. https://rrcsearch3.neubus.com/ (last accessed February 3, 2016).

Railroad Commission of Texas (RRC). 2016c. Oil and Gas Completions Query Online Database. http://www.rrc.state.tx.us/about-us/resource-center/research/online-research-queries/ (last accessed February 3, 2016).

Reagan, M.T., G.J. Moridis, N.D. Keen, and J.N. Johnson. 2015. Numerical simulation of the environmental impact of hydraulic fracturing of tight/shale gas reservoirs on near-surface groundwater: Background, base cases, shallow reservoirs, short-term gas, and water transport. *Water Resources Research* 51, no. 4: WR016086.

Refsgaard, J.C., J.P. van der Sluijs, J. Brown, and P. van der Keur. 2006. A framework for dealing with uncertainty due to model structure error. *Advances in Water Resources* 29, no. 11: 1586 – 1597.

Roussel, N.P., R. Manchanda, and M.M. Sharma. 2012. Implications of fracturing pressure data recorded during a horizontal completion on stage spacing design. Paper 152631 in *SPE Hydraulic Fracturing Technology Conference*, February 6 – 8, The Woodlands, Texas.

Saiers, J.E., and E. Barth. 2012. Comment on "Potential contaminant pathways from hydraulically fractured shale aquifers" by T. Myers. *Groundwater* 50, no. 6: 826 – 828.

Scott, R.J. 1977. The Austin Chalk-Buda Trend of South Texas. *Gulf Coast Association of Geological Societies Transactions* 27: 164 – 168.

Shapiro, S.A., and C. Dinske. 2009a. Scaling of seismicity induced by nonlinear fluid-rock interaction. *Journal of Geophysical Research B: Solid Earth* 114, no. B09307: 1 – 14.

Shapiro, S.A., and C. Dinske. 2009b. Fluid-induced seismicity: Pressure diffusion and hydraulic fracturing. *Geophysical Prospecting* 57, no. 2: 301 – 310.

Shapiro, S.A., C. Dinske, and E. Rothert. 2006. Hydraulic-fracturing controlled dynamics of microseismic clouds. *Geophysical Research Letters* 33, no. 14.

Shapiro, S.A., E. Huenges, and G. Borm. 1997. Estimating the crust permeability from fluid-injection-induced seismic emission at the KTB site. *Geophysical Journal International* 131, no. 2: F15 – F18.

Shelkholeslami, B.A., B.W. Schlottman, F.A. Seidel, and D.M. Button. 1991, Drilling and production aspects of horizontal wells in the Austin Chalk. *Journal of Petroleum Technology* 43, pp. 773-779.

Sheng, J.J. and K. Chen. 2014. Evaluation of the EOR potential of gas and water injection in shale oil reservoirs. *Journal of Unconventional Oil and Gas Resources* 5: 1 – 9.

Silverman, B. W. 1986. Density Estimation for Statistics and Data Analysis. New York: Chapman and Hall.

Sneddon, I. 1946. The distribution of stress in the neighbourhood of a crack in an elastic solid. Paper in *Proceedings of the Royal Society of London A: Mathematical, Physical and Engineering Sciences* 187, no. 1009: 229 – 260.

Snyder, R.H., and M. Craft. 1977. Evaluation of Austin and Buda Formations from core and fracture analysis. *Gulf Coast Association of Geological Societies Transactions*: 27: 376 – 385.

Stapp, W.L. 1977. The geology of the fractured Austin and Buda formations in the subsurface of South Texas. *Gulf Coast Association of Geological Societies Transactions* 27: 208 – 229

Stegent, N.A., A.L. Wagner, J. Mullen, and R.E. Borstmayer. 2010. Engineering a Successful Fracture-Stimulation Treatment in the Eagle Ford Shale. Paper 136183 in *Tight Gas Completions Conference*, November 2 – 3, San Antonio, Texas.

Stegent, N.A., K. Ferguson, and J. Spencer. 2011. Comparison of Frac Valves vs. Plug-and-Perf Completion in the Oil Segment of the Eagle Ford Shale: A Case Study. Paper 148642 in *Canadian Unconventional Resources Conference*, November 15 – 17, Calgary, Alberta.

Stegent, N.A., L.M. Leotaud, W. Prospere, and C.P. Veillette. 2010. Cement technology improves fracture initiation and leads to successful treatments in the Eagle Ford Shale. Paper 137441 in *SPE Tight Gas Completions Conference*, November 2 – 3, San Antonio, Texas.

Suliman, B., R. Meek, R. Hull, H. Bello, D. Portis, and P. Richmond. 2013. Variable Stimulated Reservoir Volume (SRV) Simulation: Eagle Ford Shale Case Study. Paper 1582061 in *Unconventional Resources Technology Conference*, August 12 – 14, Denver, Colorado.

Sun, A.Y., R. Green, S. Swenson, and M. Rodell. 2012. Toward calibration of regional groundwater models using GRACE data. *Journal of Hydrology* 422: 1 – 9.

Syfan Jr, F.E., T.T. Palisch, and J.C. Dawson. 2013. 65 Years of Fracturing Experience: The Key To Better Productivity Is Not What We Have Learned, But What We Have Forgotten and Failed To Utilize! Paper 166107 in *SPE Annual Technical Conference and Exhibition*, September 30 – October 2, New Orleans, Louisiana.

Texas Water Development Board (TWDB). 2016. Groundwater Database (GWDB) Reports. http://www.twdb.texas.gov/groundwater/data/gwdbrpt.asp (last accessed February 27, 2016).

Thorkildsen, D., and R.D. Price. 1991. Ground-water resources of the Carrizo-Wilcox aquifer in the Central Texas Region. Texas Water Development Board Report 332. Austin, Texas.

Tian, Y., W.B. Ayers, and D. McCain Jr. 2013. The Eagle Ford Shale Play, South Texas: Regional Variations in Fluid Types, Hydrocarbon Production and Reservoir Properties. Paper 16808 in *International Petroleum Technology Conference*, March 26 – 28, Beijing, China.

Tonkin, M., and J. Doherty. 2009. Calibration-constrained Monte Carlo analysis of highly parameterized models using subspace techniques. *Water Resources Research* 45, no. 12.

Tonkin, M., J. Doherty, and C. Moore. 2007. Efficient nonlinear predictive error variance for highly parameterized models. *Water Resources Research* 43, no. 7.

Townsend-Small, A., T.W. Ferrara, D.R. Lyon, A.E. Fries, and B.K. Lamb, B. K. 2016. Emissions of coalbed and natural gas methane from abandoned oil and gas wells in the United States. *Geophysical Research Letters* 43, no. 5: 2283 – 2290.

Tran D., A. Settari, and L. Nghiem. 2013. Predicting Growth and Decay of Hydraulic-Fracture Width in Porous Media Subjected to Isothermal and Nonisothermal Flow. *SPE Journal* 18, no. 4: 781 – 794.

Vazquez, M., and H.D. Beggs. 1980. Correlations for fluid physical property prediction. *Journal of Petroleum Technology* 32, no. 6: 968 – 970.

Vecchia, A.V., and R.L. Cooley. 1987. Simultaneous confidence and prediction intervals for nonlinear regression models with application to a groundwater flow model. *Water Resources Research* 23, no. 7: 1237 – 1250.

Vengosh, A., R.B. Jackson, N. Warner, T.H. Darrah, A. Kondash. 2014. A critical review of the risks to water resources from unconventional shale gas development and hydraulic fracturing in the United States. *Environmental Science & Technology* 48, no. 15: 8334 – 8348.

Vrugt, J.A. 2016. Markov chain Monte Carlo simulation using the DREAM software package: Theory, concepts, and MATLAB implementation. *Environmental Modelling & Software* 75: 273 – 316.

Walls, J.D., and S.W. Sinclair. 2011. Eagle Ford shale reservoir properties from digital rock physics. *First Break* 29, no. 6: 97 – 101.

Wang, Z., S.A. Stout, and M. Fingas. 2006. Forensic fingerprinting of biomarkers for oil spill characterization and source identification. *Environmental Forensics* 7, no. 2: 105 – 146.

Warner D.L. 2001. Technical and economic evaluation of the protection of saline ground water under the safe drinking water act and the UIC regulations: report prepared for Groundwater Protection Council.

Warner N.R., R.B. Jackson, T.H. Darrah, S.G. Osborn, A. Down, K. Zhao, A. White, and A. Vengosh. 2012. Geochemical evidence for possible natural migration of Marcellus Formation brine to shallow aquifers in Pennsylvania. *Proceedings of the National Academy of Sciences* 109, no. 30: 11961-11966.

Warner, D.L., L.F. Koederitz, and R.C. Laudon. 1997. Application of an area-of-review (AOR) concept to the East Texas Field and other selected Texas oilfields: report prepared by the University of Missouri-Rolla, for U.S. Department of Energy, 402 pp.

Warner, D.L., L.F. Koederitz, S. Dunn-Norman, and R.C. Laudon. 1996. Application of an AOR variance methodology to the Permian Basin, Texas: report prepared for The American Petroleum Institute, 288 pp.

Yeh, N.S., M.J. Davison, and R. Raghavan. 1986. Fractured Well Responses in Heterogeneous Systems—Application to Devonian Shale and Austin Chalk Reservoirs. *Journal of Energy Resources Technology* 108, no. 2: 120 – 130.

Yu, G. and R. Aguilera. 2012. 3D analytical modeling of hydraulic fracturing stimulated reservoir volume. Paper 153486 in *SPE Latin America and Caribbean Petroleum Engineering Conference*, 16 – 18 April, Mexico City, Mexico.

Zimmer, U. 2011. Calculating stimulated reservoir volume (SRV) with consideration of uncertainties in microseismic-event locations. Paper 148610 in *Canadian Unconventional Resources Conference*, November 15 – 17, Calgary, Alberta, Canada.